WAVE-INDUCED VIBRATIONS IN FIXED OFFSHORE STRUCTURES

by

WILLIAM C. NOLAN

Lieutenant, United States Coast Guard
B.S., U.S. Coast Guard Academy

and

VERNON C. HONSINGER

Lieutenant, United States Navy
B.S., U.S. Naval Academy

SUBMITTED IN PARTIAL FULFILLMENT

OF THE REQUIREMENTS FOR THE

DEGREE OF NAVAL ENGINEER

AND THE DEGREE OF

MASTER OF SCIENCE IN NAVAL ARCHITECTURE

AND MARINE ENGINEERING

at the

MASSACHUSETTS INSTITUTE OF TECHNOLOGY

May 1962

Signatures of Authors _____

Department of Naval Architecture and
Marine Engineering, 19 May 1962

Certified by _____
Thesis Supervisor

Accepted by _____
Chairman, Departmental Committee on
Graduate Students

WAVE-INDUCED VIBRATIONS IN FIXED OFFSHORE STRUCTURES by WILLIAM C. NOLAN and VERNON C. HONSINGER. Submitted to the Department of Naval Architecture and Marine Engineering on 19 May 1962 in partial fulfillment of the requirements for the Master of Science degree in Naval Architecture and Marine Engineering and the Professional degree, Naval Engineer.

ABSTRACT

The object of this thesis is to develop a procedure for calculating the dynamic displacement response of the platform of a fixed offshore structure acted upon by a regular wave train. The structure considered has four legs in a square configuration, with the waves impinging normal to one side of the square. The procedure may be manipulated for use with other leg configurations and wave directions.

The thesis is written in a manner useful to a designer of fixed offshore structures. An iterative procedure may be used to arrive at the critical wave-displacement combination.

The types of waves considered are those for which Stokes' 3rd approximation applies. A modified version of Morison's theory is used for drag forces. Families of curves are presented for use in predicting these forces and their centroids. The curves, plotted in dimensionless form, show the limits of applicability of Stokes' 3rd approximation. MacCamy-Fuchs diffraction theory is used for inertia forces.

To calculate the dynamic response of the platform the authors fit the vibration problem of the structure to the classical theory for a linear, single-degree-of-freedom system. The wave forces are expressed in terms of a Fourier series. Displacements are calculated for twelve positions in one wave cycle, and a displacement curve is drawn. A simple tabular form is presented for calculating these displacements.

Computer programs (in FORTRAN) are given for performing the bulk of the force and displacement calculations men-

tioned above. The theoretical procedure for unbraced and braced leg configurations is tested by experiment for 32 cases. For these tests the ratio of maximum theoretical to experimental displacements varies from about 0.5 to 1.7.

It is concluded that the designer should incorporate a factor of ignorance of 3 in his design.

The authors show that the largest waves are not necessarily the most critical for the structure. Rather, the critical design wave is a function of the frequency ratio (wave frequency/structure natural frequency). The designer must consider a range of significant waves which give frequency ratios of about 1.1 or less.

It is recommended that calculations be performed for some real structures in ocean waves. From a comparison of the results with observed data a revised factor of ignorance might be obtained.

In Appendix I an approach to the solution for vortex shedding forces and frequencies in a train of surface waves is presented. Existing vortex theories are modified to apply to a vertical cylinder in finite amplitude waves, and boundaries are set on the predicted maximum forces. Experiments are conducted from which vortex forces are seen to fall within the boundary limits set by theory. The experiments also validate the proposed theory that the shedding frequency is a predictable integral multiple of wave frequency. It is recommended that a procedure be developed for determining platform displacements due to these forces.

Thesis Supervisor: Donald R.F. Harleman

Title: Associate Professor of Hydraulics

TABLE OF CONTENTS

		Page
Abstract		ii
Table of Contents		iv
List of Figures		vi
List of Tables		viii
List of Symbols		ix
Acknowledgements		xiv
I.	Introduction	1
II.	Procedure	4
	A. Theoretical	4
	B. Experimental	42
III.	Results	54
IV.	Discussion of Results	71
V.	Conclusions	76
VI.	Recommendations	77
VII.	Appendix	79
	A. Details of Theoretical Procedure	80
	B. Sample Theoretical Calculations	91
	C. Summary of Theoretical Calculations	100
	D. Computer Programs	103
	E. Sample Calculations for Experimental Data	114
	F. Summary of Calculations for Experimental Data	117
	G. Supplementary Discussion of Results	124
	1. Theory and Experiment	124
	2. Computer	127

TABLE OF CONTENTS
(continued)

		Page
H.	Original Experimental Data	132
I.	Vortex Shedding on a Vertical Cylinder in a Wave Train	138
J.	Literature Citations	166

LIST OF FIGURES

Figure	Title	Page
I	Definition Sketch of a Wave	10
II	Steady State Drag Coefficient versus Reynold's Number for Circular Cylinder	15
III	Drag Force Centroids for Wave Height/Wave Length (H/L) and Water Depth/Wave Length (d/L) Ratios	18
IV	Drag Force Multiplier (A) - Crest Region	19
V	Drag Force Multiplier (B) - Trough Region	20
VI	Influence Fraction	35
VII	Photograph of Wave Tank	44
VIII	Photograph of Braced Structure Model	44
IX	Photograph of Single Cylinder in Position for Measuring Transverse Forces	47
X	Photograph of Braced Structure Model in Position for Measuring Displacement	49
XI	Photograph Showing Scheme for Recording Platform Displacement	49
XIIa-XIIp	Theoretical and Experimental Platform Displacements	55-70
XIII	Ratio of Maximum Positive Theoretical and Experimental Platform Displacements vs. Frequency Ratio ω/ω_n for Each Run of the Thesis Results	73
XIV	Simple Beam Representation of One Leg	80
XV	Portal Representation of Unbraced Structure	86

LIST OF FIGURES
(continued)

Figure	Title	Page
XVI	Tabular Calculation for Platform Displacement	97
XVIIa-XVIId	Theoretical and Experimental Longitudinal and Transverse Forces, $\frac{1}{2}$" Cylinder	119-122
XVIII	Typical Wave Gage Calibration	133
XIX	Typical Force Gage Calibration	134
XX	Typical Sanborn Recorder Longitudinal Force and Wave Profile Traces	135
XXI	Typical Sanborn Recorder Transverse Force and Wave Profile Traces	135
XXIIa-XXIId	Experimental Transverse Forces, 1" Cylinder	159-162

LIST OF TABLES

Table	Title	Page
I	Magnification Factors	29
II	Phase Angles	29
III	Experimental Wave Characteristics	51
IV	Wave Characteristics	100
V	Various Coefficients for Drag Force Determination	101
VI	Theoretical Forces and Force Centroids on a Single Leg	101
VII	Structure Natural Frequencies	102
VIII	Experimental Wave Characteristics	117
IX	Experimental Wave Forces, $\frac{1}{2}$" Cylinder	118
X	Experimental Damping and Structure Natural Frequencies	123
XI	Trough Velocities Associated with Critical Wave Parameters	129
XII	Water Temperatures	132
XIII	Experimental Data for Free (Natural) Oscillations of the Structure Model	137
XIV	Wave Periods and Period Parameters	156
XV	Wave Parameters for Transverse Force Determination	157
XVI	Comparison of Theoretical and Experimental Transverse Force Results	158

LIST OF SYMBOLS

A = dimensionless drag force multiplier in crest region (14)

B = dimensionless drag force multiplier in trough region (15)

C = wave celerity, ft./sec.

C/C_c = damping coefficient as fraction of critical damping (32,37)

C_D = drag coefficient associated with R

$C_{D_{trough}}$ = drag coefficient associated with R_{trough}

C_L = lift coefficient associated with vortex shedding

D = leg diameter, ft.

D_B = bracing diameter, ft.

E = Young's modulus, lbs./in.^{2}

F = general force, lbs.

F_D = maximum drag force on a leg in crest region, lbs.

$(F_D)_t$ = maximum drag force on a leg in trough region, lbs.

F_I = maximum inertia force on a leg in crest region, lbs.

$(F_I)_t$ = maximum inertia force on a leg in trough region, lbs.

F_L = maximum transverse force on a vertical cylinder caused by vortex shedding, lbs.

F_1 = force defined by (50), lbs.

F_2 = force defined by (52), lbs.

F_3 = force defined by (54), lbs.

H = wave height measured from crest to trough, ft.

H_{max} = theoretical limit on wave height, ft.

I = moment of inertia associated with bending of one leg, $in.^4$

J = $2\pi d/L$ (1)

L = wave length, ft.

M = general moment, ft.-lb.

N = number of legs

N' = number of legs in one row (parallel to wave crests)

P = general force on one leg, lbs.

P_o = force applied at level of platform, lbs.

R = Reynold's number associated with wave crest (18)

R_{trough} = Reynold's number associated with wave trough (19)

S = distance from bottom to mean particle position, ft.

S' = distance from bottom to actual particle position, ft.

$\bar{S}'$ = distance from bottom to point of application of F_D, ft.

$\bar{S}_I$ = distance from bottom to point of application of F_I, ft.

$\bar{S}_t'$ = distance from bottom to point of application of $(F_D)_t$, ft.

$(S_t)_{crit}$ = defined on p. 128, ft.

S_c = cylinder Strouhal number (88)

T = wave period, sec.

$(T_s)_c$ = time required to shed one vortex in wave crest (94), sec.

$(T_s)_t$ = time required to shed one vortex in wave trough (95), sec.

U = horizontal component of particle velocity at surface, ft./sec.

U_{max} = horizontal component of particle velocity at crest surface, ft./sec.

U_{trough} = horizontal component of particle velocity at trough surface, ft./sec.

W = platform weight, lbs.

a = height at which P acts, ft.

d = water depth, ft.

g = gravitational constant, normally 32.2 ft./sec.^{2}

h = leg spacing, ft.

k = spring constant, lbs./in.

ℓ = leg length, ft.

ℓ_B = cumulative length of all bracing below the still water level, ft.

m = vibrating mass, slugs

n_c = number of vortices shed during crest passage

n_t = number of vortices shed during trough passage

q = damped natural frequency of structure, rad./sec.

r_D = drag force ratio defined by (63)

r_I = inertia force ratio defined by (65)

r_m = mass ratio defined by (59)

t = time, sec.

u = horizontal component of particle velocity, ft./sec.

u_{bottom} = horizontal component of particle velocity at ocean bottom under wave trough, ft./sec.

u_{max} = horizontal component of particle velocity under wave crest, ft./sec.

$(u_{max})_{crit}$ = defined on p. 157, ft./sec.

$(u_{max})_y$ = horizontal component of particle velocity under crest at bottom of cylinder, ft./sec.

$\sqrt{\overline{u^2_{max}}}$ = root mean square of velocity distribution in wave crest, ft./sec.

u_{trough} = horizontal component of particle velocity under wave trough, ft./sec.

$\sqrt{\overline{u^2_{trough}}}$ = root mean square of velocity distribution in wave trough, ft./sec.

w = weight/unit length of leg, lbs./ft.

x = platform longitudinal displacement, in direction of wave propagation, in.

$\dot{x}$ = dx/dt

x_o = amplitude of platform longitudinal displacement, in.

x_{STATIC} = longitudinal platform displacement if force is applied statically (39), in.

y = vertical displacement of particle from mean position, ft.; in Appendix I, distance of bottom of cylinder above tank bottom, ft.

y' = distance above tank bottom to point where period parameter is 12.5 (p. 148), ft.

y_{max} = vertical displacement of particle from mean position under wave crest, ft.

y_{trough} = vertical displacement of particle from mean position under wave trough, ft.

γ = specific weight, lbs./ft.^{3}

δ = logarithmic decrement of damped free oscillations (42)

η = distance to wave surface from still water level, ft.

η_o = height of wave crest above still water level, ft.

θ = wave phase angle (=90° at crest), degrees

ν = kinematic viscosity, ft.^{2}/sec.

π = 3.14159 .....

ρ = mass density of water, slugs/ft.^{3}

ϕ = phase angle by which displacement lags force (40), degrees

ϕ_{RL} = general lag angle for forces acting on rear legs (48), degrees

ω = wave frequency; general frequency of applied force, radians/sec.

ω_c = vortex shedding frequency in crest region, radians/sec.

ω_n = undamped natural frequency of structure, radians/sec.

ω_s = general vortex shedding frequency, radians/sec.

ω_t = vortex shedding frequency in trough region, radians/sec.

ACKNOWLEDGEMENTS

The authors particularly express their appreciation to their Thesis Supervisor, Associate Professor Donald R.F. Harleman, for his interest and assistance in the preparation of this thesis.

Appreciation is also expressed to Professor Robert J. Hansen, the Thesis Advisor.

Discussion with Mr. Robert A. Vanstone of Brewer Engineering Laboratories, Inc., Marion, Massachusetts, concerning mainly his work in measuring platform motions on Texas Tower Number Four, was especially helpful at the time when the authors were formulating their thesis.

Appreciation is expressed to the Civil Engineering Branch of the United States Coast Guard for supplying plans and design computations for Buzzards Bay and Brenton Reef Light Stations.

Several friends of the authors have expressed an interest in this thesis and a willingness to be helpful in any way possible. These persons remain anonymous, but their support is deeply appreciated.

The thesis computations were done in part on the IBM 7090 Computer at the Computation Center of Massachusetts Institute of Technology, Cambridge, Massachusetts.

I. INTRODUCTION

The problem of wave-induced vibrations in fixed offshore structures suddenly was cast into the public news focus when on January 15, 1961, the United States Air Force Texas Tower Number Four collapsed 80 miles off the New Jersey coast in a heavy storm with the attendant loss of 28 lives [1]*.

Prior to that incident, and since, no one has computed the dynamic displacements of such a structure acted upon by wave forces, to the best of the authors' knowledge. The design approach has been to make the natural frequency of the structure relatively high (about 50 cycles per minute) and then simply treat the wave force as if it were statically applied. This method is crude at best, and can be very misleading.

During the winter of 1958-59 a platform motion study [2] was made of Texas Tower No. 4. It was observed that the tower platform displacements were greater for 10 and 11 ft. waves (about ± 3 in.) than for 30 ft. waves. Obviously the highest wave was not the most critical for this structure.

---

* Numbers in brackets refer to literature citations, Appendix J.

The Air Force was interested in platform motions of Texas Tower No. 4 because they wanted to know what errors might be introduced into the installed aircraft-tracking radar system. (For this particular situation it was felt that rotational motion would probably be more of a problem than translational motion.)

This thesis develops a method of calculating the dynamic translation displacements of a fixed offshore structure in a regular wave train. The theory developed has been experimentally checked by the authors. The experimental model was patterned somewhat similar to the United States Coast Guard's Buzzards Bay Light Station, located off the coast of Massachusetts [3].

The Coast Guard has initiated a long range program of replacing lightships by fixed offshore structures. The two completed to date (Buzzards Bay and Brenton Reef Light Stations) are braced structures with four legs. The U.S. Navy built a similar but considerably larger structure at Argus Island, near Bermuda. The U.S. Air Force built three Texas Towers, which were three-legged structures. Many other fixed offshore structures have been built in the past also, particularly in connection with drilling and mining operations in the Gulf of Mexico. The potential exists [4] for many more offshore oil-drilling rigs to be built around the world in the years to come.

There has been at least one case reported [5] in which vortex shedding was important in waves. In that case after a one week storm a two foot diameter pile suffered a fatigue failure caused by transverse vibrations of 2.5 seconds period in 12 feet high waves of 13 seconds period. The authors of this thesis suspected that vortex shedding forces might have a noticeable effect on offshore structures. Some investigation of this subject has been included in this thesis. The authors concluded from their literature survey that no previous work has been done on the question of vortex shedding forces on a stationary vertical cylinder in a wave train.

II. PROCEDURE

A. Theoretical Procedure

1. Hydrodynamics

General

This section deals only with those forces on a cylindrical pile acting in a direction parallel to that of wave propagation. These forces are termed longitudinal forces to distinguish them from the transverse or "lift" forces caused by vortex shedding. The transverse forces, although requiring consideration in a practical structure design, caused such small displacements of the model under study that it was not feasible to obtain experimental verification of an analytic approach. Because of this, the transverse force investigation, both theoretical and experimental, is included as Appendix I and is not discussed further in this section.

The ultimate design procedure would be to make use of a statistical analysis of ocean wave and energy spectra in the development of the input forcing functions for the structure displacement problem.

Steps have been taken in this direction, for example [6], although the problems encountered, not only in obtaining a sufficient scope of reliable data [7], but also in applying this data to the development of a useful design criteria, have yet to be solved. For this reason the authors are restricting the investigation to a regular train of surface waves whose forces are capable of relatively simple mathematical superposition.

In the past a typical design procedure has been to decide upon a "design wave," which is the largest wave to be expected (within specified confidence limits) over the planned lifetime of the structure. Using applicable wave theory, one may then determine the wave forces and moments acting over an incremental length. These may be summed up in a tabular form to give the total force and moment. [8, 3]. Some designs, also, have considered a breaking wave of size somewhat smaller than the design wave [9, 10].

If the dynamics of the problem are considered it is obvious that this design wave may not be the wave which causes the greatest excursions (or stresses) in the structure. Rather it is to be expected that a wave (of significent height) whose fundamental or some low order harmonic corresponds closely to the natural frequency of the structure may be the critical wave from a design standpoint. This possibility has been indicated

where, over an extended period of observation, a 7.5 foot wave caused greater platform motion of Texas Tower No. 2 than much larger waves did.[9] A similar observation is cited in the Introduction for Texas Tower No. 4.

A serious situation also may exist when the wave length is approximately equal to the leg spacing, for in this case the fundamental wave forces (and possibly some harmonics) will be in phase.

The proposed procedure, therefore, presents a method whereby several waves of various lengths and steepness may be considered over the range of possible water depths. The critical displacement-wave combination is then arrived at by an iterative process. To allow for a solution by this method within a reasonable length of time families of curves are developed such that total force and moment may be determined by a simple multiplication. This is intended to supplant the tedious incremental tabulation and summation mentioned previously. The curves (Figures III, IV, V) are presented in terms of dimensionless parameters such that they may be applied to any situation for which the proposed theory is applicable.

A pile spacing greater than 10 pile diameters has been found experimentally to be large enough such that proximity effects are negligible. [11] This spacing is exceeded, not only in the vast majority of offshore

structures of the type considered, but also for the model which was the object of the authors' experimental study.

Wave Theory

H = wave height, measured from crest to trough.

L = wave length.

d = water depth.

η_o = height of wave crest above still water level.

Several theories on wave motions have been developed and tested experimentally with varying degrees of success. These theories are found to be applicable over finite ranges of wave parameters and water depths, with no one theory satisfying all conditions. Since the waves of interest in this study are of the relatively shallow water finite amplitude type, two theories seem to be of particular interest - namely, Stokes' third approximation and the Solitary wave theory. These theories are discussed in detail elsewhere (for example [4, 12, 13, 14]) and will not be repeated here. However, for purposes of evaluating this study, the following limits of applicability may be noted from these references.

Stokes' 3rd approximation:

a.) $(\eta_o/H) \leq 0.625$

b.) $(H/L) \leq 0.142$

Solitary wave:

a.) waves at or near breaking point

b.) $(d/L) \longrightarrow 0$

Theoretical limits on ocean wave parameters:

a.) $(\eta_o/H) \leq 0.75$

b.) $(H/L) \leq 0.142$

c.) $H_{max} = 0.78 \ (d-(H-\eta_o))$ for shallow water

d.) from the above, $(H/d) \leq 0.653$

Using the maximum value of (η_o/H) from Stokes' theory and the value of H_{max} above, one sees that $(H/d)_{max}$ is 0.603 by Stokes' theory. There is a gap between this value and 0.653 for which the solitary wave theory would appear to be more applicable. However, waves have been observed breaking on Martha's Vineyard with values of $H/d = 0.588$. [15]

Because this present investigation must be limited, it was decided to use only Stokes' 3rd approximation. For the solitary wave and other theories the method of approach in determining forces and force centroids basically would

be the same, with the curve families of this thesis enlarged to include their particular ranges. Bretschneider [14] has developed graphs which appear to be a good starting point for determining the range of applicability of the several theories, as well as values of H, L, η_b and maximum crest velocity (U_{max}) for design waves. These values could serve as first trial inputs for the procedure to be presented here. For a conservative estimate of the force exerted by a breaking wave on a piling a value of 4 times the force as determined from Stokes' theory for a wave of the same height may be used. [16]

For reference purposes the applicable formulas from Stokes' 3rd approximation are included here in dimensionless form. [17] The reader is referred to the list of symbols at the beginning of this thesis and Figure I for use with these equations.

Let C = wave celerity, ft./sec.

$$J = 2\pi d/L \tag{1}$$

The vertical displacement of a particle from its mean position is given by (2)

$$\frac{y}{d} = \frac{1}{2d/H}\left\{\left[\frac{\sinh(J\,S/d)}{\sinh J}\right]\sin\theta - \left[\frac{3}{8}\,\frac{\pi}{L/H}\,\frac{\sinh(2J\,S/d)}{(\sinh J)^4}\right]\cos 2\theta\right\} \tag{2}$$

be the same, with the curve families of this thesis enlarged to include their particular ranges. Bretschneider [14] has developed graphs which appear to be a good starting point for determining the range of applicability of the several theories, as well as values of H, L, η_0 and maximum crest velocity (U_{max}) for design waves. These values could serve as first trial inputs for the procedure to be presented here. For a conservative estimate of the force exerted by a breaking wave on a piling a value of 4 times the force as determined from Stokes' theory for a wave of the same height may be used. [16]

For reference purposes the applicable formulas from Stokes' 3rd approximation are included here in dimensionless form. [17] The reader is referred to the list of symbols at the beginning of this thesis and Figure I for use with these equations.

Let C = wave celerity, ft./sec.

$$J = 2\pi d/L \tag{1}$$

The vertical displacement of a particle from its mean position is given by (2)

$$\frac{y}{d} = \frac{1}{2d/H}\left\{\left[\frac{\sinh(J\,S/d)}{\sinh J}\right]\sin\theta - \left[\frac{3}{8}\,\frac{\pi}{L/H}\,\frac{\sinh(2J\,S/d)}{(\sinh J)^4}\right]\cos 2\theta\right\} \tag{2}$$

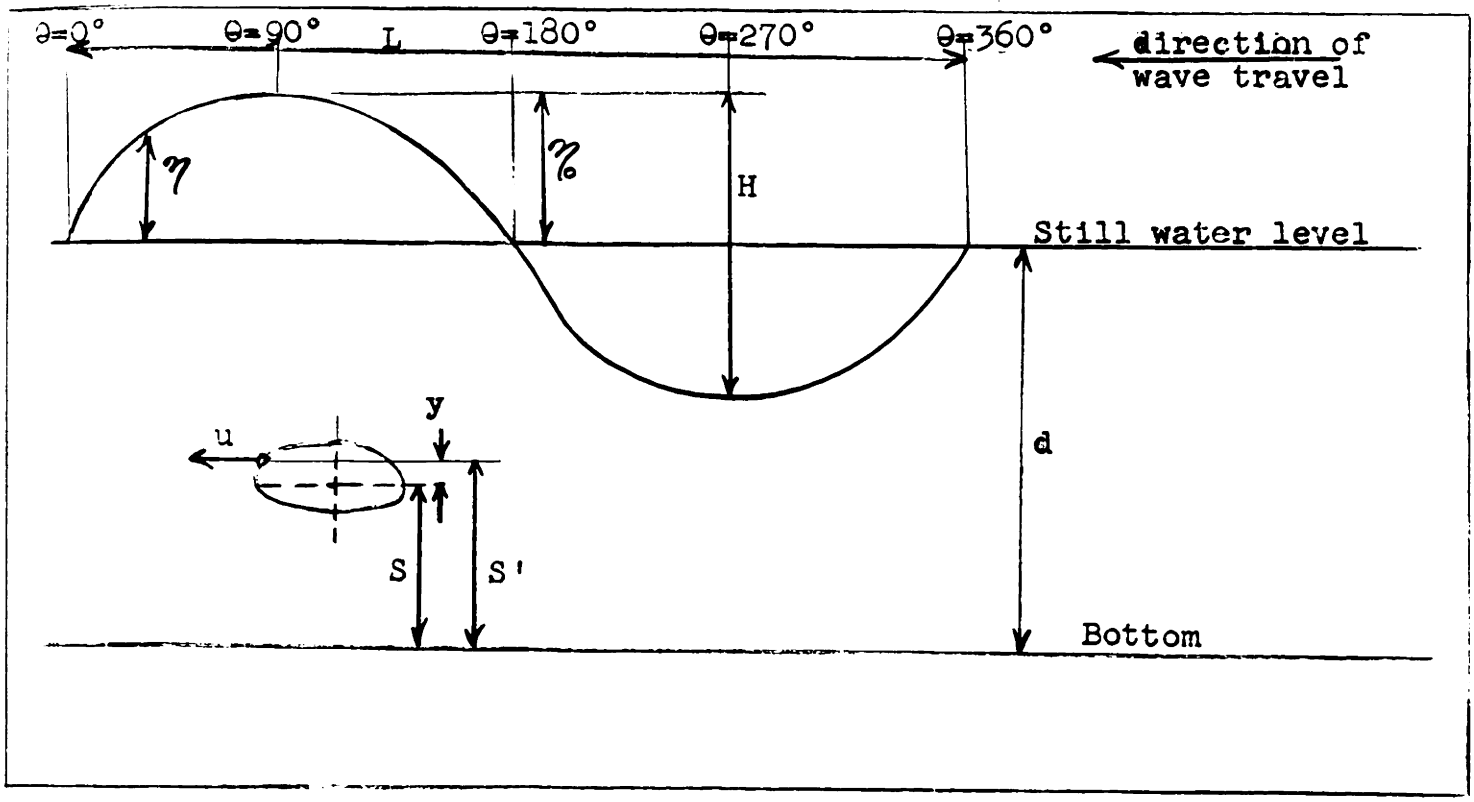

Figure I. Definition Sketch of a Wave

At the wave crest (2) becomes

$$\frac{y_{max}}{d} = \frac{1}{2\ d/H}\left\{\frac{\sinh(J\ S/d)}{\sinh J} + \frac{3}{8}\frac{\pi}{L/H}\ \frac{\sinh(2J\ S/d)}{(\sinh J)^4}\right\} \qquad (3)$$

and at the trough,

$$\frac{y_{trough}}{d} = \frac{1}{2\ d/H}\left\{\frac{-\sinh(J\ S/d)}{\sinh J} + \frac{3}{8}\frac{\pi}{L/H}\ \frac{\sinh(2J\ S/d)}{(\sinh J)^4}\right\} \qquad (4)$$

At the still water level (S/d = 1), (2) gives the wave profile

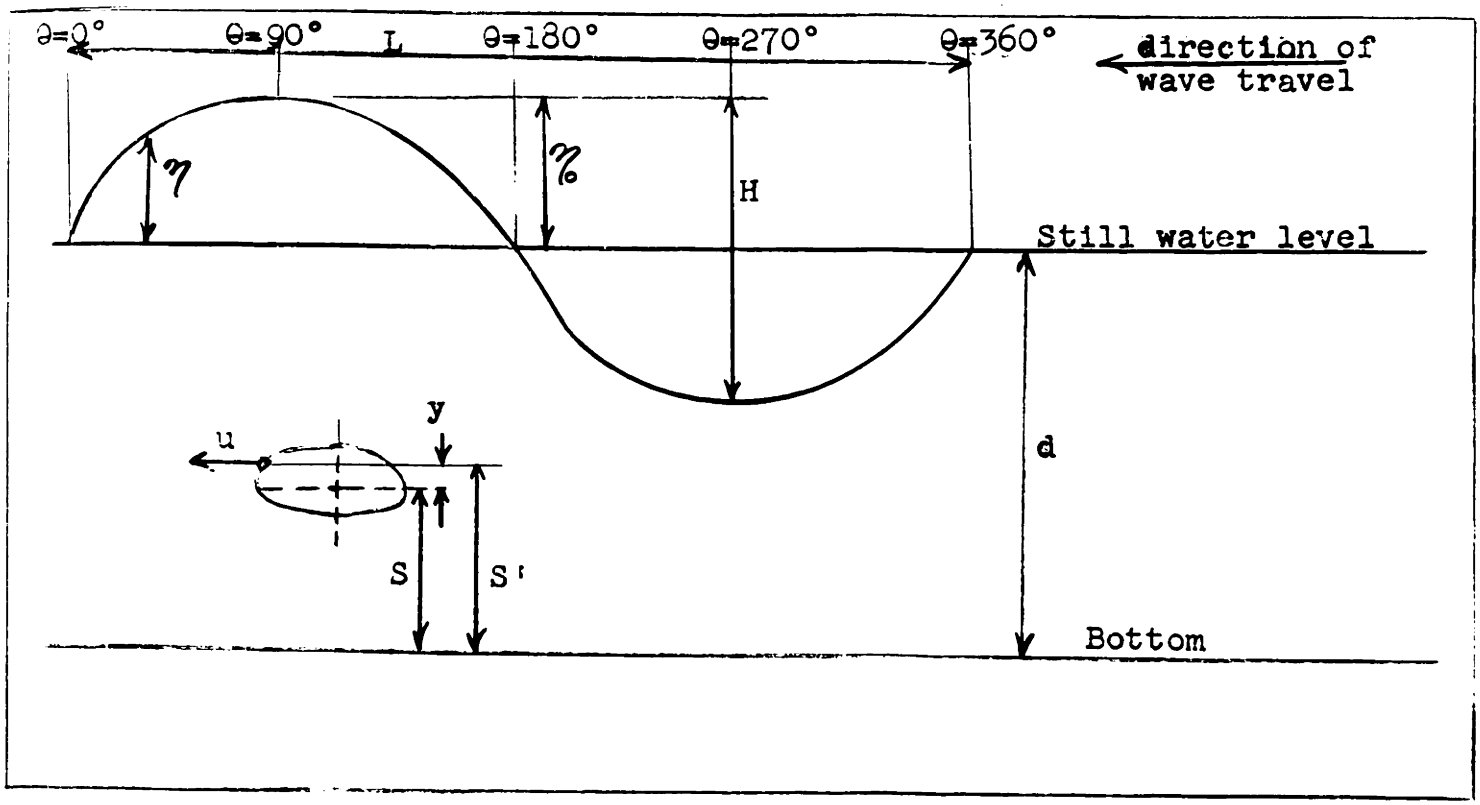

Figure I. Definition Sketch of a Wave

At the wave crest (2) becomes

$$\frac{y_{max}}{d} = \frac{1}{2\ d/H}\left\{\frac{\sinh(J\ S/d)}{\sinh J} + \frac{3}{8}\frac{\pi}{L/H}\ \frac{\sinh(2J\ S/d)}{(\sinh J)^4}\right\} \qquad (3)$$

and at the trough,

$$\frac{y_{trough}}{d} = \frac{1}{2\ d/H}\left\{\frac{-\sinh(J\ S/d)}{\sinh J} + \frac{3}{8}\frac{\pi}{L/H}\ \frac{\sinh(2J\ S/d)}{(\sinh J)^4}\right\} \qquad (4)$$

At the still water level (S/d = 1), (2) gives the wave profile

$$\frac{\eta}{d} = \frac{1}{2\,d/H}\left\{\sin\theta - \left[\frac{3}{8}\frac{\pi}{L/H}\,\frac{\sinh(2J)}{(\sinh J)^4}\cos 2\theta\right\}\right. \qquad (5)$$

From (5), with $\theta = 90°$ the height of the crest above the still water level is

$$\frac{\eta_0}{d} = \frac{1}{2\,d/H}\left\{1 + \frac{3}{8}\frac{\pi}{L/H}\,\frac{\sinh(2J)}{(\sinh J)^4}\right\} \qquad (6)$$

and for $\theta = 270°$ the distance to the trough is

$$\frac{\eta_0 - H}{d} = \frac{1}{2\,d/H}\left\{-1 + \frac{3}{8}\frac{\pi}{L/H}\,\frac{\sinh(2J)}{(\sinh J)^4}\right\} \qquad (7)$$

The wave celerity is

$$\frac{C}{\sqrt{gd}} = \sqrt{\frac{1}{J}\tanh J\left\{1 + \left(\frac{\pi}{L/H}\right)^2\left[\frac{2(\cosh 2J)^2 + 2\cosh 2J + 5}{8(\sinh J)^4}\right]\right\}} \qquad (8)$$

The particle velocity at any depth S/d is

$$\frac{u}{\sqrt{gd}} = \frac{\pi}{L/H}\cdot\frac{C}{\sqrt{gd}}\left\{\left[\frac{\cosh(J\,S/d)}{\sinh J}\right]\sin\theta - \left[\frac{\pi}{L/H}\cdot\frac{1}{(\sinh J)^2}\left(-\frac{1}{2}+\frac{3}{4}\,\frac{\cosh(2J\,S/d}{(\sinh J)^2}\right.\right.\right.$$

$$\left.\left.\left.\right)\right]\cos 2\theta + \frac{\pi}{L/H}\cdot\frac{1}{2}\left[\frac{\cosh(2J\,S/d)}{(\sinh J)^2}\right]\right\} \qquad (9)$$

At the wave crest (9) becomes

$$\frac{u_{max}}{\sqrt{gd}} = \frac{\pi}{L/H}\cdot\frac{C}{\sqrt{gd}}\left\{\frac{\cosh(J\,S/d)}{\sinh J} + \frac{\pi}{L/H}\cdot\frac{1}{(\sinh J)^2}\left(-\frac{1}{2}+\frac{3}{4}\,\frac{\cosh(2J\,S/d)}{(\sinh J)^2}\right)\right.$$

$$\left. + \frac{\pi}{L/H}\cdot\frac{1}{2}\left[\frac{\cosh(2J\,S/d)}{(\sinh J)^2}\right]\right\} \qquad (10)$$

At the wave trough (9) becomes

$$\frac{u_{trough}}{\sqrt{gd}} = \frac{\pi}{L/H}\cdot\frac{C}{\sqrt{gd}}\left\{-\frac{\cosh(J\,S/d)}{\sinh J} + \frac{\pi}{L/H}\cdot\frac{1}{(\sinh J)^2}\left(-\frac{1}{2}+\frac{3}{4}\,\frac{\cosh(2J\,S/d)}{(\sinh J)^2}\right)\right.$$

$$\left. + \frac{\pi}{L/H}\cdot\frac{1}{2}\left[\frac{\cosh(2J\,S/d)}{(\sinh J)^2}\right]\right\} \qquad (11)$$

Force Theory

Using Stokes' 3rd approximation for wave motions, D.R.F. Harleman and W.C. Shapiro of the Massachusetts Institute of Technology Hydrodynamics Laboratory have developed a force theory which shows good agreement with experiment. [17] In developing this theory they applied certain modifications to Morison's Force Theory for drag and the MacCamy-Fuchs Diffraction Theory for inertia forces. In this thesis the authors will utilize the approach as presented by Harleman and Shapiro. Families of curves will be developed from their equations, these curves to be used for the iterative design procedure mentioned previously.

As will be shown the only forces of interest are the maximum values of the drag and inertia components for both crest and trough regions.

F_D = maximum drag force in crest region

$(F_D)_t$ = maximum drag force in trough region

F_I = maximum inertia force in crest region

$(F_I)_t$ = maximum inertia force in trough region

D = cylinder diameter

$$F_D = \frac{\gamma D d^2 C_D A}{2} \tag{12}$$

$$(F_D)_t = \frac{-\gamma D d^2 C_{D\,trough} B}{2} \tag{13}$$

where

$$A \equiv \int_0^{1+\eta_o/d} \frac{u^2_{max}}{gd} \cdot d(S'/d) \tag{14}$$

$$B \equiv \int_0^{1+\frac{\eta_o - H}{d}} \frac{u^2_{trough}}{gd} \cdot d(S'/d) \tag{15}$$

and S' is the vertical distance to the actual particle position and is therefore equal to the mean particle position S plus or minus the vertical displacement y.

For the crest $S' = S + y_{max}$ (16)

and for the trough $S' = S - y_{trough}$ (17)

It can be seen that (14) and (15) do not lend themselves to regular integration, but must be solved graphically or by some other means. The steady state drag coefficients C_D and $C_{D\ trough}$ to be used in (12) and (13), respectively, are determined as functions of Reynolds numbers, defined as follows:

$$R = \frac{\sqrt{\overline{u^2}_{max}}}{\nu} D = \frac{D}{\nu}\sqrt{\frac{g\,d\,A}{1+\eta_o/d}} \tag{18}$$

$$R_{trough} = \frac{\sqrt{\overline{u^2}_{trough}}}{\nu} D = \frac{D}{\nu}\sqrt{\frac{g\,d\,B}{1+\left(\frac{\eta_o - H}{d}\right)}} \tag{19}$$

where $\sqrt{\overline{u^2}_{max}}$ and $\sqrt{\overline{u^2}_{trough}}$ are the root mean squares of the velocity distributions for the crest and trough, respectively.

$$\sqrt{\overline{u^2}_{max}} = \sqrt{\frac{A\,g\,d^2}{d+\eta_o}} \tag{20}$$

$$\sqrt{\overline{u^2}_{trough}} = \sqrt{\frac{B\,g\,d^2}{d+(\eta_o - H)}} \tag{21}$$

In (18) and (19), A and B are determined from (14) and (15), respectively, and η_o/d, $\frac{\eta_o - H}{d}$ from (6) and (7),

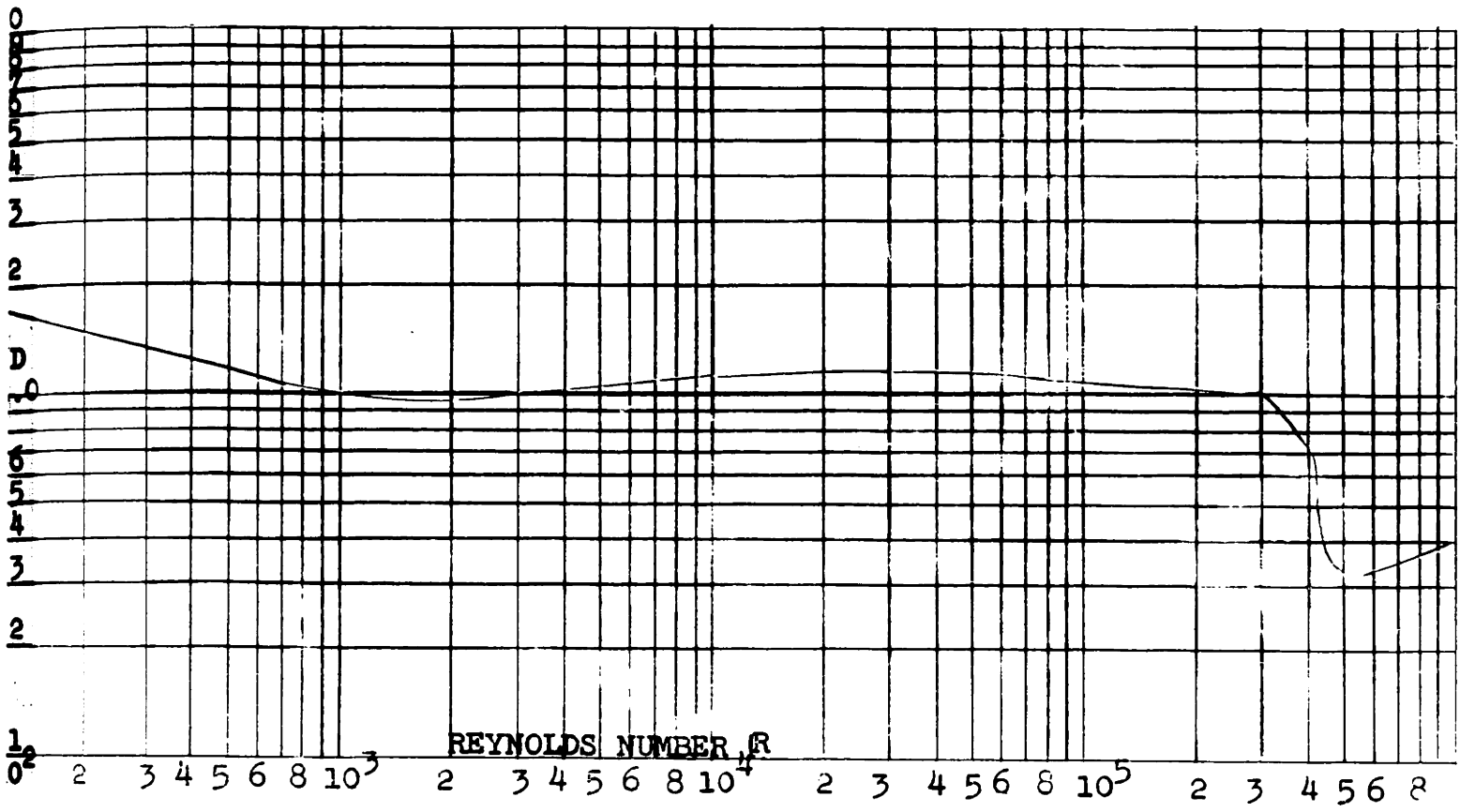

Figure II. Steady state drag coefficient versus Reynolds number for circular cylinders, [17, 18].

respectively. Figure II is a plot of steady state C_D vs. R for circular cylinders.

$$F_I = \frac{\gamma \pi D^2 H}{4 \cosh J} \sinh I \cos \theta \qquad (22)$$

$$(F_I)_t = \frac{\gamma \pi D^2 H}{4 \cosh J} \sinh I \cos \theta \qquad (23)$$

where $I = J + \frac{\pi}{L/H} \sin \theta$ (24)

and θ is that angle of wave position ($0° \leq \theta < 180°$ for (22), and $180° \leq \theta < 360°$ for (23)) such that F_I and $(F_I)_t$ are maximized, respectively. Because θ will be very nearly equal to 0° and 180° for these situations, it can be seen from (24) that little error (and great simplification) is introduced by letting $\theta = 0°$ and 180° in (22) and (23), respectively.

This gives $$F_I = -(F_I)_t = \frac{\gamma \pi D^2 H}{4} \tanh J \qquad (25)$$

Let $\bar{S}'$ = center of action of the force F_D and

$(\bar{S}')_t$ = center of action of the force $(F_D)t$

Then $$\frac{\bar{S}'}{d} = \frac{\int_0^{1+\eta_o/d} S'/d \; \frac{u_{max}^2}{gd} \, d(S'/d)}{A} \qquad (26)$$

$$\frac{(\bar{S}')_t}{d} = \frac{\int_0^{1+\frac{\eta_o - H}{d}} S'/d \; \frac{u_{trough}^2}{gd} \, d(S'/d)}{B} \qquad (27)$$

$\bar{S}_I$ = center of action of force F_I

$$\bar{S}_I = \frac{\gamma D^2 LH}{8 F_I \cosh J} \left[1 + J \sinh J - \cosh J \right] \qquad (28)$$

Harleman and Shapiro have shown that $\overline{S}'$ can be assumed constant for $0^{\circ} \leq \theta \leq 180^{\circ}$, and $(\overline{S}')_t$ can be assumed constant for $180^{\circ} \leq \theta \leq 360^{\circ}$ with little loss in accuracy. Also, with the assumption that $\overline{S}_I$ is equal for crest and trough by (28), it is reasonable to assume that it is constant for any value of θ.

By use of (5,7,10,11,14,15,26,27) values of A and B for (12,13,18,19) and $\frac{\overline{S}'}{d}$ and $\frac{(\overline{S}')t}{d}$ for (26) and (27) were computed for families of the parameters H/L and d/L on an IBM 7090 digital computer.

The results are plotted in Figures III, IV, and V in dimensionless form. Values of H/d equal to 0.603, which was mentioned as the approximate limit of applicability of Stokes' theory, and 0.653, which is the maximum value this parameter may obtain (page 8), are also shown in these figures. These values indicate the boundary for use of the figures, as well as the boundary up to which the solitary wave theory could be used to extend the range of applicability. The computer program, representative output, and comments are included as Appendix D. In addition to A, B, $\frac{\overline{S}'}{d}$, and $(\frac{\overline{S}'}{d})_t$, the following are given as outputs:

$$\frac{\eta_o}{d}$$

$$\frac{H-\eta_o}{d}$$

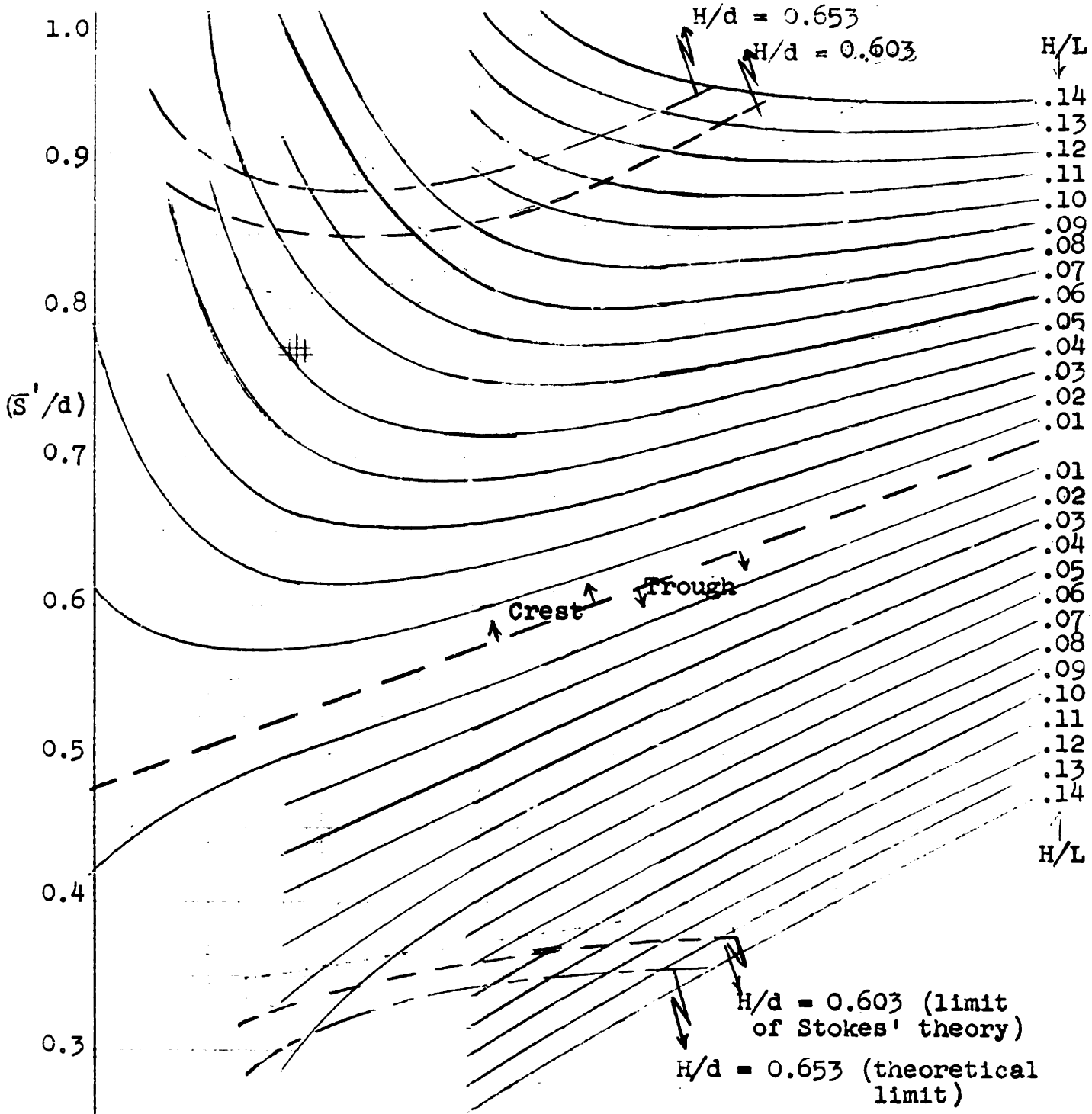

Figure III

Drag Force Centroids for Wave Height/Wave Length (H/L) and Water Depth/Wave Length (d/L) Ratios.

$(\bar{S}'/d)$ = centroid/depth ratio for crest

$(\bar{S}'_{trough}/d)$ = centroid/depth ratio for trough

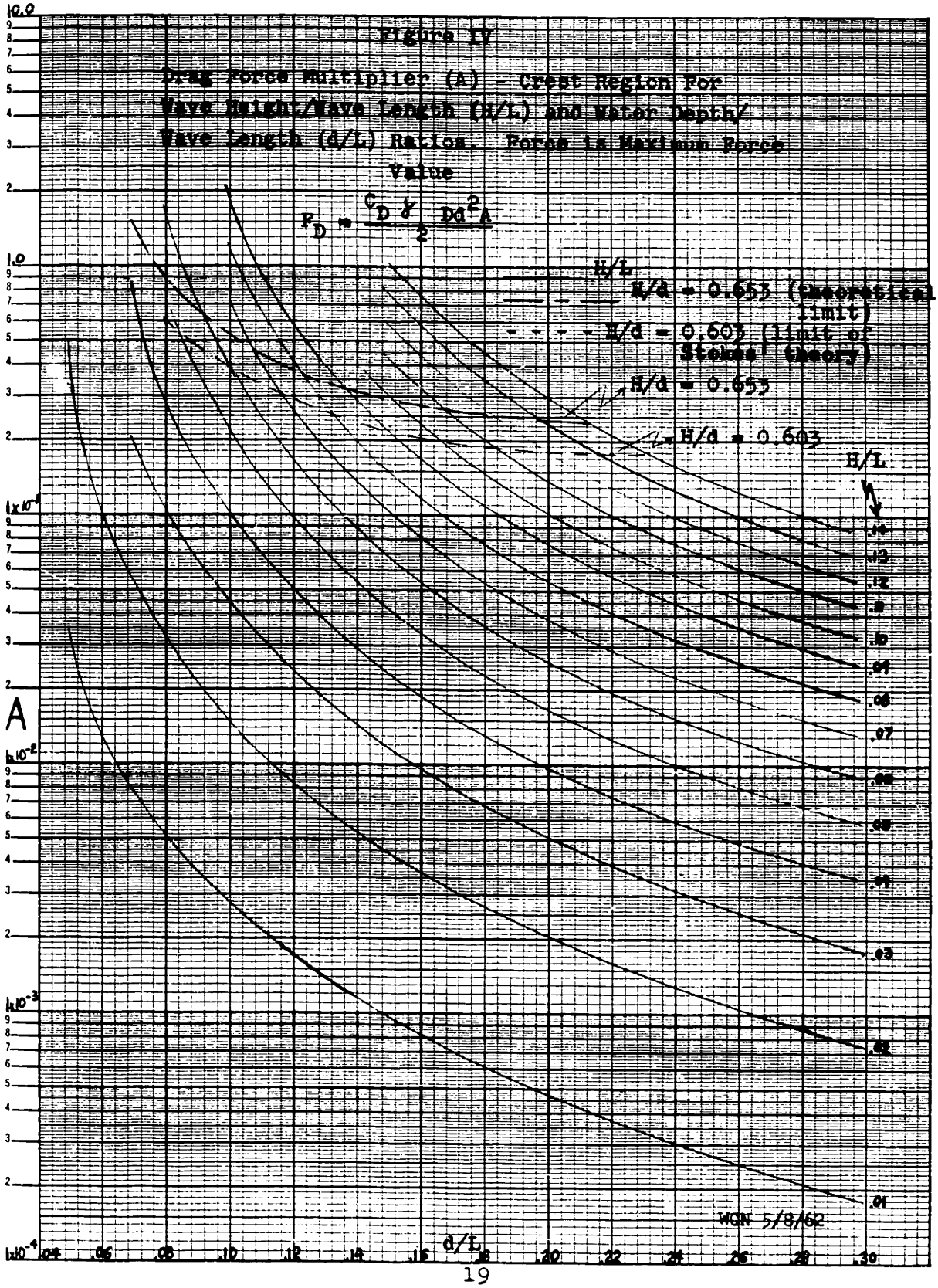
Figure IV
Drag Force Multiplier (A) - Crest Region For Wave Height/Wave Length (H/L) and Water Depth/Wave Length (d/L) Ratios. Force is Maximum Force Value
$F_D = \frac{C_D \gamma}{2} D d^2 A$
H/L
H/d = 0.653 (theoretical limit)
H/d = 0.603 (limit of Stokes' theory)
H/d = 0.653
H/d = 0.603
H/L
A
d/L
WQN 5/8/62

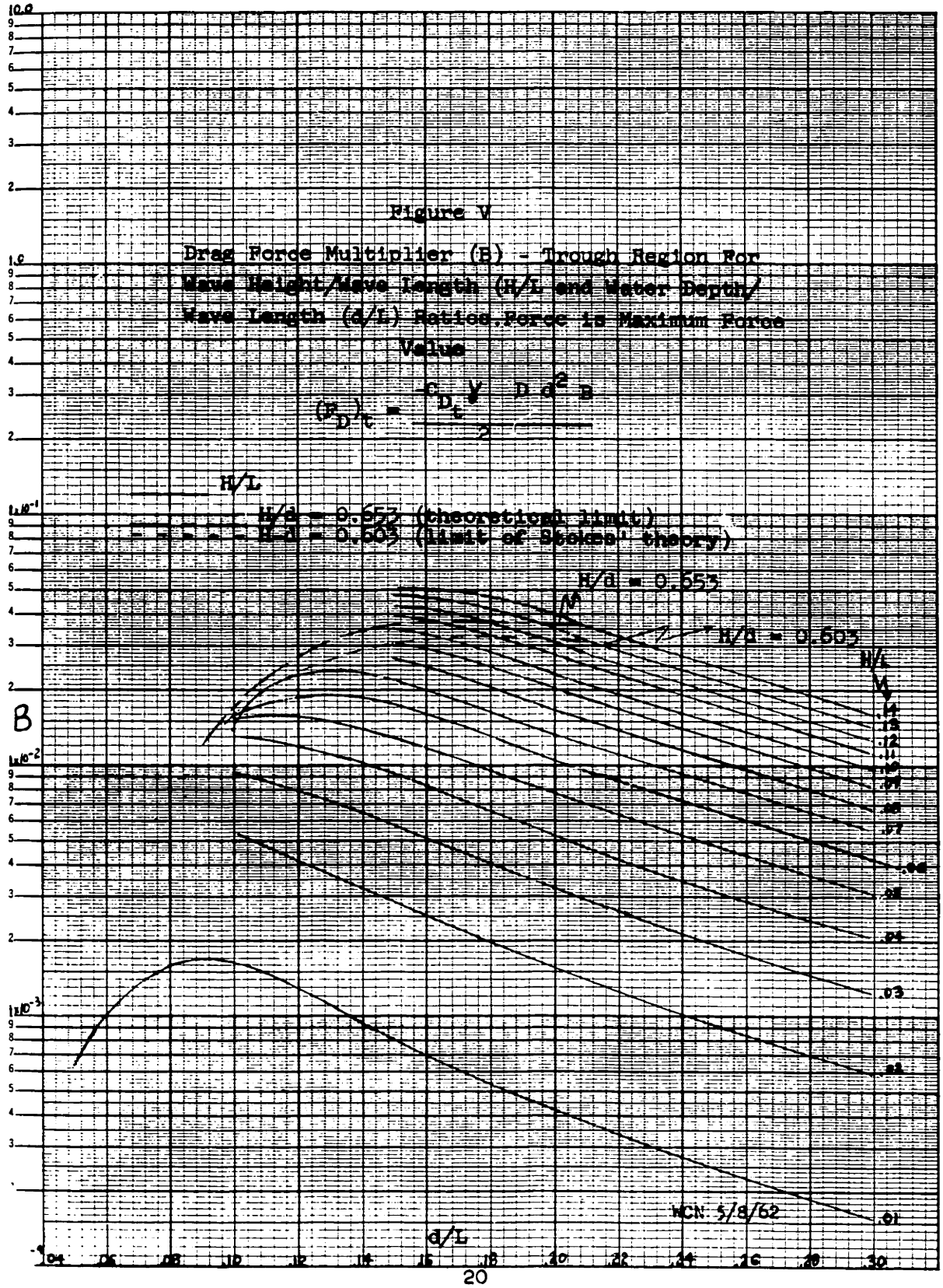
Figure V
Drag Force Multiplier (B) - Trough Region For Wave Height/Wave Length (H/L and Water Depth/ Wave Length (d/L) Ratios. Force is Maximum Force Value
$(F_D)_t = \frac{C_{D_t} \gamma D d^2 B}{2}$
H/L
H/d = 0.553 (theoretical limit)
H/d = 0.503 (limit of Stokes' theory)
H/d = 0.553
H/d = 0.503
B
d/L
HCN 5/8/62

$$\frac{u_{max}}{\sqrt{gd}} \text{ at surface} = \frac{U_{max}}{\sqrt{gd}}$$

$$\frac{u_{trough}}{\sqrt{gd}} \text{ at surface} = \frac{U_{trough}}{\sqrt{gd}}$$

Velocity profiles are also given for $\frac{u_{max}}{\sqrt{gd}}$, $\frac{u_{max}^2}{gd}$, $\frac{u_{trough}}{\sqrt{gd}}$ and $\frac{u_{trough}^2}{gd}$ vs. $\frac{S'}{d}$.

Design Force Procedure

It has been shown [17] that drag force is a function of $\sin^2\theta$, while, for the assumption that F_I occurs at $\theta = 0°, 180°$, inertia force is a function of $\cos\theta$. The forcing functions for use in the differential equations of platform displacements will therefore be of the following form:

$$0° \leq \theta \leq 180° \qquad F = F_D \sin^2\theta + F_I \cos\theta \qquad (29)$$

$$180° \leq \theta \leq 360° \qquad F = (F_D)_t \sin^2\theta + F_I \cos\theta \qquad (30)$$

For convenience the formulas and procedures used in the determination of these forces and their points of application are summarized below.

$$F_D = \frac{\gamma D d^2 C_D A}{2} \qquad (12)$$

$$(F_D)_t = \frac{-\gamma D d^2 C_{D \text{ trough}} B}{2} \qquad (13)$$

$$F_I = \frac{\gamma \pi D^2 H}{4} \tanh J \qquad (25)$$

C_D from Figure II for $R = \frac{D}{\nu}\sqrt{\frac{g d A}{1 + \eta_o/d}}$ (18)

$C_{D \text{ trough}}$ from Figure II for $R = \frac{D}{\nu}\sqrt{\frac{g d B}{1 + (\frac{\eta_o - H}{d})}}$ (19)

A from Figure IV

B from Figure V

$$\frac{\eta_o}{d} = \frac{1}{2\, d/H}\left\{1 + \frac{3}{8}\frac{\pi}{L/H}\frac{\sinh (2J)}{(\sinh J)^4}\right\} \qquad (6)$$

or from computer output (not plotted)

$$\frac{\eta_o - H}{d} = \frac{\eta_o}{d} - \frac{H}{d} \qquad (31)$$

$\frac{\bar{S}'}{d}$ and $\frac{(\bar{S}')t}{d}$ from Figure III

$$\bar{S}_I = \frac{\gamma D^2 LH}{8 F_I \cosh J}\left[1 + J \sinh J - \cosh J\right] \qquad (28)$$

2. Vibrations

General

Once the wave forces on the legs have been determined the next problem is to calculate the resulting displacement of the platform as a function of time, or wave position Θ with respect to the front (upstream) legs of the structure.

This thesis considers only the longitudinal displacement x of the platform, taken as positive in the direction of wave propagation. It has been observed that the transverse vibrations in the experimental runs were relatively negligible, with an amplitude of perhaps three percent of that of the longitudinal vibrations: For the dimensions of real structures the transverse vibrations may be as important as the longitudinal vibrations.

This thesis does not consider wind force and its effect on platform displacement. Certainly with large waves there will also be high wind, and the wind-caused displacement must be added to that induced by the waves. In a steady wind the problem is one of statics, not vibrations, unless vortex shedding is important. A useful discussion of wind loads is given in [4] . Water currents can be treated in the same way.

The structure considered has a square platform of weight W, supported on four (N=4) legs of length ℓ and diameter D, arranged in a square configuration of leg spacing h on a side. The case of no leg bracing is considered first, after which the case of added bracing is considered.

The investigation is limited to the case of the waves impinging normal to one face of a square configuration of legs. Once the reader understands the concept of this procedure he should be able to manipulate the procedure to fit any practical leg configuration and a limited number of angles of wave impingement. When the direction of wave propagation is not parallel to an axis of symmetry of the braced leg configuration, the calculations become complicated by the facts that generally the platform translation is not in the direction of the applied force and that rotation of the platform may become significant.

The legs of the thesis model are fixed at the base. This condition was assumed for the Argus Island structure [19]. In the case of Texas Tower No. 4 the footings beneath each leg were 25 feet in diameter filled with cement, and sunk or embedded into the ocean floor to a depth of 18 feet. After the collapse divers reported that the footings were apparently in good condition with-

out any evidence of fracture, movement, or scour [20] . The opinion was that the footings were not cocked out of a perpendicular plane with the ocean floor [21] . In other words, the assumption of fixed footings was valid for Texas Tower No. 4.

The legs of the thesis model are fixed at the platform. This assumption was made in the design of Texas Tower No. 4. Later investigation [2] indicated that the actual restraint condition was closer to being pin-ended than fixed.

As a practical matter in the consideration of vibrations, it should be pointed out that large quantities of surging oil or water in tanks may amplify tower motion. This problem generally can be reduced by installing several small tanks in lieu of one large tank and by installing internal baffling in the tanks.

Reference [20] on the collapse of Texas Tower No. 4 provides much useful and interesting food-for-thought for the designer of fixed offshore structures.

The reader interested in experiments with models should realize that it is not possible to scale model results to fit the prototype. The problem is that drag and inertia components of the wave force do not scale in the same manner. Consequently the reader should center his interest in the concept of this thesis, and

not on the numerical results for any particular run.

Classical Vibration Theory

The approach considered will be to fit the vibration problem of the structure to the classical theory for a linear, single-degree-of-freedom system. There are many sources in the literature where one may find this theory. The authors have chosen to follow the notation of Den Hartog [22].

From Newton's Law one can arrive at the following differential equation of forces:

$$m\ddot{x} + C\dot{x} + kx = P_o \sin \omega t \qquad (32)$$

where
- x = displacement, a function of time
- $\dot{x} = dx/dt$ = velocity
- $\ddot{x} = d^2x/dt^2$ = acceleration
- m = mass with single degree of freedom
- C = damping coefficient
- k = spring constant
- P_o = magnitude of applied force
- ω = circular frequency of applied force
- t = time

The steady state solution to (32) can be written as:

$$x = x_o \sin(\omega t - \phi) \qquad (33)$$

where x_o and ϕ are as yet unknown, and:

x_o = displacement amplitude

ϕ = phase angle by which x lags $P_o \sin \omega t$

Insert (33) into (32) to obtain:

$$x_o = \frac{P_o}{\sqrt{(C\omega)^2 + (k - m\omega^2)^2}} \qquad (34)$$

$$\phi = \text{arc tan} \frac{C\omega}{k - m\omega^2} \qquad (35)$$

From consideration of free vibration without damping one can find that the undamped natural frequency ω_n is:

$$\omega_n = \sqrt{\frac{k}{m}} \qquad (36)$$

From consideration of free vibration with damping one can define critical damping C_c as:

$$C_c = 2\sqrt{mk} = 2m\omega_n \qquad (37)$$

For values of damping C less than C_c the free vibration is truly oscillatory. For values of C greater than C_c the free "vibration" is not oscillatory, but rather the mass creeps back exponentially to its equilibrium position from an initial displacement.

Insert (36) and (37) into (34) and (35) to obtain:

$$\frac{x_o}{x_{STATIC}} = \frac{1}{\sqrt{\left[1-\left(\frac{\omega}{\omega_n}\right)^2\right]^2 + \left[2\frac{C}{C_c}\cdot\frac{\omega}{\omega_n}\right]^2}} \tag{38}$$

$$\text{where } x_{STATIC} = \frac{P_o}{k} \tag{39}$$

$$\phi = \text{arc tan } \frac{2\frac{C}{C_c}\cdot\frac{\omega}{\omega_n}}{1-\left(\frac{\omega}{\omega_n}\right)^2} \tag{40}$$

It will prove useful to have numerical tables for expressions (38) and (40) for entering arguments of $\frac{\omega}{\omega_n}$ and small values of C/C_c. Table I is presented for values of $\frac{x_o}{x_{STATIC}}$. Table II is presented for values of ϕ.

Unbraced Structure

Mass m must represent the mass of the platform and a certain portion of the mass of the legs. By applying Rayleigh's Energy Method to this case (Appendix A) it is possible to compute:

$$m = \frac{1}{g}\left(W + \frac{13}{35}Nw\ell\right) \tag{41}$$

TABLE I - MAGNIFICATION FACTORS (38)

ω/ω_n \ c/c_c	0	0.01	0.02	0.03	0.04	0.05	0.06	0.07	0.08
0	1.00	1.00	1.00	1.00	1.00	1.00	1.00	1.00	1.00
0.25	1.07	1.07	1.07	1.07	1.07	1.07	1.07	1.07	1.07
0.50	1.33	1.33	1.33	1.33	1.33	1.33	1.33	1.33	1.33
0.70	1.96	1.96	1.96	1.96	1.95	1.94	1.94	1.93	1.92
0.80	2.78	2.78	2.77	2.76	2.74	2.72	2.68	2.65	2.62
0.85	3.60	3.59	3.58	3.55	3.50	3.45	3.39	3.31	3.24
0.90	5.26	5.24	5.19	5.06	4.92	4.76	4.58	4.39	4.20
0.95	10.21	10.03	9.54	8.85	8.09	7.35	6.69	6.07	5.54
1.00	∞	50	25	16.7	12.5	10.0	8.33	7.14	6.25
1.05	9.81	9.61	9.09	8.35	7.59	6.84	6.18	5.60	5.09
1.10	4.76	4.74	4.66	4.55	4.40	4.22	4.04	3.84	3.66
1.15	3.10	3.09	3.07	3.04	2.98	2.92	2.84	2.77	2.69
1.20	2.27	2.27	2.26	2.24	2.22	2.19	2.16	2.12	2.08
1.30	1.45	1.45	1.45	1.44	1.43	1.43	1.42	1.40	1.39
1.50	0.80	0.80	0.80	0.80	0.80	0.80	0.79	0.79	0.79
1.75	0.48	0.48	0.48	0.48	0.48	0.48	0.48	0.48	0.48
2.00	0.33	0.33	0.33	0.33	0.33	0.33	0.33	0.33	0.33
3.00	0.12	0.12	0.12	0.12	0.12	0.12	0.12	0.12	0.12
5.00	0.04	0.04	0.04	0.04	0.04	0.04	0.04	0.04	0.04

TABLE II - PHASE ANGLES (degrees) (40)

0	0	0	0	0	0	0	0	0	0
0.25	0	0	1	1	1	2	2	2	2
0.50	0	1	2	2	3	4	5	5	6
0.70	0	2	3	5	6	8	9	11	12
0.80	0	3	5	8	10	12	15	17	20
0.85	0	4	7	10	14	17	20	23	26
0.90	0	5	11	16	21	25	30	34	37
0.95	0	11	21	30	38	44	49	54	57
1.00	0/0	90	90	90	90	90	90	90	90
1.05	180	168	158	148	140	134	129	125	121
1.10	180	174	168	162	157	152	148	144	140
1.15	180	176	172	168	164	160	157	153	150
1.20	180	177	174	171	168	165	162	159	156
1.30	180	178	176	174	171	169	167	165	163
1.50	180	179	177	176	174	173	172	170	169
1.75	180	179	178	177	176	175	174	173	172
2.00	180	179	178	178	177	176	175	175	174
3.00	180	180	179	179	178	178	177	177	177
5.00	180	180	180	179	179	179	179	178	178

where g = gravitational constant, normally 32.2 ft/sec.^{2}
w = weight/unit length of leg
N = number of legs

If the configuration had been such that the legs were considered to be pinned to the platform the fraction to be used in the second term of (41) would be 33/140 (Appendix A).

It is shown in Appendix A that the added mass effect (of accelerated water mass) is negligible in still water. For forced vibrations there is the further consideration that the water particles are moving with wave orbital velocities. For this latter situation it is simply assumed that added mass is negligible. Later in the experimental results (Appendix G) it will be seen that this assumption is valid.

For damping C it is necessary to resort to experiment to determine values of $\frac{C}{C_c}$ for the plastic model of this thesis. The damping consists of structural damping in the plastic and viscous damping by the water. Again from Den Hartog [22] for the case of free vibrations with viscous damping one finds that the logarithmic decrement δ fits the following relationships:

$$\delta \equiv \log_e \frac{x_1}{x_2} \qquad (42)$$

where x_1 and x_2 are two successive positive (or negative) decaying displacement amplitudes.

$$\delta = \frac{2\pi}{\sqrt{1 - \left(\frac{C}{C_c}\right)^2}} \cdot \frac{C}{C_c} \tag{43}$$

For values of C/C_c up to 8%, and somewhat larger, the following approximation is "exact" within sliderule accuracy:

$$\frac{C}{C_c} \approx \frac{1}{2\pi}\delta \tag{44}$$

With this expression one can calculate values of structural damping by observing free vibrations in air, assuming that the air causes negligible damping.

For completeness at this time it is noted that:

$$\omega_n = \frac{q}{\sqrt{1 - \left(\frac{C}{C_c}\right)^2}} \tag{45}$$

where q = damped natural frequency

With this expression one can calculate experimental values of ω_n.

It is shown in Appendix A that in still water for these particular experiments the theoretical viscous

damping is 11% maximum of the structural damping. In the steady state vibrations there is the further consideration that the velocity associated with viscous damping is not $\dot{x}$ but is the velocity relative to the water particles, which are moving with wave orbital velocities. For these reasons viscous damping by the water is neglected. The experimental results (Appendix F) support this action.

In Appendix A the following expression is derived for spring constant k:

$$k = \frac{12NEI}{\ell^3} \tag{46}$$

where E = Young's modulus

and I = moment of inertia associated with bending of one leg

Actually k must be determined experimentally for the plastic model of this thesis because a unique value of E cannot be obtained from a handbook for the plastic.

From (36,41,46):

$$\omega_n = \frac{12gNEI}{\ell^3 (W + \frac{13}{35} N w \ell)} \tag{47}$$

The forcing function in (32) is $P_o \sin \omega t$. The expression for the wave force is not this simple, but if it can be represented by a series of terms of the form $P_o \sin \omega t$ one can find an equal number of terms for x, each with its own phase angle. By superposition of these terms one can calculate the platform displacement x.

The forces acting on each leg are equal in magnitude. The forces on the front legs are in phase (because of the direction of wave impingement on the structure). The forces on the rear legs are likewise in phase with each other, but they lag the forces on the front legs by a lag angle ϕ_{RL}, which one can deduce to be:

$$\phi_{RL} = \frac{360\ h}{L} \text{ degrees} = \frac{2\pi h}{L} \text{ radians} \qquad (48)$$

For the drag force acting on one leg it has been stated (29,30) that in the range $0° \leq \theta \leq 180°$ the force can be expressed as $F_D \sin^2 \omega t$. At $\theta = 90°$ the line of action of this force is at a height $\bar{s}'$ above the bottom. For $180° \leq \theta \leq 360°$ the drag force is $(F_D)_{trough} \sin^2 \omega t$, which acts at a height $(\bar{s}')_t$. The inertia force acting on one leg can be expressed as $F_I \cos \omega t$, acting at a height $\bar{s}_I$ when $\theta = 0°, 180°$.

Only a fraction of these forces can be considered to act directly on the platform. Let P_o represent the force required at the level of the platform to produce the same static deflection as force P acting at height a on a leg of length ℓ. An influence fraction P_o/P has been computed in Appendix A, with the numerical results given in Figure VI.

It has been stated earlier that F_D can be considered to act at $\bar{s}'$ throughout the range $0° \leq \theta \leq 180°$. This means that in this range:

$$\frac{a}{\ell} = \frac{\bar{s}'}{\ell} \tag{49}$$

Use Figure VI, and write

$$F_1 = F_D \cdot \frac{P_o}{P} \tag{50}$$

With similar reasoning:

$$\frac{a_t}{\ell} = \frac{(\bar{s}')t}{\ell} \tag{51}$$

$$F_2 = -(F_D)_t \cdot \frac{P_o}{P_t} \tag{52}$$

(F_2 is a positive number.)

FIGURE VI - INFLUENCE FRACTION $\frac{P_o}{P}$

Fraction $\frac{P_o}{P}$ of Force P to be Considered Acting On Platform When P Acts at Height a on an Unbraced Leg of Length ℓ.

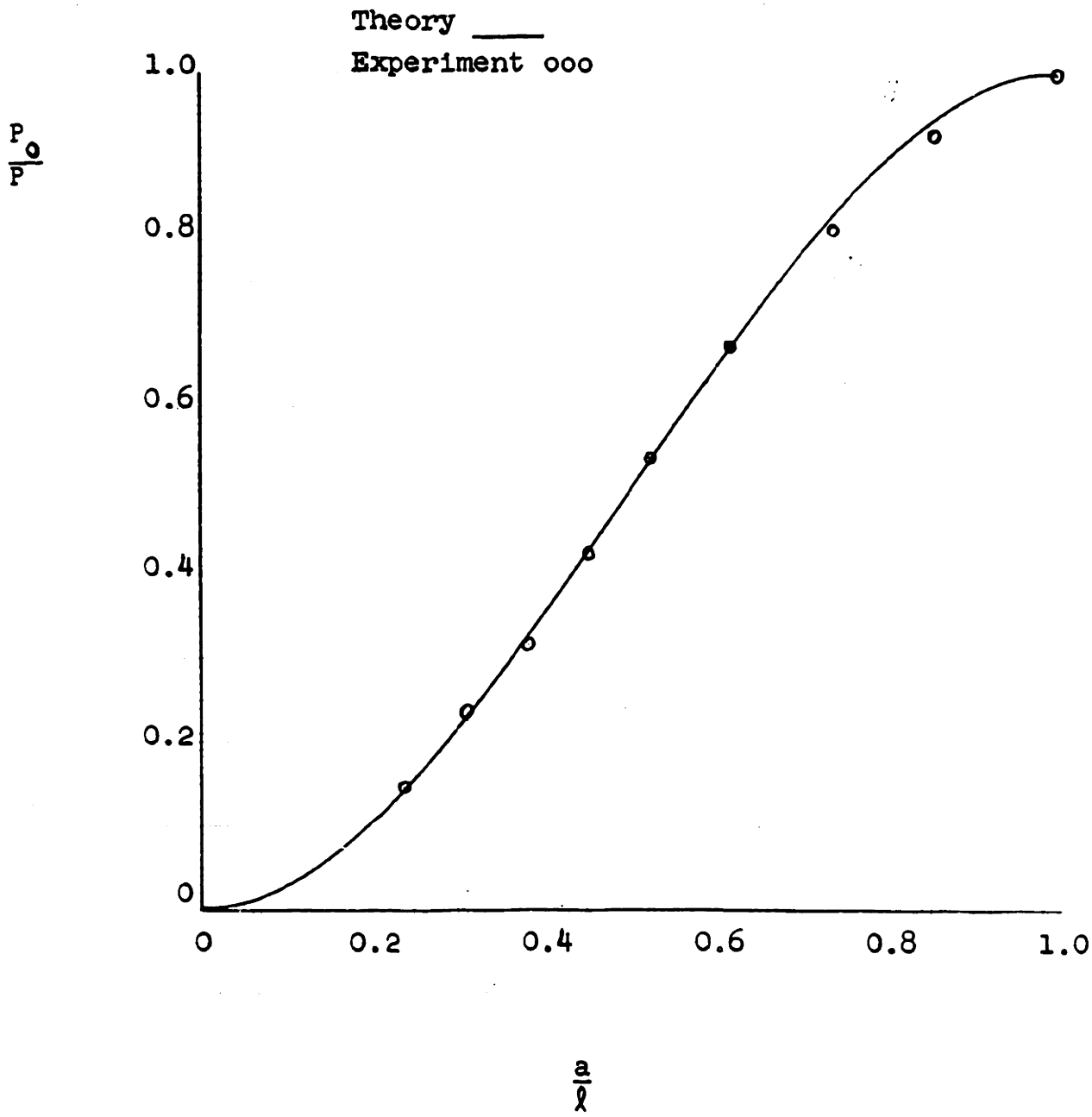

VCH 4/13/62

$$\frac{a_I}{\ell} = \frac{\bar{s}_I}{\ell} \tag{53}$$

$$F_3 = F_I \cdot \frac{P_o}{P_I} \tag{54}$$

Now one can write expressions for the force acting on the platform due to the force acting on one front leg.

$$\text{force} = F_1 \sin^2 \omega t + F_3 \cos \omega t \quad (0° \leq \omega t \leq 180°) \tag{55}$$

$$\text{force} = -F_2 \sin^2 \omega t + F_3 \cos \omega t \quad (180° \leq \omega t \leq 360°) \tag{56}$$

A Fourier series is calculated in Appendix A to represent this force. For the cases considered in this thesis only five terms are significant. The following expression results:

$$F(t) = \frac{F_1 - F_2}{4} + \frac{4}{3\pi}(F_1 + F_2) \sin \omega t$$

$$- \frac{4}{15\pi}(F_1 + F_2) \sin 3\omega t + F_3 \cos \omega t$$

$$- \frac{(F_1 - F_2)}{4} \cos 2\omega t \tag{57}$$

The angle ϕ_{RL} has been defined (48) for a harmonic force varying as ωt. One can deduce that if the force

varies as $n\omega t$ the appropriate lag angle is $n\phi_{RL}$.

$$\text{lag angle} = n\phi_{RL} \tag{58}$$

At this point all of the necessary theory is available for computing displacement x as a function of θ at the front legs. One has simply to set up a convenient method for a hand numerical calculation. Fortunately a simple tabular method can be found. For purposes of illustration it seems best to show this method in conjunction with a sample calculation. The reader is therefore referred to Appendix B.

The numerical calculation can also be performed on a digital computer. Such a program was used in the preparation of the Results, Section III. The program is given in Appendix D.

Braced Structure

The solution to the problem for a braced structure may be approached by applying rough modifications to the solution for the unbraced structure.

For mass m it was found previously (41) by Rayleigh's Energy Method that 13/35 of the mass of the legs should be added to the mass of the platform.

Assume that the same ratio holds for the bracing and legs of the braced structure. Define the ratio r_m as:

$$r_m = \frac{\text{mass of legs + mass of bracing}}{\text{mass of legs}} \tag{59}$$

The assumption is:

$$m = \frac{1}{g}(W + \frac{13}{35} r_m N w \ell) \tag{60}$$

From (36,46,60):

$$\omega_n = \sqrt{\frac{12gNEI}{\ell^3(W + \frac{13}{35} r_m N w \ell)}} \tag{61}$$

In the design of the Argus Island structure the fraction $\frac{1}{2}$ was used in lieu of $\frac{13}{35}$. [23] It appears that this fraction was assumed, not derived.

Damping for the plastic model must be determined experimentally, as before (44).

> "In most metal structures, nearly all the damping observed can be attributed to the technique of fabrication. For example, a good weld can be distinguished from a poor one by its effect on the part's ringing after impact: the poorer the joint, the more damping. Riveted joints generally contribute more damping than welded ones, and bolted joints more than riveted ones." *

* Hamme, R.N., [24, p. 37-2]

"Bare steel structures, particularly welded rather than riveted, have very low damping ranging from perhaps 1.0 to 3.0 per cent of critical damping." *

If a designer is in doubt as to what damping exists in his structure he will generally be well advised to assume the smallest reasonable value in order to be on the "safe side."

Stiffness k remains as expressed in (46) for the thesis model because no bracing was added in planes where it would have stiffened the structure for resistance to longitudinal forces. If such bracing had been added, experimental displacements would not have been large enough to be observable.

For a normal braced structure one must compute appropriate values for stiffness k and influence fraction $\frac{P_o}{P}$. A good textbook on this matter is [25]. Probably two values of $\frac{P_o}{P}$ will be sufficient to fair a curve, because the curve will be very similar in shape to that of Figure VI.

The case of Texas Tower No. 4 provides an interesting lesson in engineering with regard to stiffness furnished by the bracing. On this tower the bracing consisted of pin connected tension members. It was concluded [2] that the underwater bracing was essentially ineffective

* Housner, G.W., [24, p. 50-20]

for platform excursions up to ± 3 inches because of the large clearances in the pin connections. The lesson is that joints should be welded, which is the method usually used.

It is seen in (12,13) that drag force varies directly with leg diameter D. It is seen in (25) that inertia force varies directly as D^2. For each of these forces the line of action is independent of D. Assume that if bracing existed whose long dimension was parallel to the direction of wave propagation the wave forces on this bracing would be negligible compared to the forces on the bracing whose long dimension was parallel to the wave crests. Let ℓ_B be the cumulative length of all of the hydrodynamically significant underwater bracing (below the still water level), of diameter D_B. For simplicity assume that the wave forces on a length d(d = water depth) of bracing are the same as if the bracing were uniformly distributed in one additional leg of diameter D_B. These assumptions lead to the following relationships for forces acting on the braced structure:

$$(F_D)_B = r_D \cdot F_D,\ (F_1)_B = r_D \cdot F_1,\ (F_2)_B = r_D \cdot F_2 \qquad (62)$$

where

$$r_D = 1 + \frac{\ell_B}{Nd}\left(\frac{D_B}{D}\right) \qquad (63)$$

for platform excursions up to ± 3 inches because of the large clearances in the pin connections. The lesson is that joints should be welded, which is the method usually used.

It is seen in (12,13) that drag force varies directly with leg diameter D. It is seen in (25) that inertia force varies directly as D^2. For each of these forces the line of action is independent of D. Assume that if bracing existed whose long dimension was parallel to the direction of wave propagation the wave forces on this bracing would be negligible compared to the forces on the bracing whose long dimension was parallel to the wave crests. Let ℓ_B be the cumulative length of all of the hydrodynamically significant underwater bracing (below the still water level), of diameter D_B. For simplicity assume that the wave forces on a length d(d = water depth) of bracing are the same as if the bracing were uniformly distributed in one additional leg of diameter D_B. These assumptions lead to the following relationships for forces acting on the braced structure:

$$(F_D)_B = r_D \cdot F_D,\ (F_1)_B = r_D \cdot F_1,\ (F_2)_B = r_D \cdot F_2 \qquad (62)$$

where

$$r_D = 1 + \frac{\ell_B}{Nd}\left(\frac{D_B}{D}\right) \qquad (63)$$

$$(F_I)_B = r_I \cdot F_I, \quad (F_3)_B = r_I \cdot F_3 \tag{64}$$

where $$r_I = 1 + \frac{\ell_B}{Nd}\left(\frac{D_B}{D}\right)^2 \tag{65}$$

With these modified values for the forces to be used in (57) one can make a hand calculation for displacement x as in Appendix B, or a computer calculation as in Appendix D.

Vibration Stresses

Up to this point no mention has been made of stresses. It should be obvious that if platform displacement is greater for the dynamic situation than for the static situation the attendant vibration stresses throughout the structure will also be greater by the same ratio. (Deflections are "small," and the stress-strain relationship is linear elastic.)

The maximum dynamic displacement has been obtained from the plots of x vs θ that resulted from carrying out the foregoing procedure. As a result of the calculation for stiffness k there is available a moment (and force) distribution (which is simply related to a stress distribution by simple beam theory). The stress distribution is for a selected force, which

results in a calculated platform displacement. This static displacement is the denominator of the sought-for ratio. All values in the static stress distribution are multiplied by this ratio to arrive at the vibration stress distribution.

In addition to the vibration stresses one must also take into account static stresses due to such causes as wind forces, current forces, column loads, thermal effects, fabrication, etc. These stresses can be superposed to arrive at the total stress at any point.

B. Experimental Procedure

The experimental work of this thesis was carried out in the Wave Tank of the Hydrodynamics Laboratory of Massachusetts Institute of Technology in March 1962.

The primary objective of the experiments was to measure platform displacement of a model of a fixed offshore structure under the influence of a regular train of waves. Thirty-two runs were made. In addition, runs were made to measure the longitudinal and transverse wave forces on a single vertical cylinder. More will be said later about the various runs and the data that was collected.

Most of the equipment used, with the exception of the models, was in existence prior to these particular experiments and has been described in detail in several references [17,26,27,28].

Wave Tank and Wave Generator

Figure VII is a photograph of the wave tank, which is 90 feet long, 2½ feet wide, and 3 feet deep. Basically it is a steel structure, but the walls and 40 feet of the bottom are plate glass.

At the near end of the tank there is a hinged plate wave generator, hinged to the tank bottom. A rod connects the upper end of the plate to an eccentric point on a rotating wheel. Wave height is governed by adjusting the eccentricity. Wave period is governed by adjusting the speed of rotation of the wheel. The speed can be determined by a photocell arrangement wired to an electronic counter.

At the far end of the tank there is a 35 foot long beach arrangement, whose purpose is to absorb energy and prevent (or reduce) undesirable wave reflections. For these experiments, however, it was decided to avoid wave reflection altogether by starting the wave generator for each run and recording data before the reflected wave

Figure VII - Photograph of Wave Tank

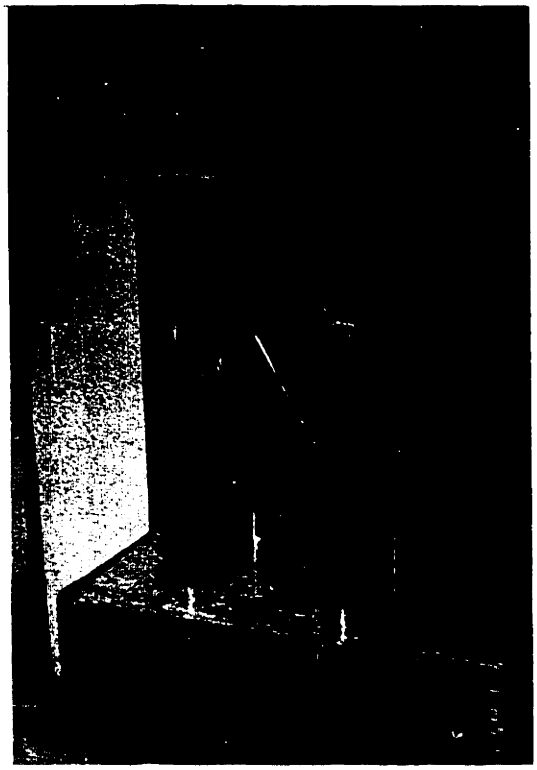

Figure VIII - Photograph of Braced Structure Model

had time to return to the model. After some trial and error with the waves to be used it was decided that data would be recorded between the passing of the eighth and ninth wave crests at the test stand for all runs.

Test Stand

The test stand is seen in Figure VII. It is located approximately 40 feet downstream from the wave generator. It consists of a triangular frame of steel angles supported by three legs of 3-inch pipe straddling the tank. The stand is guyed to the floor by steel cables to increase its rigidity. A steel angle was added to connect the stand to the laboratory wall to improve transverse rigidity, with a consequent improvement in the rigidity previously supplied by the cables.

Models

Figure VIII is a photograph of the model of a braced structure. It was fabricated of plexiglas by Forest Products, Inc., of Cambridge, Mass.

The legs are $\frac{1}{2}$ inch (actually 0.505 inch average) rod 42 inches long, with 16 inches on a side between leg centers. The leg diameter was decided upon as a

compromise between the requirments for a large diameter for adequate experimental forces and for a small diameter for adequate flexibility in order to observe deflection. The bracing is $\frac{1}{4}$ inch rod, with horizontal members located 14 and 28 inches above the base. The platform is 5/8 inch thick (actually 0.610 inch average) by 18-1/16 inches square. A 3/8 inch bolt in the center of the platform serves as a pointer for displacement measurements and holds the weights (to be discussed later). The base of the model is $\frac{1}{2}$ inch thick by 30-1/8 inches by 22 inches, with beveled leading and trailing edges. The model also was used in the unbraced condition.

Single Cylinders

In order to measure longitudinal and transverse wave forces two different aluminum cylinders were used. They were attached to the portal gage by a flange arrangement, as seen in the photograph of Figure IX. The $\frac{1}{2}$ inch cylinder cleared the tank bottom by 1/8 inch. The 1 inch cylinder cleared the tank bottom by 12-5/8 inches.

Figure IX - Photograph of Single Cylinder in Position for Measuring Transverse Forces

Movie Equipment

A 16 mm Bell and Howell movie camera was used to record platform motion and time, as seen in the photographs of Figures X and XI. Camera speeds of 24 and 48 frames/second were used.

Recorder

A four-channel direct writing model 150 Sanborn recorder was used to record wave profiles and force traces. A paper speed of 25 mm/sec was found to be most satisfactory. Time marks could be made in the paper margin upon signal from a manual push-button.

Wave Profile Measurement

Wave profiles were measured by a resistance wave gage, which can be seen in Figures IX and X. The gage consists of two platinum wires (0.008 inch diameter) insulated from each other and oriented vertically with a spacing between them of $\frac{1}{4}$ inch. When the wires are partially immersed in water an alternating current flows which is essentially directly proportional to the depth of immersion. The current

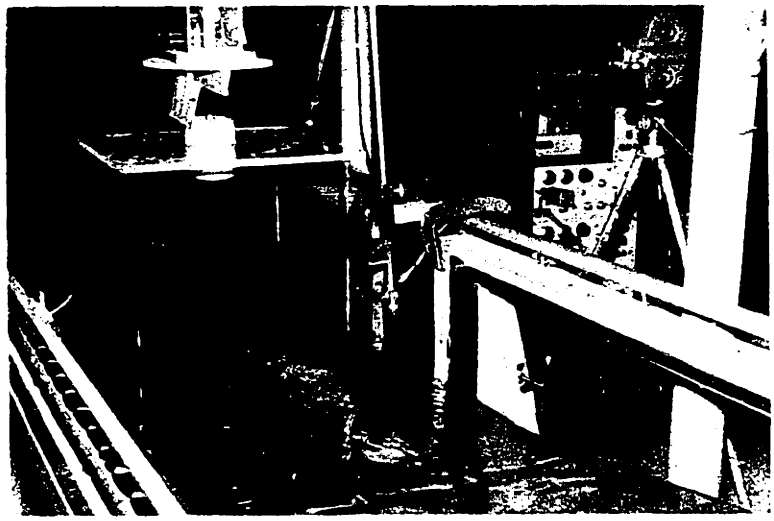

Figure X - Photograph of Braced Structure Model in Position for Measuring Displacement

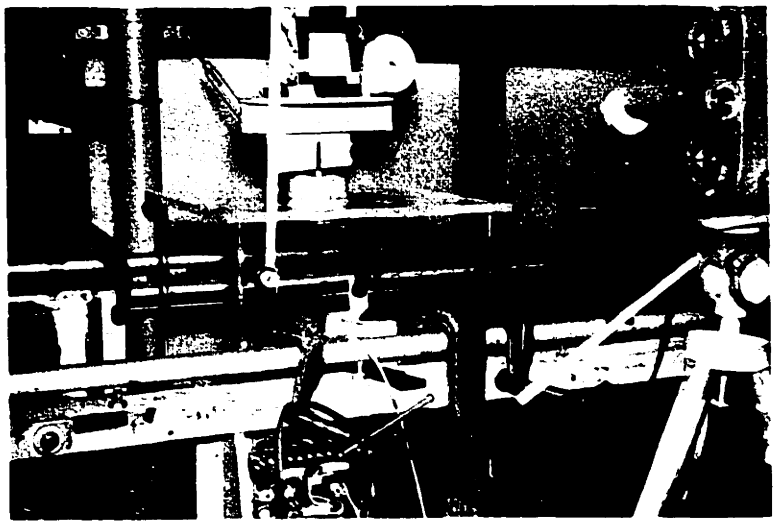

Figure XI - Photograph Showing Scheme for Recording Platform Displacement

produces a signal which is amplified and recorded by the Sanborn recorder.

The gage can be raised and lowered by a graduated rack and pinion arrangement. It is calibrated statically by raising and lowering it through known distances in still water.

Two gages are used to determine wave length. The gages are raised until their probes are immersed about $\frac{1}{4}$ inch in the wave crest. The distance between the gages is adjusted by trial and error to one wave length, at which time two crest marks will be made simultaneously on the Sanborn recorder.

Force Measurement

Horizontal forces were measured by a portal gage, seen in Figure IX directly above the cylinder flange and oriented in this case to measure transverse forces. The gage measures horizontal force in terms of shear deflection. Its design is such as to make the output essentially independent of the distance to the point of application of the force, or bending moment. A Schaevitz linear variable differential transformer is used to convert the shear deflection of the bottom plate of the gage into an electrical signal, which is amplified and recorded by the Sanborn recorder.

[illegible]

[illegible] recorder

[illegible]rce Measurement

[illegible]orizontal [illegible]rces are measured [illegible]

[illegible]. [illegible]en in Figure X [illegible]

[illegible] oriented [illegible]

[illegible]rces. [illegible] are measured [illegible]

[illegible] deflection. [illegible]

[illegible] essentially [illegible]

[illegible]

The force gage can be calibrated in the positive and negative directions by the use of weights suspended on a string which is run over a pulley. Two pulleys are seen in position on the sides of the tank in Figure IX.

Model Runs

Water depth was maintained at 27 inches throughout the experiments.

Four different waves were used, with the characteristics as listed in Table III.

TABLE III

Experimental Wave Characteristics

Wave	H(feet)	L(feet)	d/L	H/L
A	0.240	15.23	0.148	0.0158
B	0.313	10.86	0.207	0.0289
C	0.361	8.82	0.255	0.0409
D	0.404	7.33	0.307	0.0552

The model was used in two configurations, unbraced and braced. For each configuration and wave combination four structural natural frequencies were in-

vestigated by adding weights to the platform. The weights used were 0,3,6, and 10 pounds.

A total of 32 model runs was made. For each run platform displacement and time were recorded by the movie camera, and wave profile was recorded by the Sanborn recorder. A time mark was made on the recorder paper at a known time as read on the clock that appeared in the movie.

Single Cylinder Runs

Single cylinder runs were made for each wave on a $\frac{1}{2}$ inch cylinder to measure longitudinal and transverse forces. Runs were made for each wave on a 1 inch cylinder to obtain additional data on transverse forces.

For each run wave profile and force trace were recorded.

Miscellaneous Measurements

Movies were taken of the free oscillations of the unbraced and braced structures in air and in water for all combinations of the four added weights. Displacement and time were recorded for three cycles.

An experimental value of spring constant k was determined.

Experimental values of the influence fraction $\frac{P_o}{P}$ (Figure VI) were determined as a function of $\frac{a}{\ell}$.

The weight of the plastic in the model was recorded.

Water temperature was recorded.

III. RESULTS

Figure XII presents the theoretical and experimental results for platform longitudinal displacement x.

The terminology "Run AO" indicates a run with wave A and O lb. of added weight on the platform of the unbraced model. The letter "Z" specifies the braced model.

Experimental wave characteristics are given in Table III.

Values of structural damping $\frac{C}{C_c}$ used in the calculations are given in Table X.

Figure XIIa - Platform Displacements for Wave A

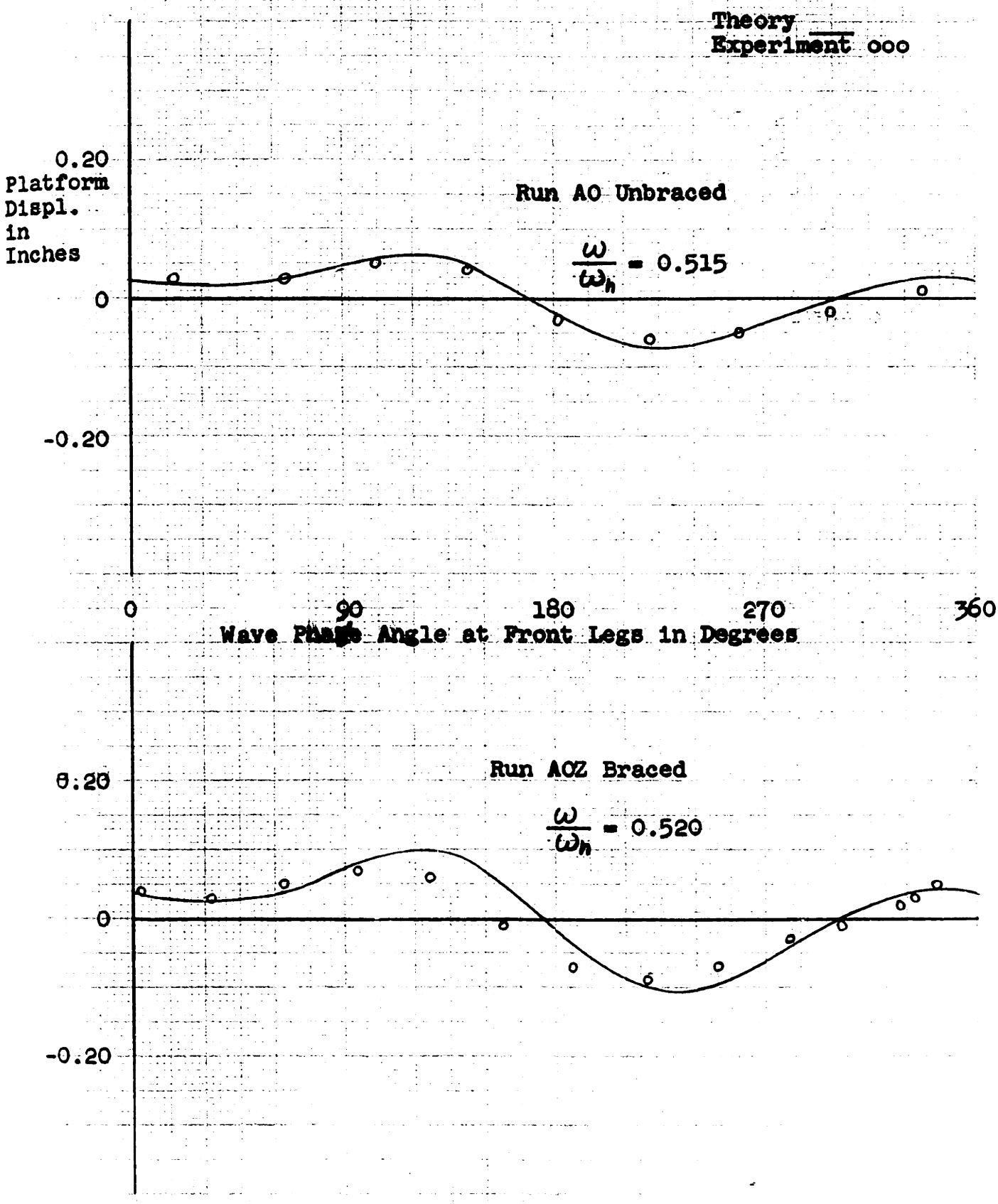

VCH 4/19/62

Figure XIIb - Platform Displacements for Wave A

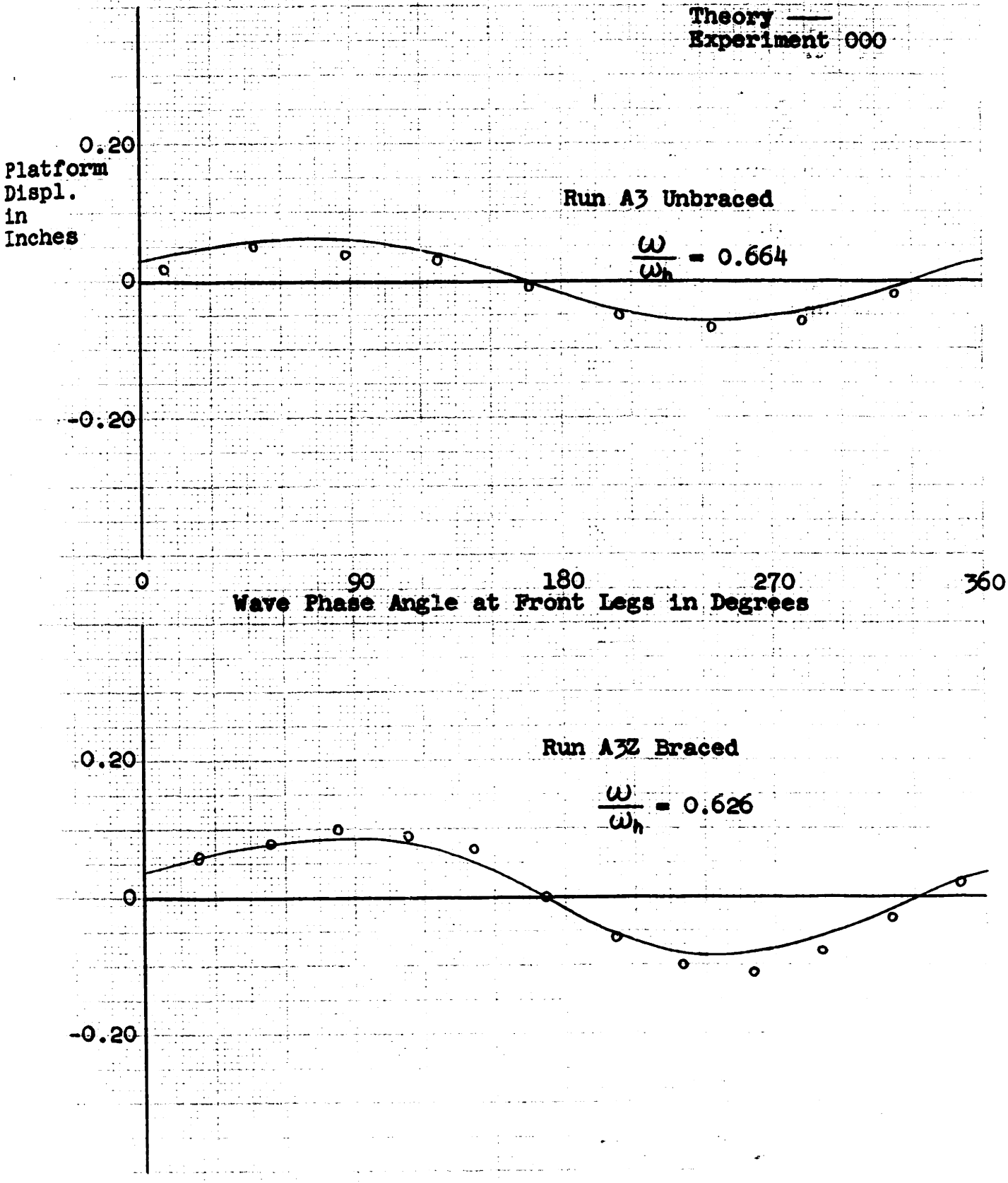

VCH 4/19/62

Figure XIIc - Platform Displacements for Wave A

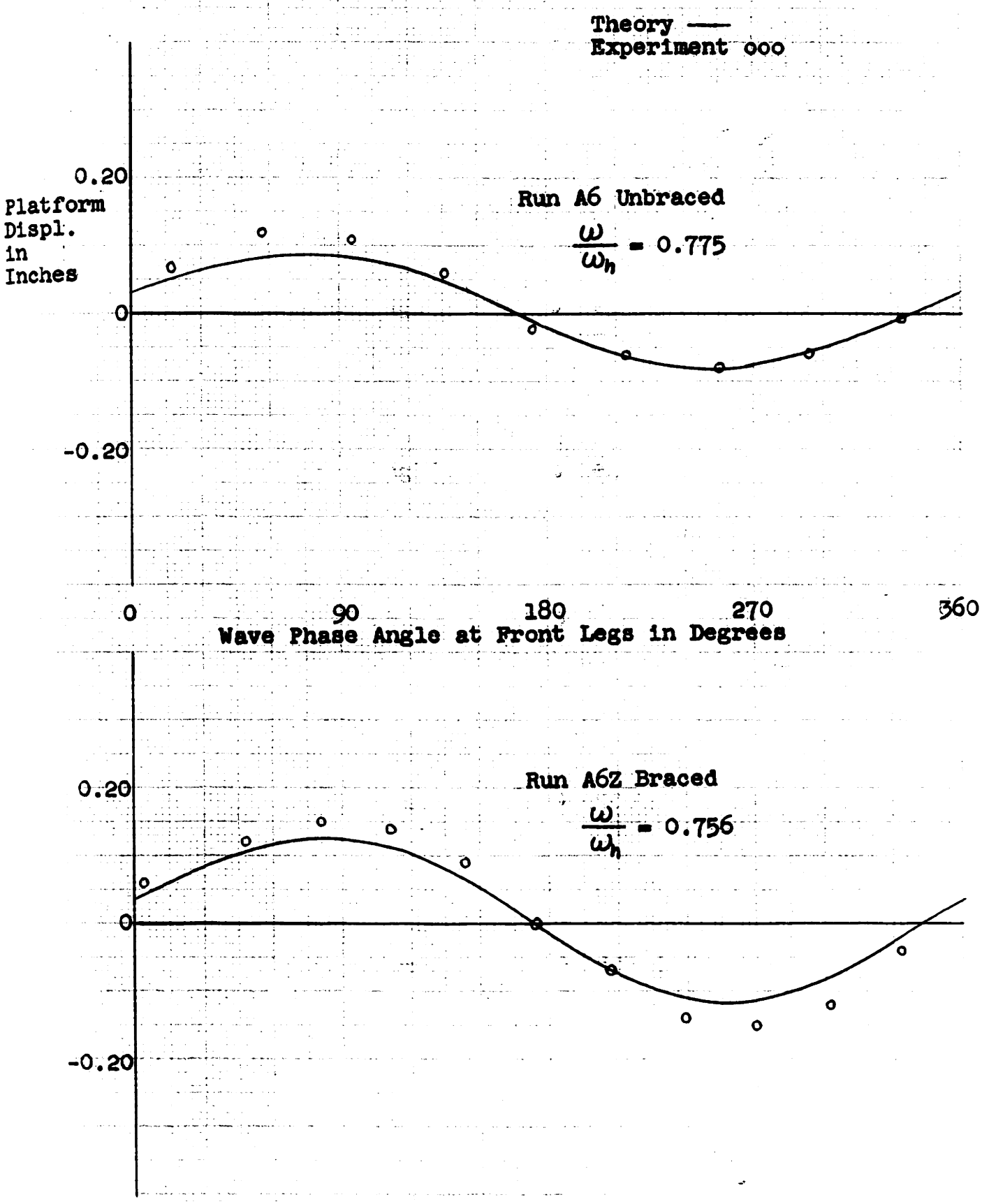

VCH 4/19/62

Figure XIId - Platform Displacements for Wave A

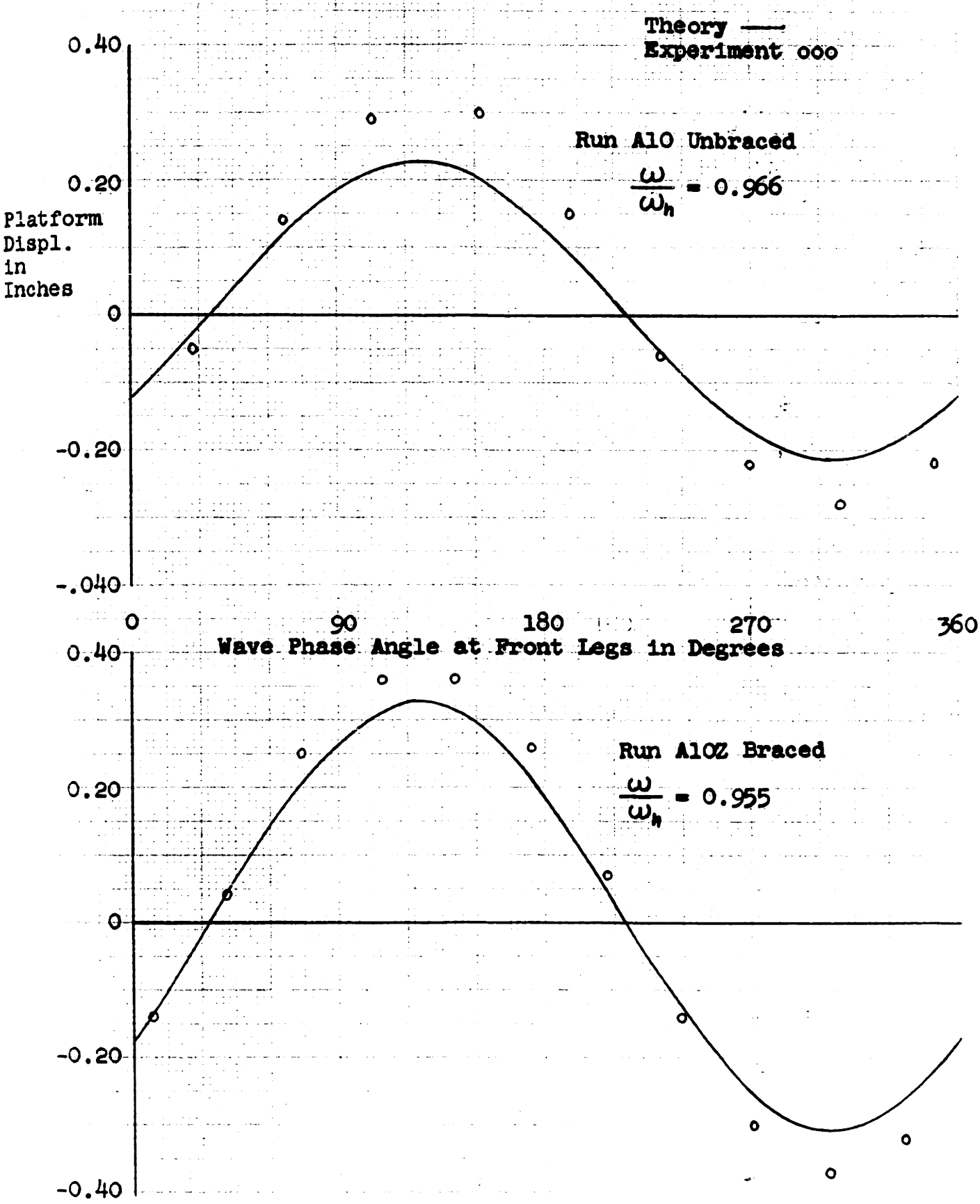

VCH 4/19/62

Figure XIIe - Platform Displacements for Wave B

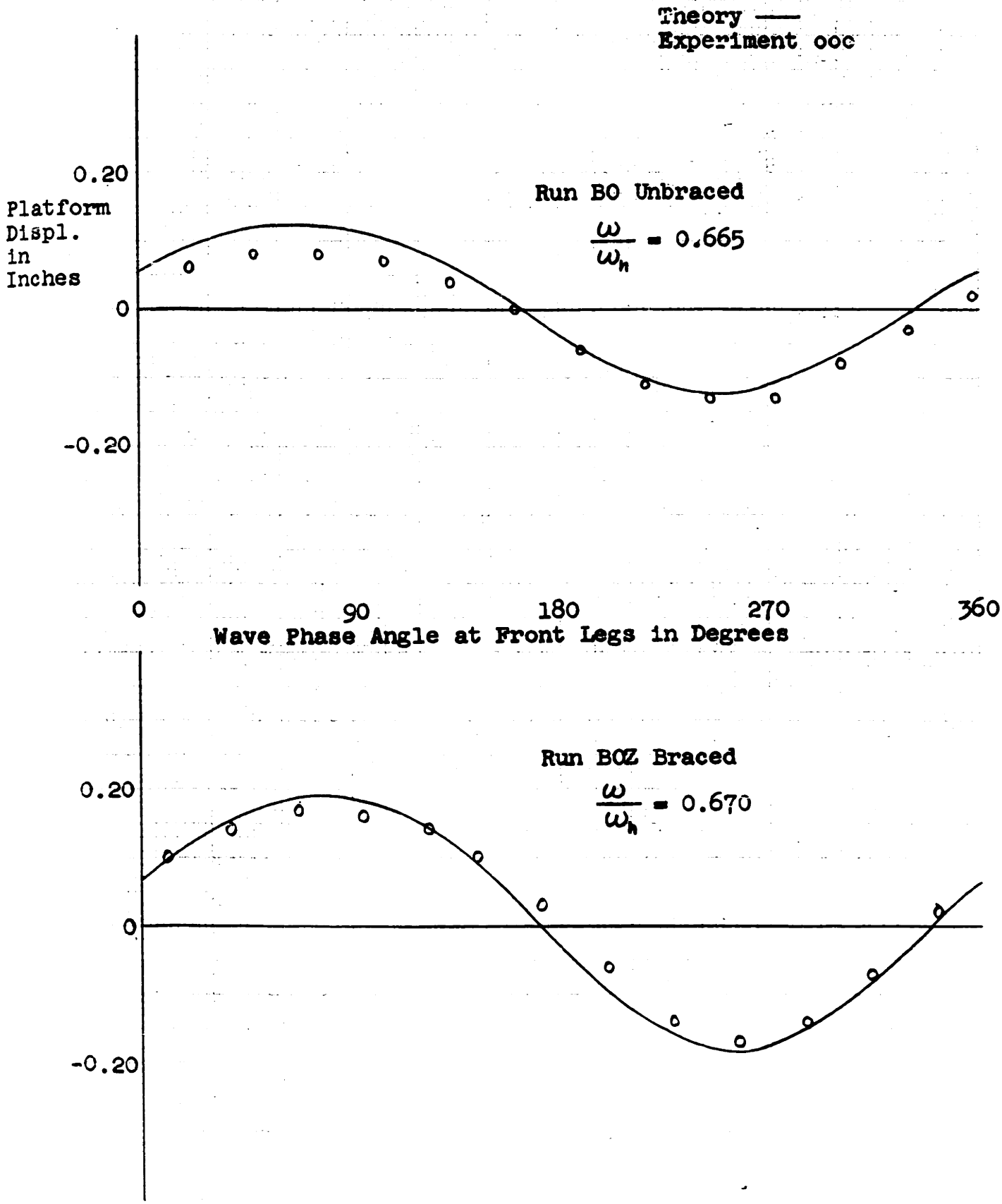

VCH 4/19/62

Figure XIIf - Platform Displacements for Wave B

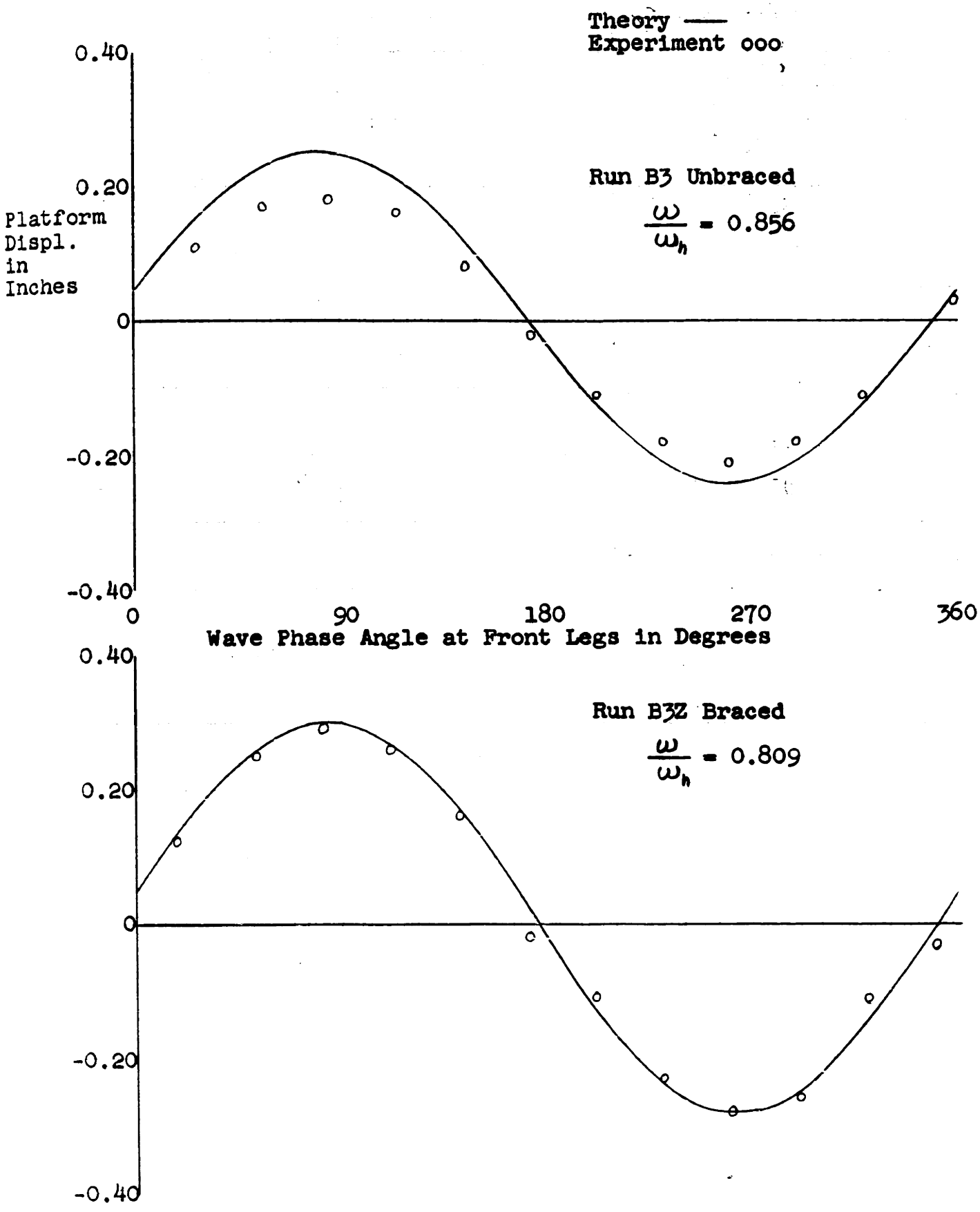

VCH 4/19/62

Figure XIIg - Platform Displacements for Wave B

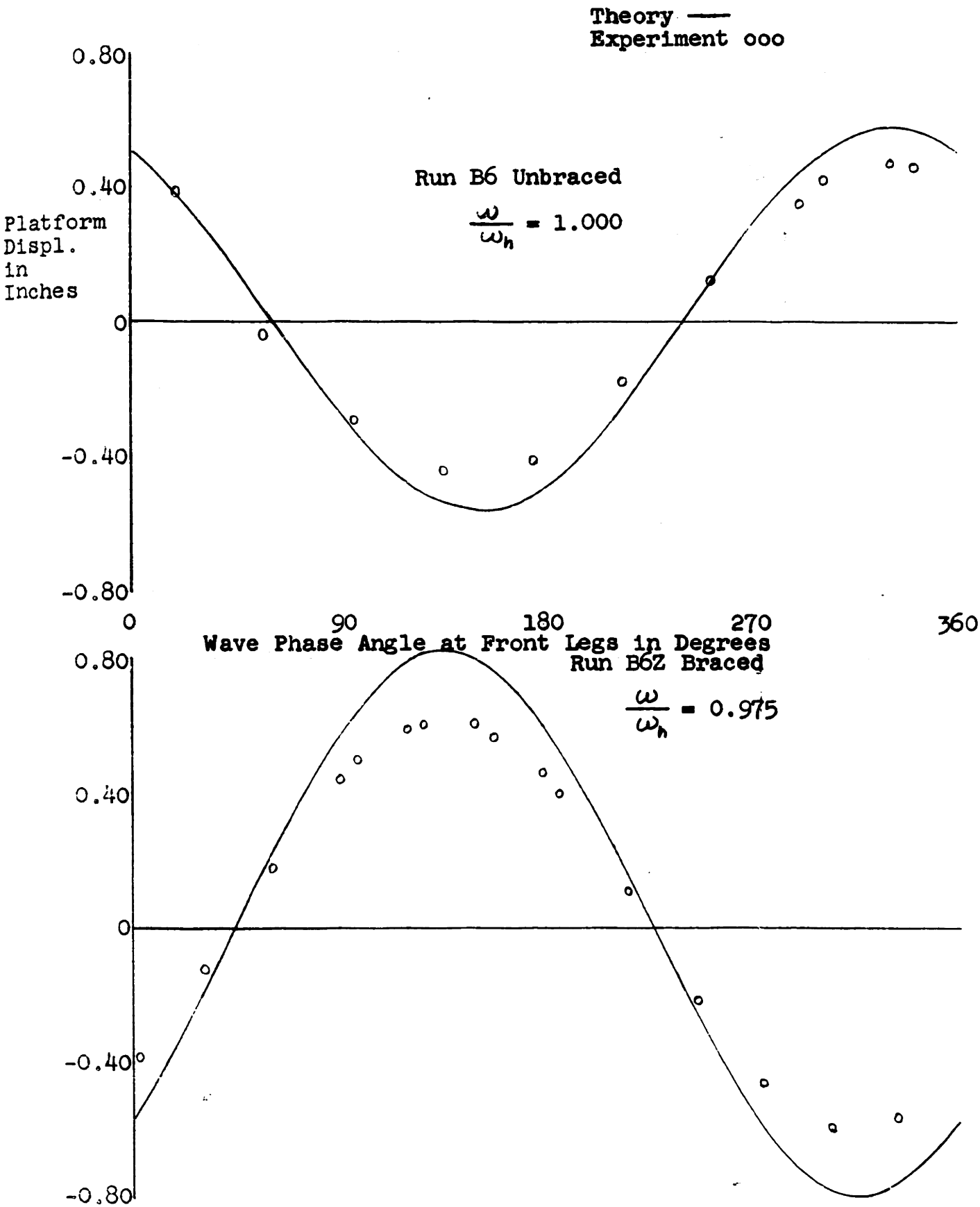

VCH 4/19/62

Figure XIIh - Platform Displacements for Wave B

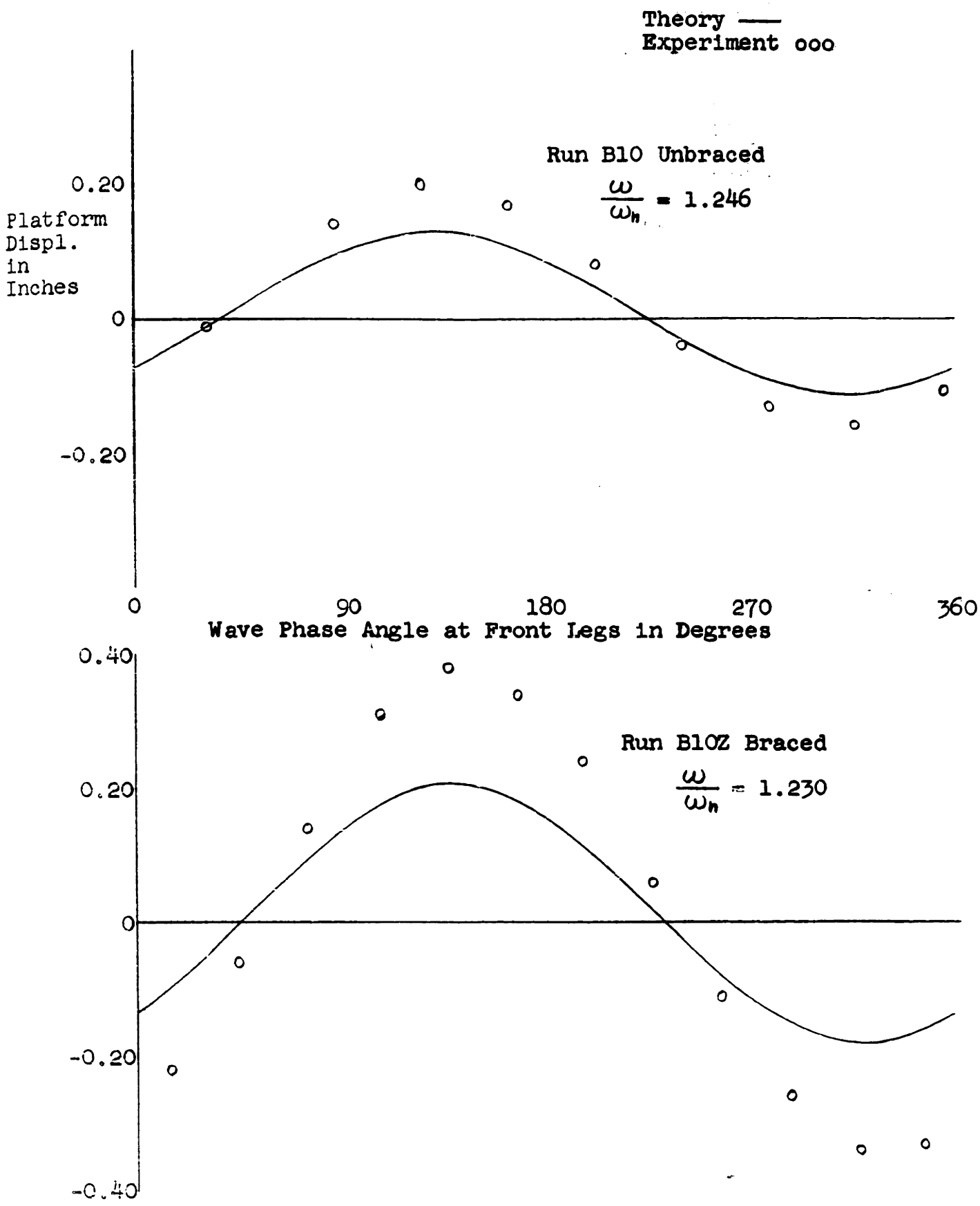

VCH 4/19/62

Figure XIIi - Platform Displacements for Wave C

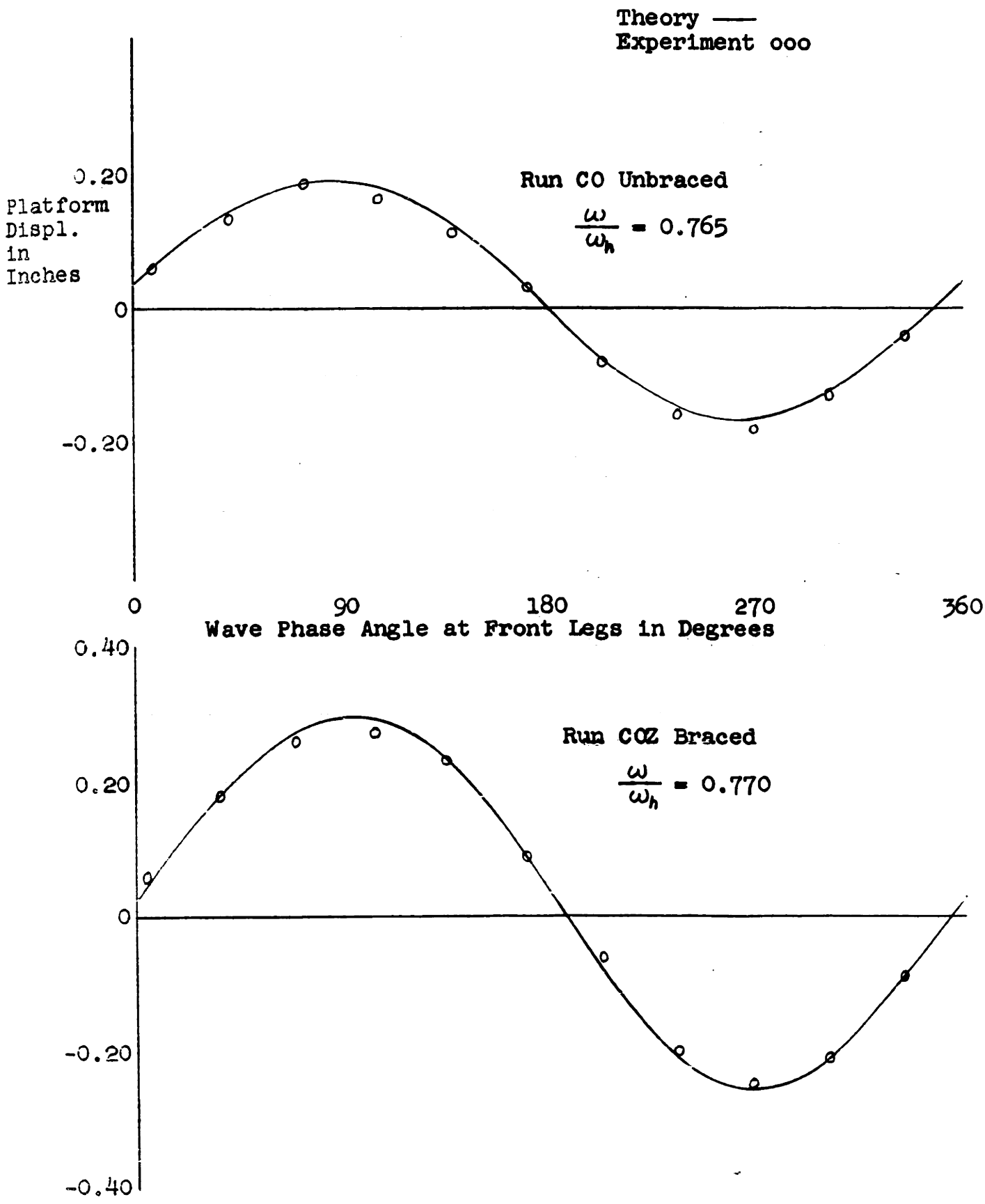

VCH 4/19/62

Figure XIIj - Platform Displacements for Wave C

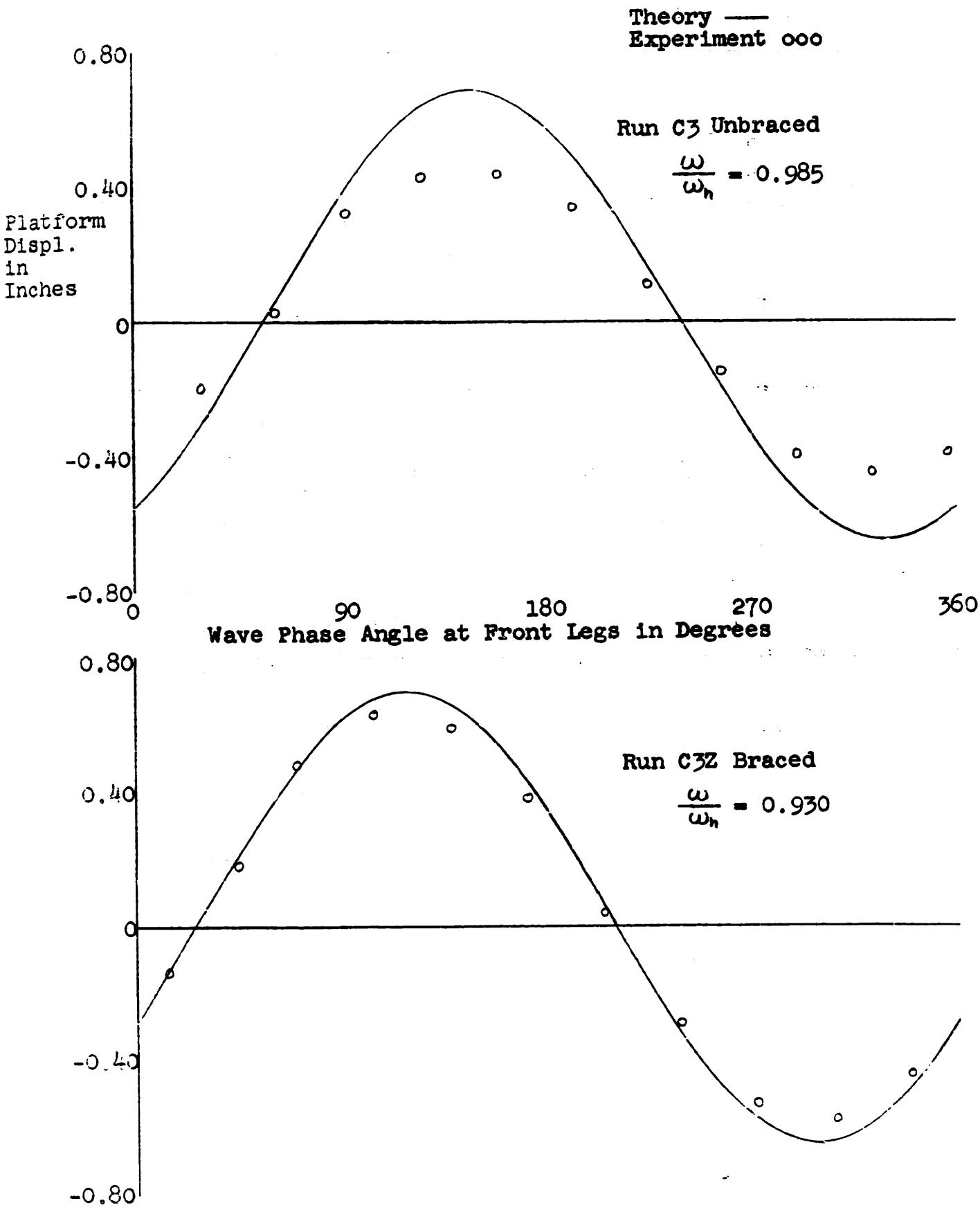

VCH 4/19/62

Figure XIIk - Platform Displacements for Wave C

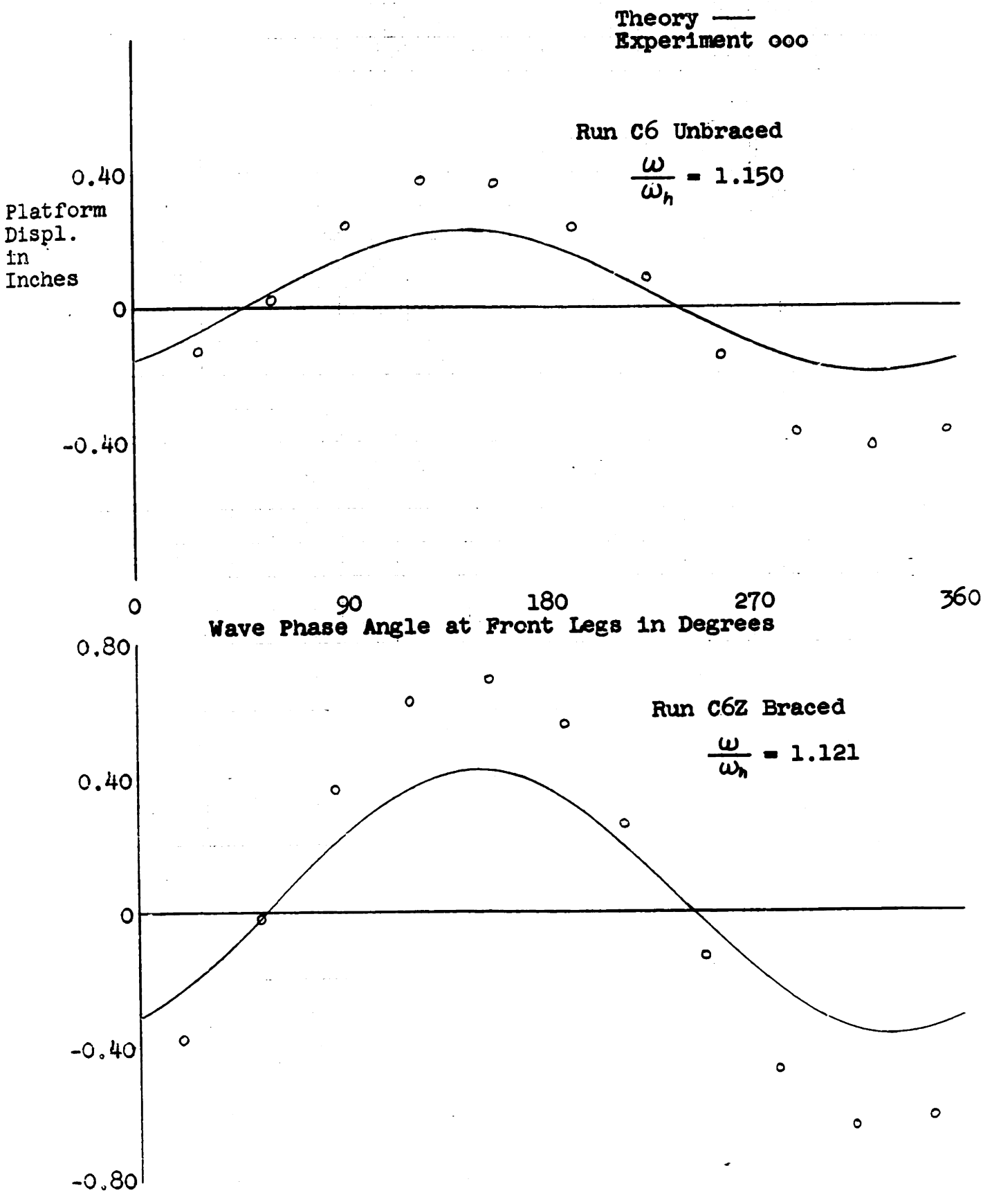

VCH 4/19/62

Figure XIIk - Platform Displacements for Wave C

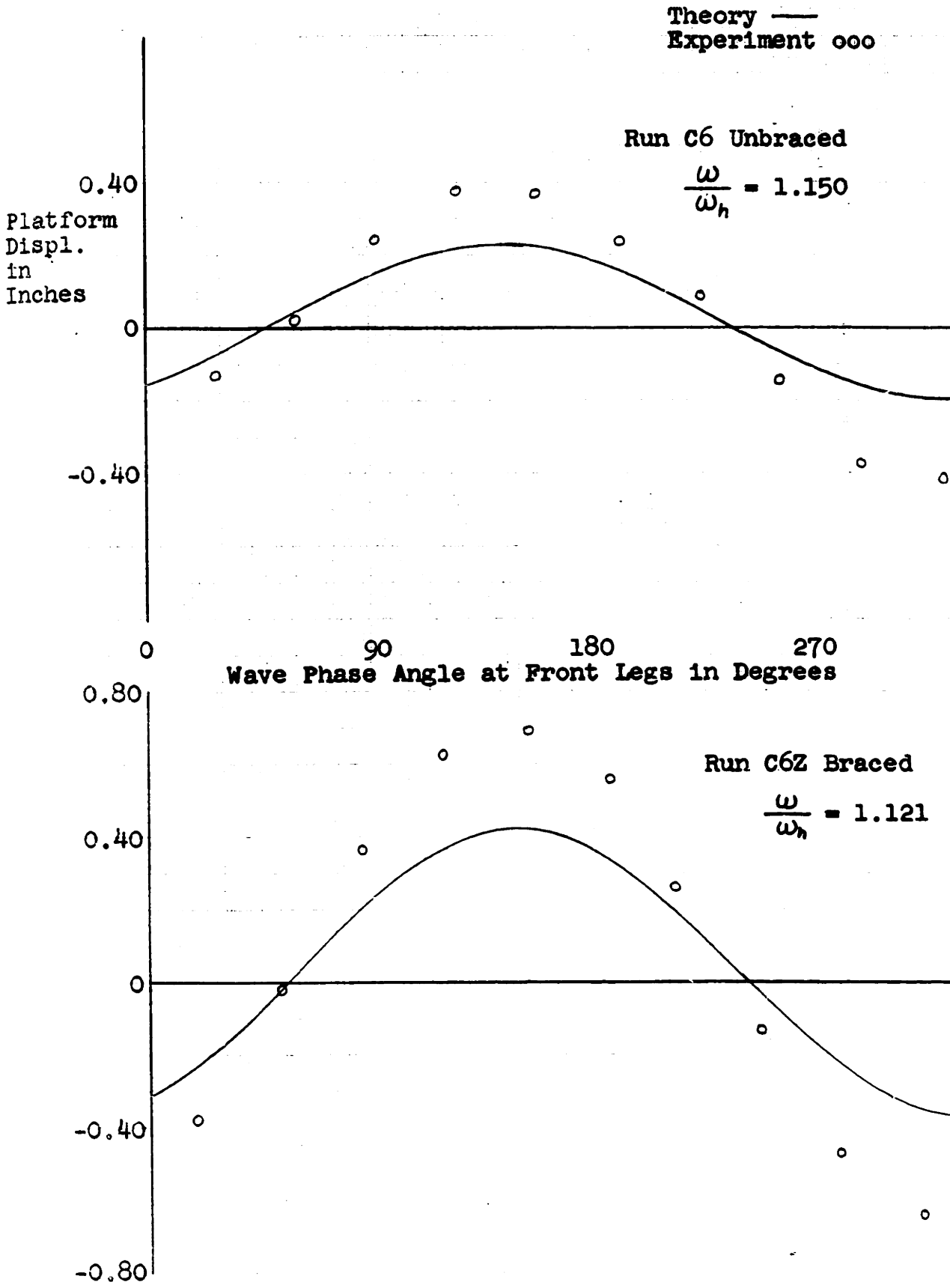

VCH 4/19/62

TO BE

CONT

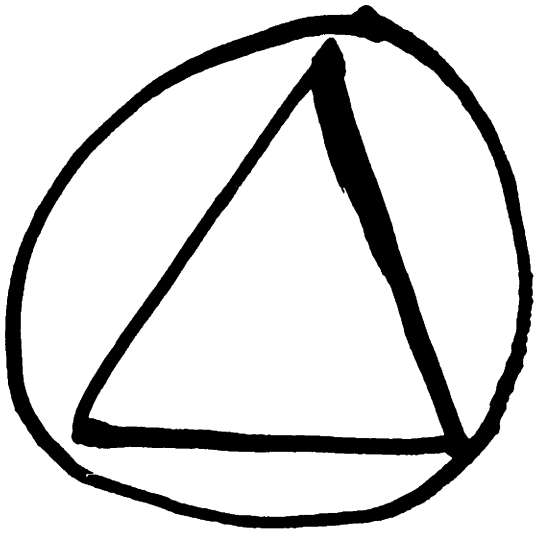

Figure XIII - Platform Displacements for Wave C

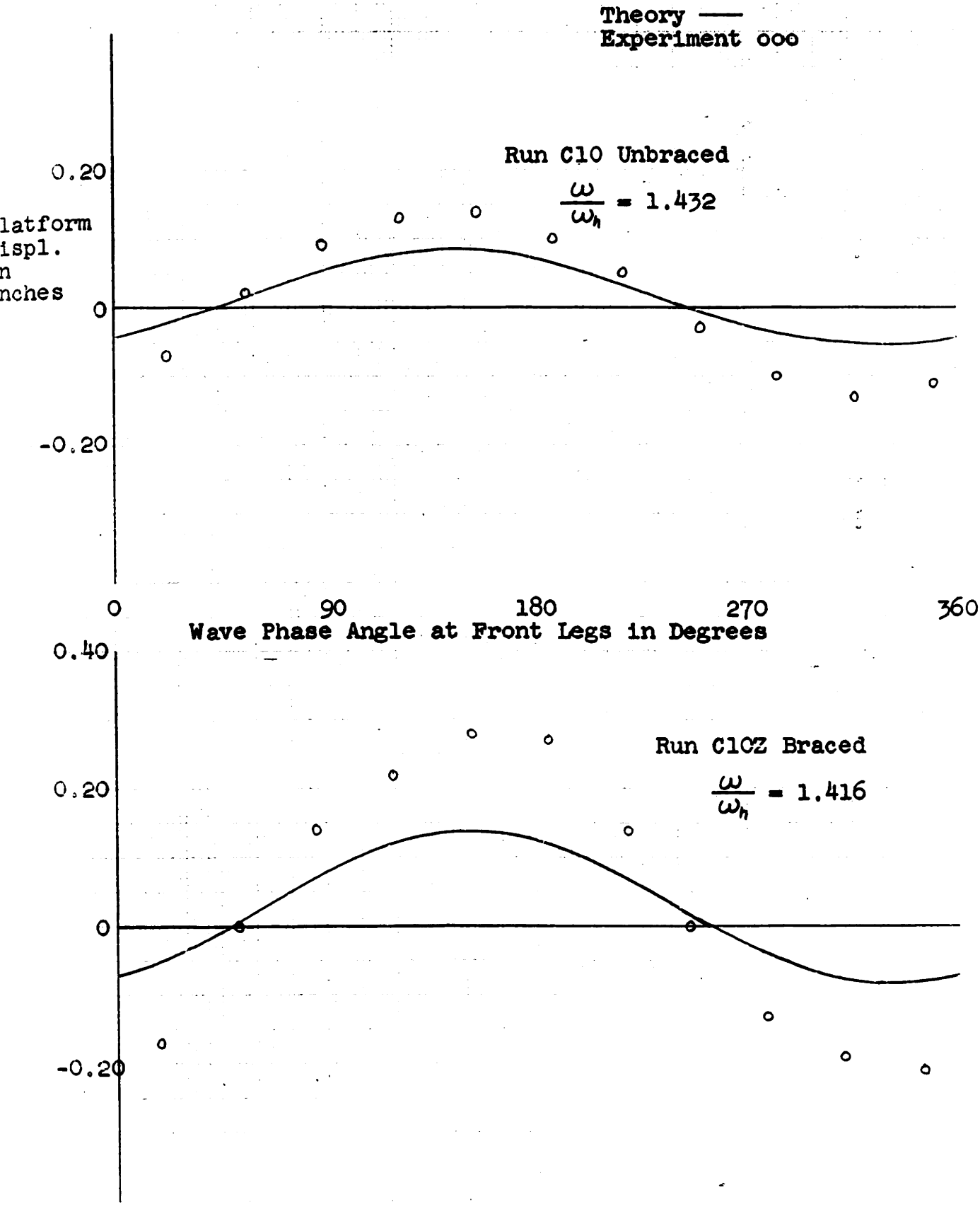

VCH 4/19/62

Figure XIIm - Platform Displacements for Wave D

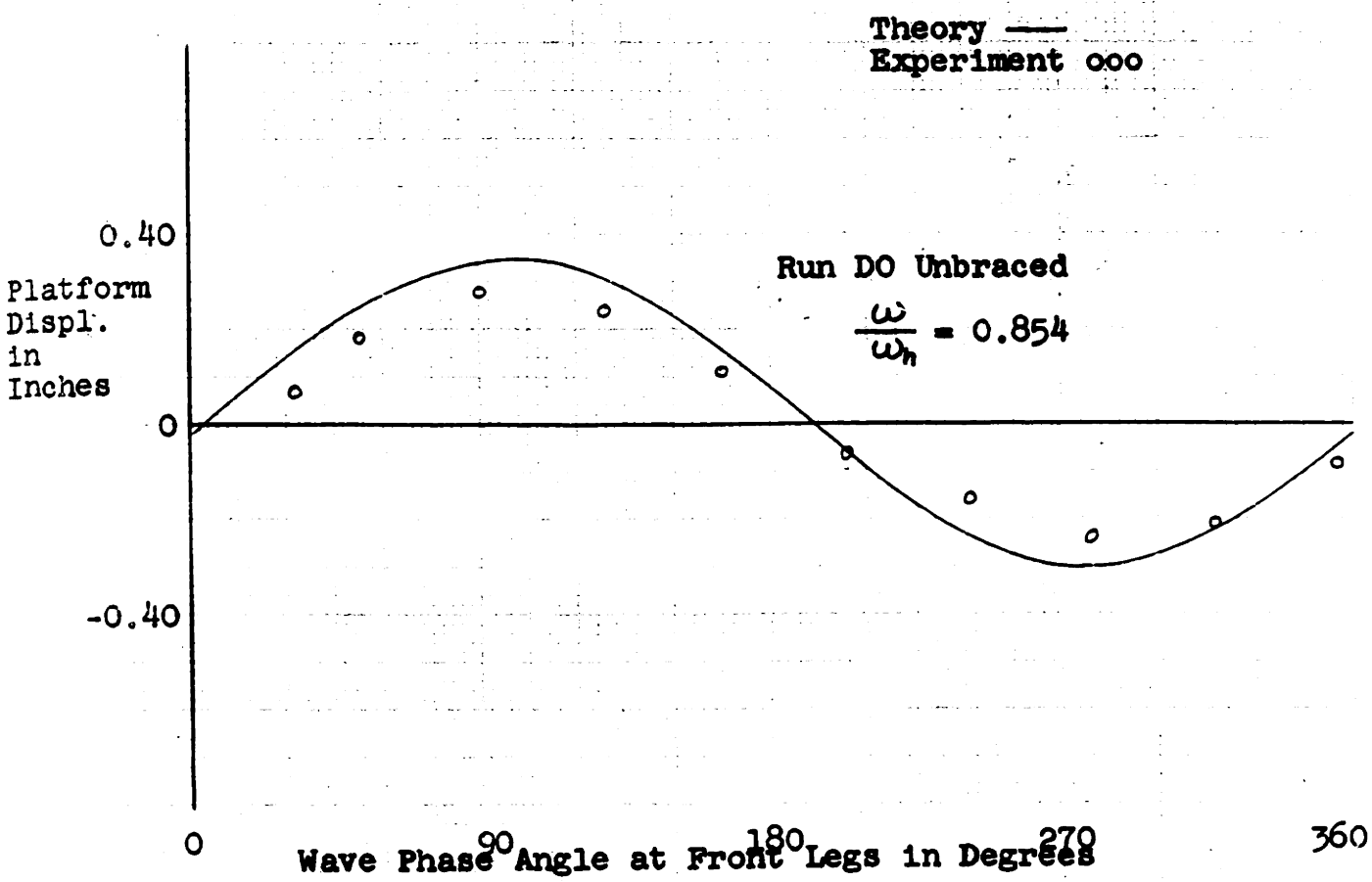

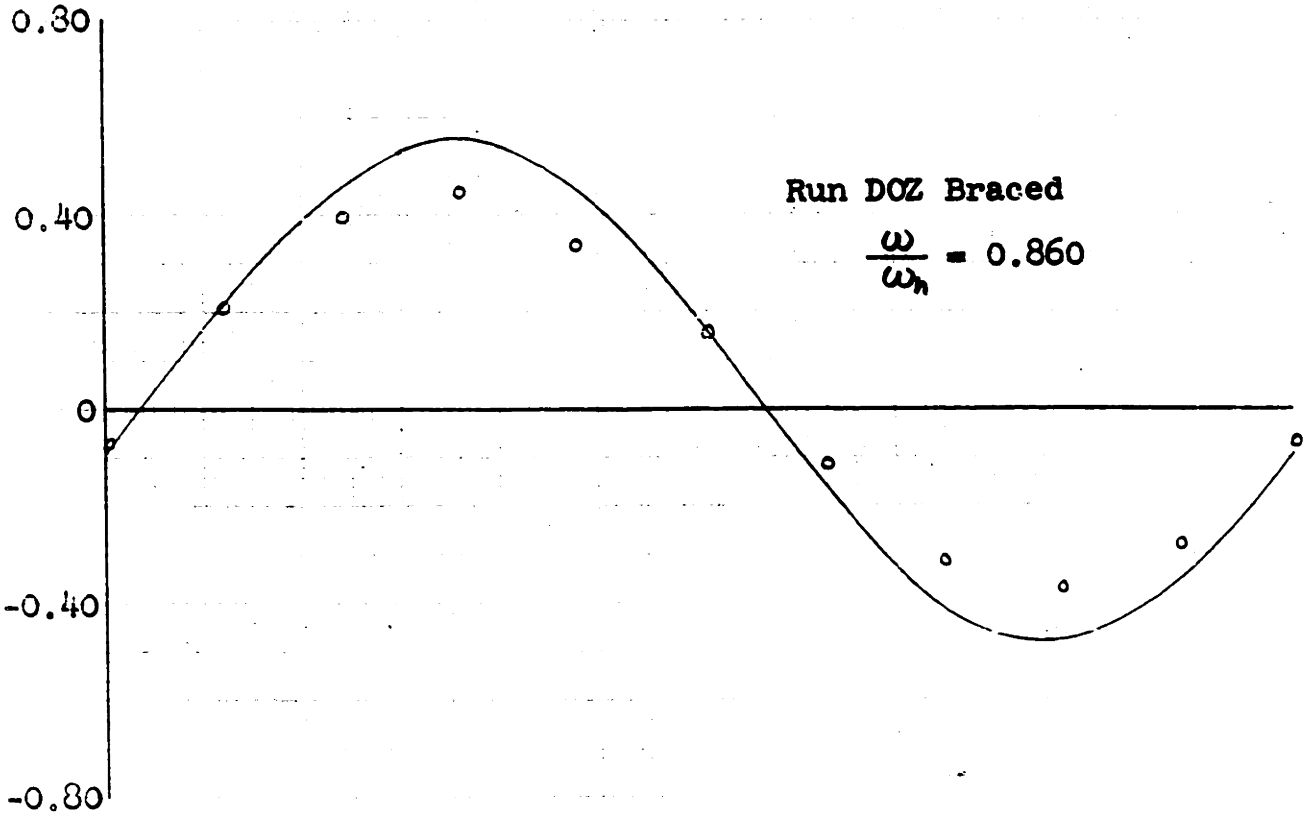

VCH 4/19/62

Figure XIIn - Platform Displacements for Wave D

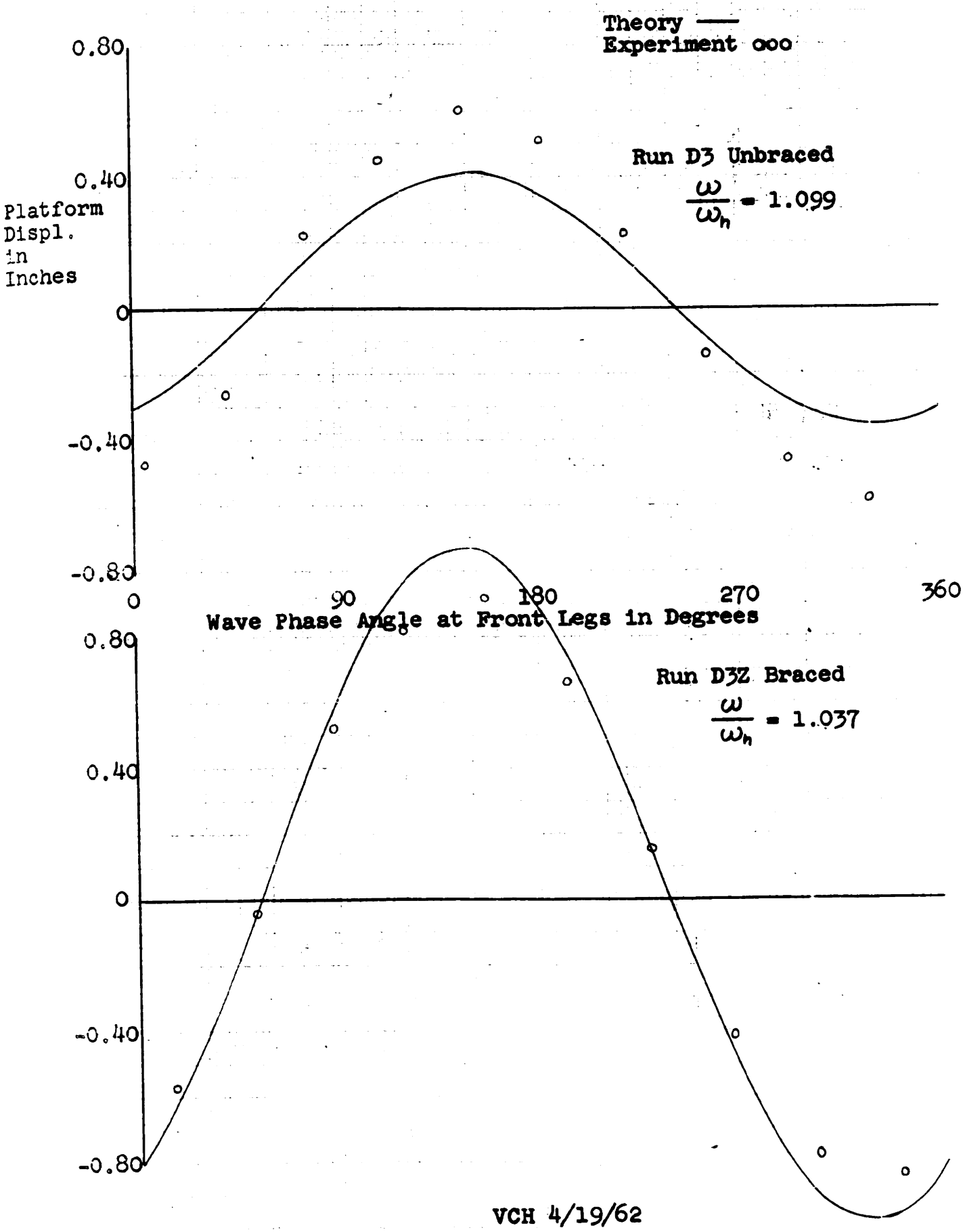

VCH 4/19/62

Figure XIIo - Platform Displacements for Wave D

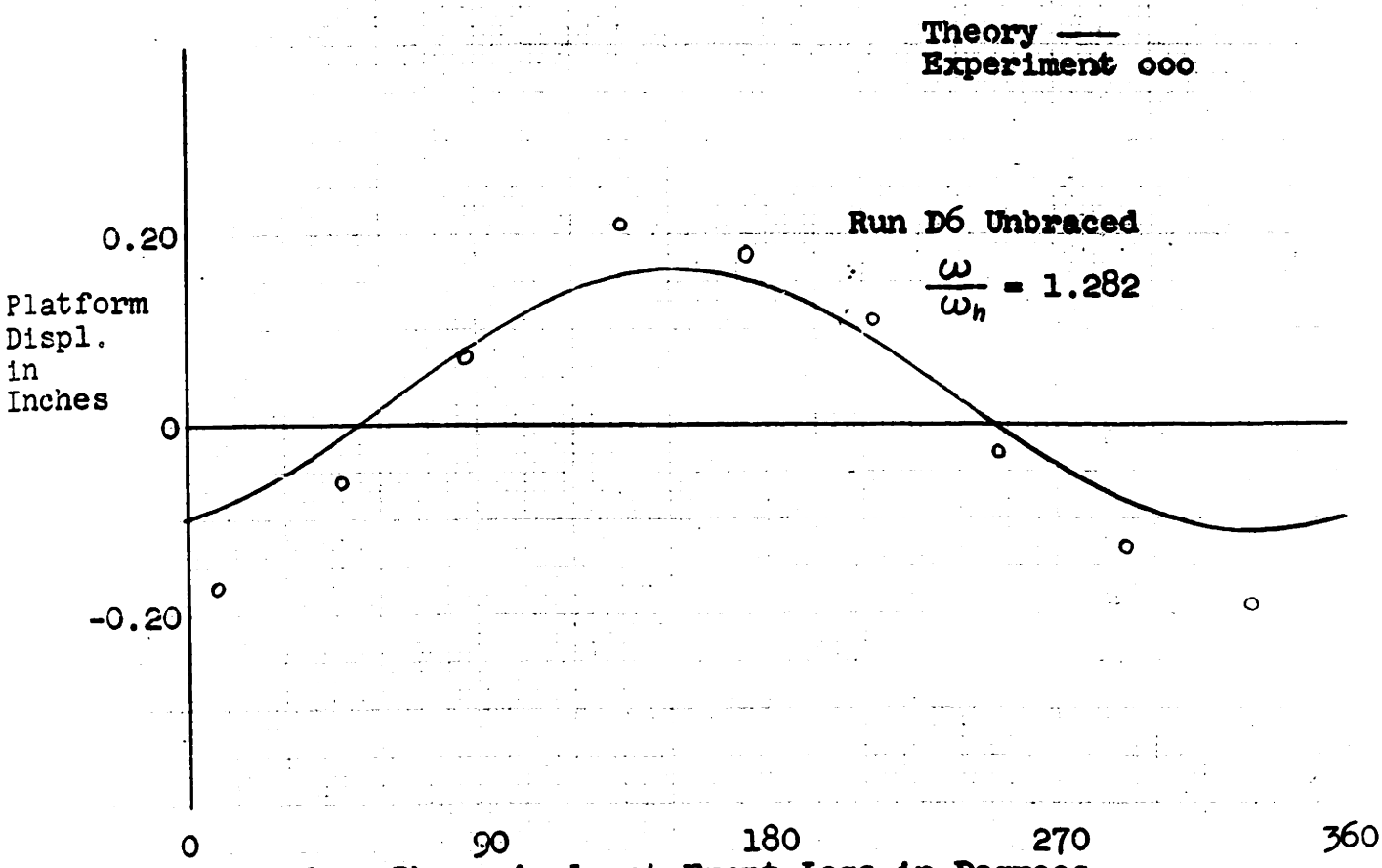

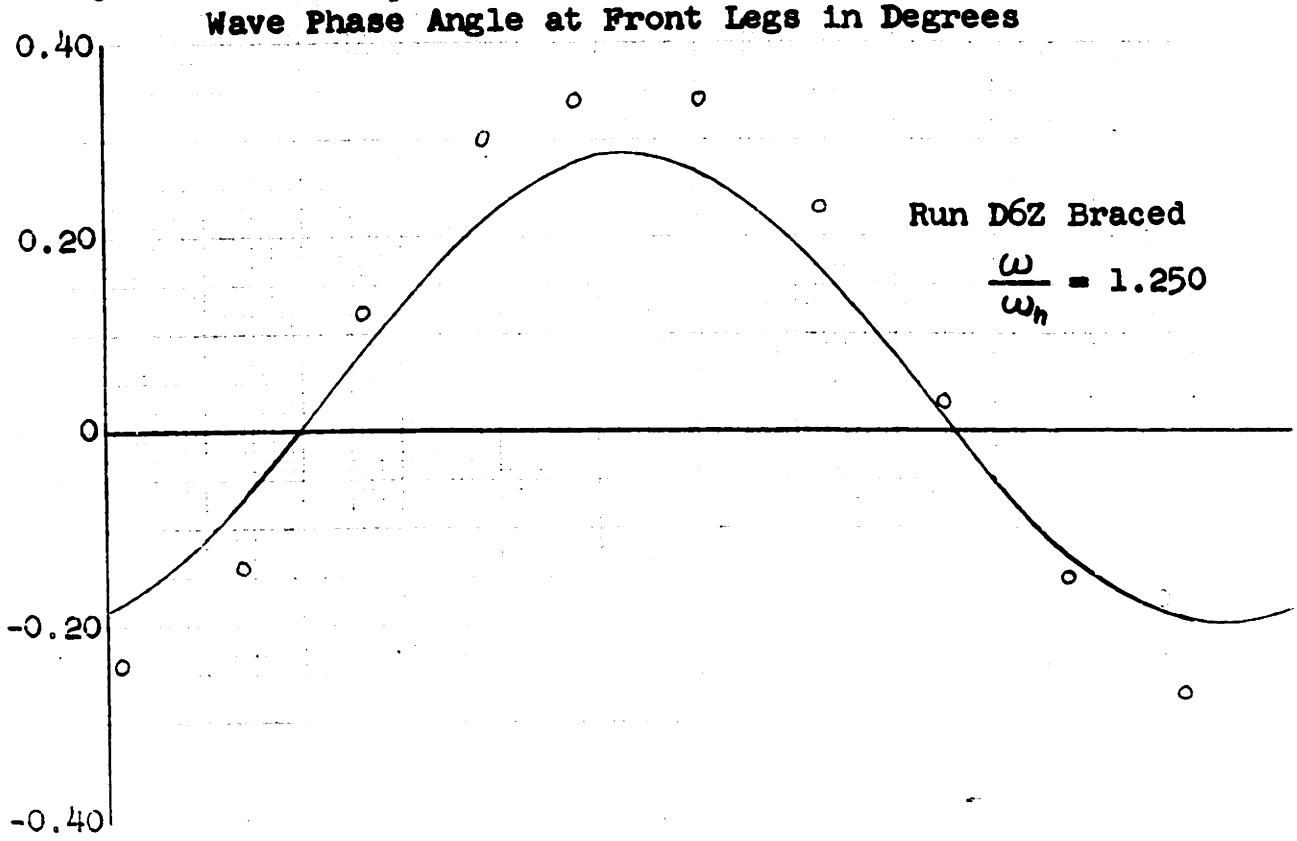

VCH 4/19/62

Figure XIIp - Platform Displacements for Wave D

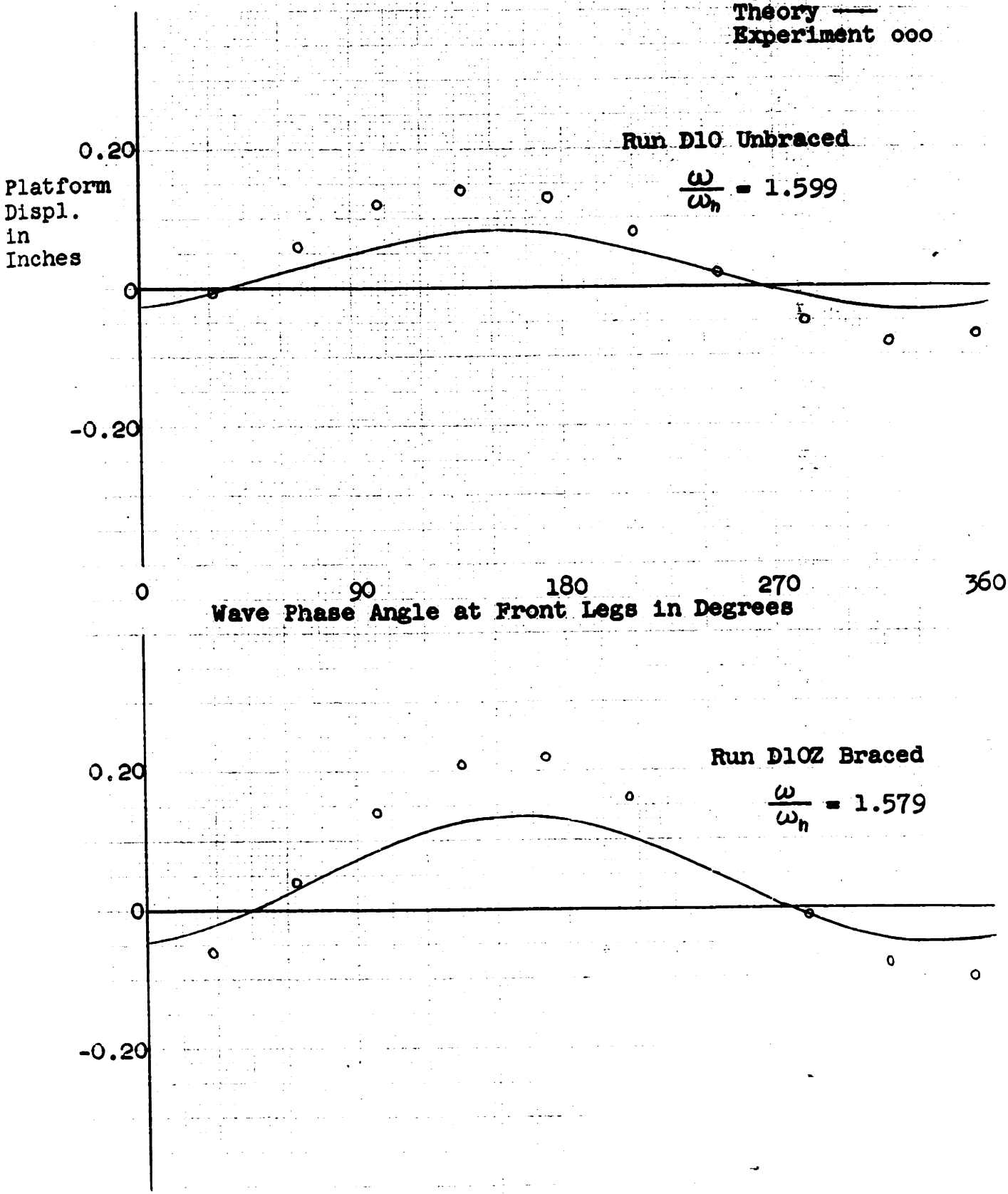

VCH 4/19/62

Figure XIIp - Platform Displacements for Wave D

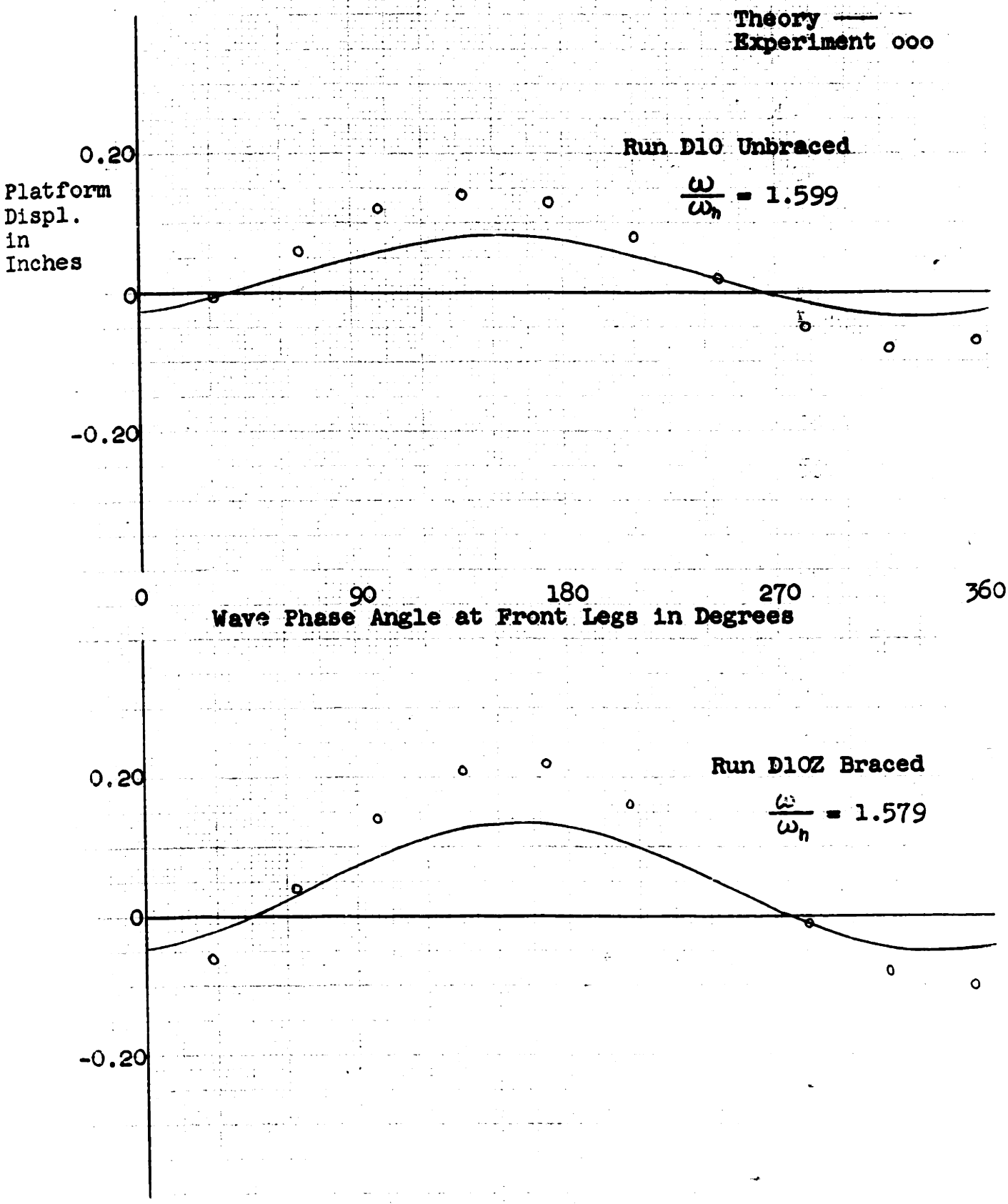

VCH 4/19/62

IV. DISCUSSION OF RESULTS

The plots of Figure XII indicate that the results of this thesis are good, in the opinion of the authors. The procedure set forth in the thesis is judged to be sound.

The reader will notice that in all cases the theoretical curve of displacement has the same shape as the experimental curve (which is not actually faired in). Of particular note are the curves of runs AO and AOZ (Figure XIIa), for which both the theoretical and experimental curves have an extra dip in the positive portion of the curve.

An attempt was made during the experiment to relate some reference time in the movie and on the Sanborn recorder paper. The procedure involved pushing a manual push-button as the second hand of the clock (one rotation = 10 seconds) passed some known time. Any human error would appear as an error in the experimentally determined phase angles θ at the front legs. The resulting data showed that the human error was so large that the data had to be discarded. Consequently

the phase relationships of the experimental points in Figure XII were adjusted to give the best fit to the theoretical curve.

If one follows a particular structure configuration (for example, 6Z) through its four runs he will see that the greatest displacements occur for those waves which give frequency ratios $\frac{\omega}{\omega_h}$ of about 1.1 or smaller. (Note that two different displacement scales are used for the plots.)

Figure XIII contains one point for each run. Each point represents the ratio of the maximum positive theoretical displacement, plotted as a function of frequency ratio $\frac{\omega}{\omega_h}$ for the particular run. The figure is intended to indicate the magnitude of the difference between the theoretical and experimental thesis results. It is seen that the displacement ratio is generally quite different from its ideal value of 1.0. Values greater than 1.0 indicate a conservative design, or overdesign. Values less than 1.0 indicate that the theory is inadequate and that the structure designed according to the theoretical procedure would be too weak. It is inferred in the previous paragraph that the designer is interested in waves for which $\frac{\omega}{\omega_h}$ is about 1.1 or less. Consequently the right-hand portion of Figure XIII is of no further concern, as a practical matter. For runs

Figure XIII - Ratio of Maximum Positive Platform Displacements, Theoretical/Experimental, vs. the Frequency Ratio $\frac{\omega}{\omega_n}$ for Each Run of the Thesis Results

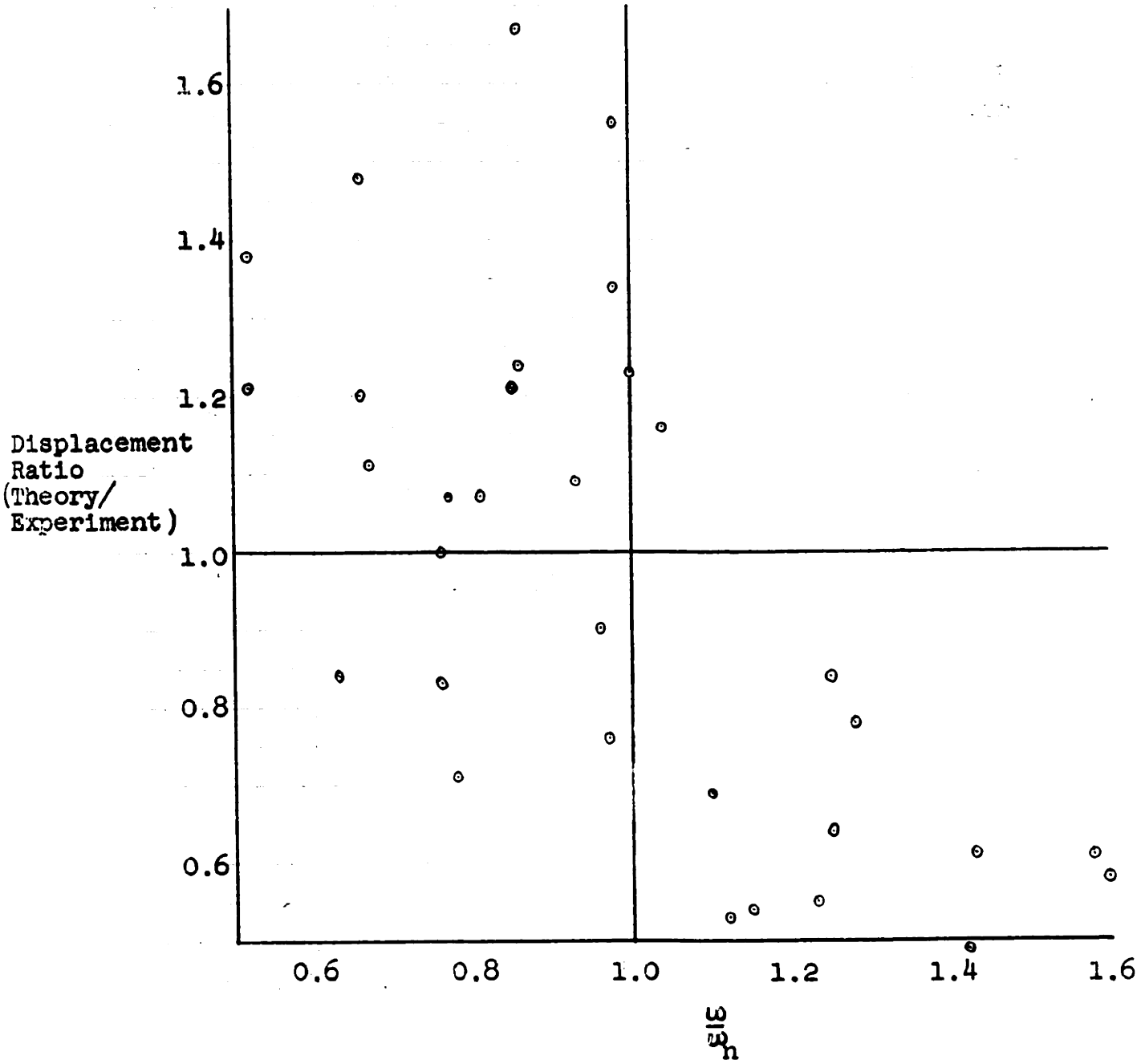

VCH 4/19/62

in which $\frac{\omega}{\omega_h}$ is less than 1.1 multiplication of the theoretical displacements by 1.5 would insure that the displacement ratios were always 1.0 or greater.

The theoretical solution for displacement is very sensitive to errors in the structural natural frequency. Computer calculations (not submitted), using both the theoretical and experimental values of ω_n obtained in this thesis (Appendix C), indicate that in some cases the maximum displacements so calculated differ by a factor of 2. The computer results show that, given two frequency ratios with all other variables the same, one may not expect that the frequency ratio nearer 1.0 will generally give the larger theoretical displacement. If a designer is in doubt about the exact natural frequency of his structure, as will be the general case in design work, he should apply a factor of ignorance of 3 to his calculated displacements. Under certain circumstances this may be extremely conservative (by a factor of about 5), but at other times it may be barely adequate. (The designer may wish to apply an additional conventional factor of safety.)

The authors desired that the theoretical calculations should test the method of determining wave forces on the structure and the method for predicting the consequent

vibrations. The calculation of theoretical ω_n was felt to be of secondary importance in testing this thesis. In order to reduce the sources of errors in the Results, therefore, the theoretical calculations were made using the experimental values of ω_n (as determined in air). Theoretical values were used for wave frequency ω, however.

Additional discussion of results is given in Appendices G and I.

V. CONCLUSIONS

1. The procedure set forth in this thesis provides a sound method of calculating the dynamic displacement of a fixed offshore structure acted upon by a passing train of regular waves.

2. The dynamic displacement of the platform may be of interest per se (p. 2). More generally, however, the dynamic displacement is required for the design stage determination of the vibration stresses throughout the structure (pp. 41-42).

3. Field test data on Texas Towers No. 2 (pp. 5-6) and No. 4 (p. 1) shows that the highest wave encountered does not necessarily produce the greatest platform displacement. Consequently, for design purposes one might not design an adequate structure simply by considering only the largest wave to be encountered, as has been the general past practice. One must consider several waves of various lengths (or periods) and steepnesses over the range of possible water depths. The critical displacement-wave combination must be arrived at by an iterative process.

4. For a particular structure with its particular natural frequency the greatest displacements occur for those waves which give frequency ratios $\frac{\omega}{\omega_h}$ of about 1.1 or smaller. For these waves the theoretical solution for displacement is generally conservative, with some exceptions.

5. A designer should apply a factor of ignorance of 3 to his calculated displacement. Under certain circumstances this may be extremely conservative (by a factor of about 5), but at other times it may be barely adequate. (The designer may wish to apply an additional conventional factor of safety.)

VI. RECOMMENDATIONS

1. This thesis advances a procedure for obtaining a "safe" design of a fixed offshore structure. At times the procedure may lead to a considerably overdesigned (excess strength) structure, which is generally poor from a cost viewpoint. It is recommended that future workers attempt to refine the procedure in order to reduce the amount of overdesign that may be involved.

2. It is recommended that some calculations be carried out for some real structures in the ocean and that the results be compared with observed data. From this work one might confirm the validity of this procedure for design purposes, and a revised factor of ignorance might be obtained. For example:

a. Were the results of the design calculations for Texas Tower No. 4 adequate? Could one predict tower collapse for the wave and wind conditions that existed when the tower did collapse? How do calculated displacements compare for some of the observed data available in [2]?

b. Perform a design calculation for the Argus Island structure and compare the results with those of [19].

c. Perform a design calculation for the Buzzards Bay Light Station structure and make a conclusion regarding the adequacy of structural strength.

3. Broaden the scope of the design data by extending the limits of Figures III, IV, and V to include solitary and breaking wave theories.

4. Develop an analogous procedure for calculating platform translation and rotation for an arbitrary angle of wave impingement.

5. Continue the investigation of vortex shedding on a vertical cylinder in a wave train (Appendix I). In a manner similar to that of this thesis calculate a Fourier series representation of the vortex shedding force and establish a procedure for calculating transverse platform displacement.

VII. APPENDIX

A. Details of Theoretical Procedure

Spring Constant k

Apply simple beam theory [29] to one leg (Figure XIV) to determine the static deflection curve for a force P_o acting at the level of the platform.

$$\frac{d^2y}{dZ^2} = \frac{M}{EI} = \frac{P_o}{EI}\left(\frac{\ell}{2} - Z\right)$$

$$\frac{dy}{dZ} = \frac{P_o}{EI}\left(\frac{\ell Z}{2} - \frac{Z^2}{2}\right)$$

$$y = \frac{P_o}{EI}\left(\frac{\ell Z^2}{4} - \frac{Z^3}{6}\right)$$

$$y_{max} = \frac{P_o \ell^3}{12EI}$$

$$\frac{y}{y_{max}} = \frac{3Z^2}{\ell^2} - \frac{2Z^3}{\ell^3}$$

By definition: $k = \frac{P_o}{y_{max}} = \frac{12EI}{\ell^3}$

For N legs: $k = \frac{12NEI}{\ell^3}$ (46)

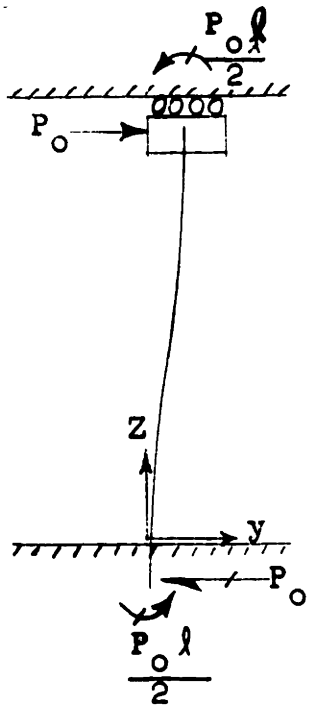

Figure XIV - Simple Beam Representation of One Leg

Rayleigh's Energy Method Applied to the Unbraced Structure

Apply Rayleigh's Energy Method [22,30] to the unbraced fixed offshore structure to determine the undamped natural

frequency ω_n. Assume simple harmonic motion for the N-legged structure. Use the static deflection curve for the elastic curve.

$$\text{Maximum kinetic energy} = \frac{W}{2g}\omega_n^2 y_{max}^2 + N\int_o^{\ell} \frac{w}{2g}\omega_n^2 y_{max}^2 \left[\frac{3Z^2}{\ell^2} - \frac{2Z^3}{\ell^3}\right]^2 dZ = \frac{\omega_n^2 y_{max}^2}{2g}(W + \frac{13}{35} Nw\ell)$$

$$\text{Maximum potential energy} = N\int_o^{\ell} \frac{M^2}{2EI} dZ = \frac{NP_o^2 \ell^3}{24EI}$$

Equate the maximum kinetic and potential energies to obtain:

$$\omega_n = \sqrt{\frac{12g\ NEI}{\ell^3(W + \frac{13}{35}Nw\ell)}} \qquad (47)$$

Use (36) and (46) to find:

$$m = \frac{1}{g}(W + \frac{13}{35}Nw\ell) \qquad (41)$$

If the configuration had been such that the legs were considered to be pinned to the platform the fraction to be used in the second term of (41) would be different from that calculated above. A calculation for this new value would proceed in a manner exactly analogous to that above. One can deduce that in calculating the spring constant k he would start with:

$$\frac{d^2y}{dZ^2} = \frac{M}{EI} = \frac{P_o}{EI}(\ell - Z)$$

The calculation would give a fraction of 33/140 to be used in the second term of (41).

Still Water Added Mass for the Unbraced Structure

Assume that the added mass for any elemental length of leg is equal to the mass of the water displaced by that leg [31], measured in terms of weight w_w per unit length. Calculate the maximum kinetic energy K.E. of this water for a condition of free vibration. Then calculate how much of this added mass unit must be placed at the level of the platform (W_w) to give the same maximum K.E.

$$N\int_o^d \frac{w_w}{2g}\omega_n^2\, y_{max}^2\left[\frac{3Z^2}{\ell^2} - \frac{2Z^3}{\ell^3}\right]^2 dZ = \frac{W_w}{2g}\omega_n^2\, y_{max}^2$$

Use this expression to calculate W_w for d = 27 in. and ℓ = 42 in.:

$$W_w = 0.03\ N\ w_w \ell$$

By comparing this quantity with those of (41) one sees that the added mass effect is small. Added mass will therefore be neglected.

Still Water Viscous Damping for the Unbraced Structure

A numerical example must be used for this calculation. Use run O-W, which is the free vibration of the unbraced structure in still water with zero pounds added to the platform in the experiment. Let $\sqrt{\overline{\dot{y}_o^2}}$ denote the root mean square velocity of the leg maximum velocity profile. Assume simple harmonic motion.

D = 0.505 in. d = 27 in. ℓ = 42 in.

$$\overline{\dot{y}_o^2} = \frac{1}{d} \int_0^d \dot{y}_{max}^2 \left[\frac{3Z^2}{\ell^2} - \frac{2Z^3}{\ell^3}\right]^2 dZ = 0.1292\ \dot{y}_{max}^2$$

$$\therefore \sqrt{\overline{\dot{y}_o^2}} = 0.359\ \dot{y}_{max}$$

This occurs at $Z = 17.0$ in., which can be found when one realizes that maximum velocity at any point Z on the leg is related to maximum displacement at that point by the constant ω_n. Enter Figure VI with $a = 17.0$ in., $a/\ell = 0.406$, and find $P_o/P = 0.360$.

For run O-W the average of the observed amplitudes for the decaying exponential displacements was 0.66 in.

The experimental natural frequency was $\omega_n = 6.13$ rad/sec. Assume q and ω_n to be numerically equal, which is very nearly true at the small values of damping which are of concern. With these numbers one can compute an average

$$\dot{y}_{max} = \omega_n \cdot y_{max} = (6.13)\left(\frac{0.66}{12}\right) = 0.337 \text{ ft./sec.}$$

$$\therefore \sqrt{\overline{\dot{y}_o^2}} = (0.359)(0.337) = 0.121 \text{ ft./sec.}$$

which gives a Reynold's number $R = \dfrac{(0.121)\left(\frac{0.505}{12}\right)}{(1.15 \times 10^{-5})} = 442.$

Enter Figure II to find steady state $C_D = 1.2$.

The maximum damping force acting on the platform is $\frac{P_o}{P} N C_D \frac{\rho}{2} A_\ell \overline{\dot{y}_o^2}$ where $A_\ell = D.d$ and $N = 4$.

This maximum damping force is calculated to be 0.00232 lb. At the low Reynold's number involved one can assume that the product of drag coefficient C_D and velocity

is constant, which means that the damping force varies directly as the first power of velocity rather than the second power. This assumption means that the maximum damping force equals $C\sqrt{\dot{y}_o^2}$ so that

$$C = \frac{P_o}{P} N(C_D \cdot \bar{\dot{y}}_o) \frac{\rho}{2} D \cdot d\sqrt{\dot{y}_o^2} = 0.0192.$$

From (41) find $m = 0.272$. From (37) find $C_c = 2m\omega_n = 3.34$. One can calculate viscous $\frac{C}{C_c} = 0.0057$, which happens to be exactly the value that was obtained experimentally. It is 11% of the observed structural damping (Table X).

With expressions for C and C_c one can write:

$$\frac{C}{C_c} = \frac{\frac{P_o}{P} N(\text{const.}) \frac{\rho}{2} D.d.(\omega_n . y_o)}{2m\,\omega_n}$$

For the experimental runs all variables in the right hand side of this expression are fixed except y_o and m. (ω_n cancels out.) If a situation is considered in which y_o is held constant, and m is varied, it is seen that viscous $\frac{C}{C_c}$ should decrease as m is increased. This trend was observed experimentally.

Influence Fraction $\frac{P_o}{P}$

Suppose that the force P acting as shown (Figure XV) on a two-legged structure causes the platform deflection y_{max}. The problem is to find what P_o acting at the platform level will cause the same y_{max}.

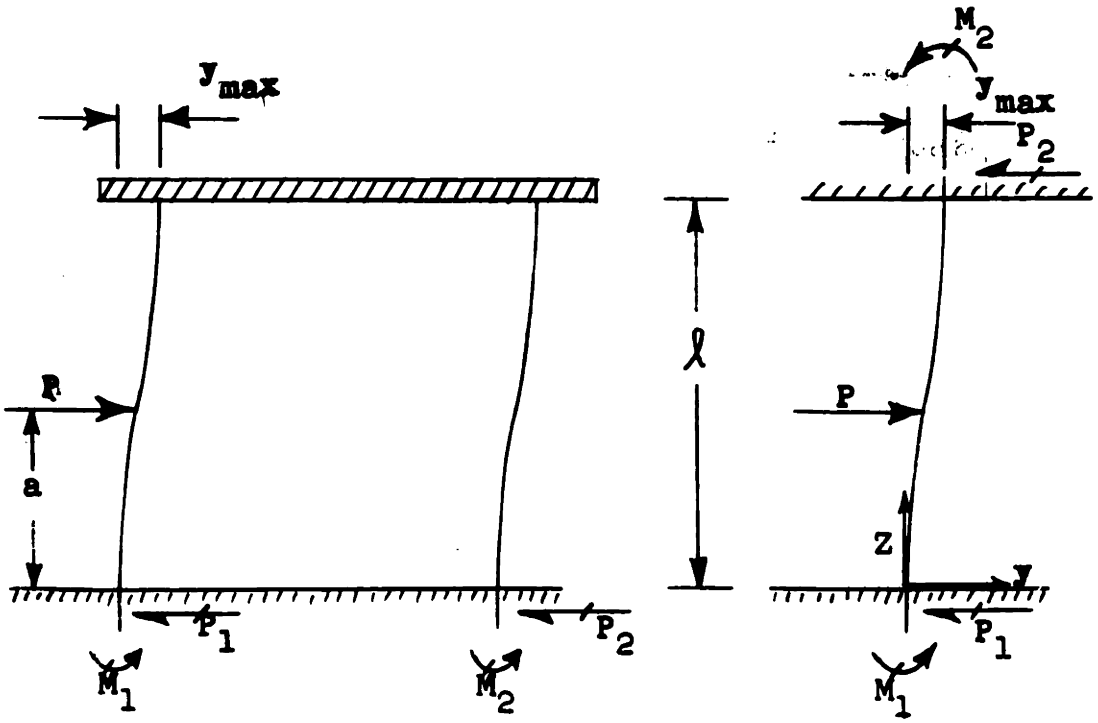

Figure XV - Portal Representation of Unbraced Structure

From (46) it can be shown that:

$$y_{max} = \frac{P_o \ell^3}{24EI} \qquad \text{and} \qquad P_2 = \frac{P_o}{2}$$

From Figure XV the reader can deduce that:

$$P_1 = P - \frac{P_o}{2} \qquad \text{(sum of forces = 0)}$$

and $$Pa = M_1 + M_2 + \frac{P_o a}{2} \qquad \text{(sum of moments = 0)}$$

For $0 \leq Z \leq a$ $\qquad M(Z) = M_1 - P_1 Z$

$$y'' = \frac{M}{EI} = \frac{1}{EI}(M_1 - P_1 Z)$$

$$y' = \frac{1}{EI}(M_1 Z - \frac{P_1 Z^2}{2})$$

$$y = \frac{1}{EI}(\frac{M_1 Z^2}{2} - \frac{P_1 Z^3}{6})$$

For $a \leq Z \leq \ell$ $\qquad M(Z) = M_1 - P_1 Z + P(Z-a)$

$$y'' = \frac{1}{EI} \quad M_1 - P_1 Z + P(Z-a)$$

$$y' = \frac{1}{EI} \quad M_1 Z - \frac{P_1 Z^2}{2} + P(\frac{Z^2}{2} - aZ) \quad + C_3$$

Equate expressions for y' at $Z = a$ to find $C_3 = \frac{Pa^2}{2EI}$

$$y = \frac{1}{EI} \quad \frac{M_1 Z^2}{2} - \frac{P_1 Z^3}{6} + P(\frac{Z^3}{6} - \frac{aZ^2}{2}) + \frac{Pa^2 Z}{2} \quad + C_4$$

Equate expressions for y at $Z = a$ to find $C_4 = \frac{-Pa^3}{6EI}$

Let $y' = 0$ for $Z = \ell$ and use $P_1 = P - \frac{P_o}{2}$

to find $M_1 = Pa(1 - \frac{a}{2\ell}) - \frac{P_o \ell}{4}$

Substitute these values for P_1 and M_1 into the expression for y and evaluate y_{max} at $Z = \ell$ to find:

$$y_{max} = \frac{1}{EI}\left[\frac{Pa^2\ell}{4} - \frac{Pa^3}{6} - \frac{P_o \ell^3}{24}\right]$$

Equate this to the previous value for y_{max} from (46) and solve for $\frac{P_o}{P}$:

$$\frac{P_o}{P} = \frac{3a^2}{\ell^2} - \frac{2a^3}{\ell^3}$$

This expression is plotted in Figure VI.

Fourier Series Representation of Force Acting on Platform

The following two expressions have been developed theoretically to represent the force acting on the platform:

$$F(t) = F_1 \sin^2 \omega t + F_3 \cos \omega t \quad (0° \leq \omega t \leq 180°) \qquad (55)$$

$$F(t) = -F_2 \sin^2 \omega t + F_3 \cos \omega t \quad (180° \leq \omega t \leq 360°) \qquad (56)$$

Many textbooks, such as [22,30], discuss Fourier series.

Let $F(t) = a_1 \sin\omega t + a_2 \sin 2\omega t + \ldots + a_n \sin n\omega t$

$+b_o + b_1 \cos\omega t + b_2 \cos 2\omega t + \ldots + b_n \cos n\omega t$

$(0° \leq \omega t \leq 360°)$

where: $a_n = \frac{\omega}{\pi} \int_o^{2\pi/\omega} F(t) \left[\sin n\omega t\right] \, dt$

$b_n = \frac{\omega}{\pi} \int_o^{2\pi/\omega} F(t) \left[\cos n\omega t\right] \, dt$

$b_o = \frac{\omega}{2\pi} \int_o^{2\pi/\omega} F(t) dt$

One can deduce that $0 = a_2 = a_4 = a_6 = \ldots$

and $0 = b_1 = b_3 = b_5 = \ldots$.

$$a_1 = \frac{\omega F_1}{\pi} \int_o^{\pi/\omega} \sin^3\omega t \, dt - \frac{\omega F_2}{\pi} \int_{\pi/\omega}^{2\pi/\omega} \sin^3\omega t \, dt = \frac{4}{3\pi}(F_1 + F_2)$$

$$a_3 = \frac{\omega F_1}{\pi} \int_o^{\pi/\omega} \left[\sin^2\omega t\right]\left[\sin 3\omega t\right] dt - \frac{\omega F_2}{\pi} \int_{\pi/\omega}^{2\pi/\omega} \left[\sin^2\omega t\right]\left[\sin 3\omega t\right] dt$$

$$= -\frac{4}{15\pi}(F_1 + F_2)$$

$$a_5 = \frac{-4}{105\pi}(F_1 + F_2)$$

$$a_7 = \frac{-4}{189\pi}(F_1 + F_2)$$

$$a_9 = \frac{-4}{693\pi}(F_1 + F_2)$$

$$b_2 = \frac{\omega F_1}{\pi}\int_0^{\pi/\omega}\left[\sin^2\omega t\right]\left[\cos 2\omega t\right]dt - \frac{\omega F_2}{\pi}\int_{\pi/\omega}^{2\pi/\omega}\left[\sin^2\omega t\right]\left[\cos 2\omega t\right]dt$$

$$= \frac{-(F_1 - F_2)}{4}$$

$$b_4 = 0 = b_6 = b_8 = \ldots.$$

$$b_o = \frac{\omega F_1}{2\pi}\int_0^{\pi/\omega}\sin^2\omega t\,dt - \frac{\omega F_2}{2\pi}\int_{\pi/\omega}^{2\pi/\omega}\sin^2\omega t\,dt = \frac{F_1 - F_2}{4}$$

$$\therefore F(t) = \frac{F_1 - F_2}{4} + \frac{4}{3\pi}(F_1 + F_2)\sin\omega t$$

$$- \frac{4}{15\pi}(F_1 + F_2)\sin 3\omega t + F_3\cos\omega t$$

$$- \frac{(F_1 - F_2)}{4}\cos 2\omega t + \ldots. \qquad (57)$$

B. SAMPLE THEORETICAL CALCULATIONS

The calculations performed to determine theoretical displacements caused by the B wave are given below.

Given:

pile diameter D = 0.5 in. (0.0417 ft.)
water depth d = 27 in. (2.25 ft.)
wave height H = 0.313 ft.
wave length L = 10.86 ft.

therefore $d/L = 0.207$ and $H/L = 0.0289$

Sample Calculation:

1. Hydrodynamics

a.) Calculate maximum drag forces and centroids on a single leg.

$0° \leq \theta \leq 180°$

$$\text{drag force} = F_D = \frac{\gamma D d^2}{2} C_D A \quad \text{where } \gamma = 62.4 \text{ lbs/ft}^3 \tag{12}$$

$$F_D = 6.58\, C_D A$$

from computer program results (Appendix D) or by interpolation of Figure IV, $A = 0.00421$

$$IR = \frac{D}{\nu}\sqrt{\frac{gdA}{1 + \eta_o/d}} \qquad (18)$$

for water temperature = 61°F, $\nu = 1.21 \times 10^{-5}$ ft.^{2}/sec.

$$\frac{\eta_o}{d} = \frac{H}{2d}\left[1 + \frac{3\pi}{8\ L/H}\ \frac{\sinh(2J)}{(\sinh J)^4}\right] \qquad (6)$$

$$J = \frac{2\pi d}{L} = 1.30$$

$\sinh(2J) = 6.69$, $\sinh J = 1.698$

$$\frac{\eta_o}{d} = \frac{0.313}{2(2.25)}\left[1 + \frac{3(3.14)(0.0289)(6.69)}{8\ (1.698)^4}\right] = 0.0715$$

$1 + \frac{\eta_o}{d}$ also could be read directly from the computer program results (Appendix D).

$$1 + \frac{\eta_o}{d} = \left(\frac{S'}{d}\right)_{max} = 1.0715$$

$$IR = \frac{0.0417}{1.21 \times 10^{-5}}\sqrt{\frac{32.2(2.25)(0.00421)}{1.0715}} = 1804$$

from Figure II for $IR = 1804$, $C_D = 0.96$

therefore $F_D = 6.58(0.96)(0.00421) = 0.0266$ lbs.

drag force centroid = $\bar{S}'$

From computer program results (Appendix D) or by interpolation of Figure III, $\frac{\bar{S}'}{d} = 0.685$

$$\bar{S}' = 0.685(2.25) = 1.542 \text{ ft.}$$

<u>$180° \leq \theta \leq 360°$</u>

$$\text{drag force} = (F_D)_t = \frac{-\gamma D d^2}{2} C_{D \text{ trough}} B \qquad (13)$$

$$(F_D)_t = -6.58 C_{D \text{ trough}} B$$

from Figure V (or Appendix D), $B = 0.00276$

$$IR_{trough} = \frac{D}{\nu}\sqrt{\frac{gdB}{1 + (\frac{\eta_o - H}{d})}} \qquad (19)$$

$$\frac{\eta_o - H}{d} = \frac{\eta_o}{d} - \frac{H}{d} \qquad (31)$$

$$\frac{\eta_o - H}{d} = 0.0715 - \frac{0.313}{2.25} = -0.0677$$

or from Appendix D, $1 + (\frac{\eta_o - H}{d}) = 0.9323$

$$IR_{trough} = \frac{0.0417}{1.21 \times 10^{-5}}\sqrt{\frac{32.2(2.25)(0.00276)}{0.9323}} = 1591$$

from Figure II for $IR_{trough} = 1591$, $C_{D \text{ trough}} = 0.925$

therefore $(F_D)_t = -6.58(0.925)(0.00276) = -0.01702$ lbs.

drag force centroid = $(\bar{S}')_t$

from Figure III (or Appendix D), $\frac{(\bar{S}')_t}{d} = 0.559$

$(\bar{S}')_t = 0.559(2.25) = 1.258$ ft.

b.) Calculate maximum inertia force and centroid on a single leg.

$$F_I = \gamma \frac{D^2}{4} \pi H \tanh J \qquad (25)$$

for $J = 1.30$, $\tanh J = 0.862$

$$F_I = 62.4\frac{(0.0417)^2}{4}(3.14)(0.313)(0.862) = 0.02295$$

$$\bar{S}_I = \frac{\gamma D^2 LH}{8 F_I \cosh J}\left[1 + J \sinh J - \cosh J\right]$$

$\sinh J = 1.698$, $\cosh J = 1.971$

$$\bar{S}_I = \frac{62.4(0.0417)^2(10.86)(0.313)}{8(0.02295)(1.971)}\left[1 + 1.3(1.698) - 1.971\right]$$

$\bar{S}_I = 1.26$ ft.

c.) Calculate wave period.

$$T = \frac{L}{C} \text{ where } C = \sqrt{\frac{gd \tanh J}{J}\left\{1+\left(\frac{\pi}{L/H}\right)^2\left[\frac{2(\cosh(2J))^2+2\cosh(2J)+5}{8\ (\sinh J)^4}\right]\right\}} \qquad (8)$$

$$C = \sqrt{\frac{32.2(2.25)(0.862)}{1.30}\left\{1+(3.14(0.0289))^2\left[\frac{2(6.77)^2+2(6.77)+5}{8(1.698)^4}\right]\right\}}$$

$C = 6.98$ ft./sec.

Therefore $T = \frac{10.86}{6.98} = 1.558$ sec.

$$\omega = \frac{2\pi}{T} = 4.03 \text{ rad./sec.}$$

C is determined internally in the computer program (Appendix D) but is not one of the outputs. A simple addition to the "WRITE OUTPUT," "DIMENSION," and "FORMAT" statements would include C as an output.

Summary of steps a,b, and c:

$F_D = 0.0266$ lbs. $\quad \bar{S}' = 1.542$ ft.
$(F_D)_t = -0.01702 \quad (\bar{S}')_t = 1.258$ ft.
$F_I = 0.02295$ lbs. $\quad \bar{S}_I = 1.26$ ft.
$\omega = 4.03$ rad./sec.

Enter these figures in the upper left-hand corner of the tabular calculation sheet, Figure XVI. (Actually in this sample calculation the numbers do not agree exactly with those of Figure XVI, which were determined at another time, but the slight differences are negligible for purposes of illustration.)

2. Vibrations

Consider run B6. This is the unbraced model with 6 lb. of added weight on the platform, in wave B.

The reader should trace the steps on Figure XVI as he reads the following explanatory notes.

Values of ω_n, $\frac{C}{C_c}$, and k are taken from Appendix F. Otherwise they would be determined as explained in the Procedure, Section II.

Values of the influence fraction $\frac{P_o}{P}$ are read from Figure VI.

The values of θ at the front legs are simply reference values. Values of platform longitudinal displacement are calculated for these twelve reference values of θ, and a curve is faired through the points (as was done in the preparation of Figure XII).

Below the values of θ the corresponding reference angles for each of the significant terms in

Θ	WAVE FORCE ON ONE LEG	S'	$\frac{a}{\ell}$	$\frac{P_o}{P}$	FORCE $\times \frac{P_o}{P}$
90°	.0262	1.544'	.441	.412	F_1=.01080
270°	.0178	1.262'	.361	.397	F_2=.00706
180°	.0230	1.260'	.360	.396	F_3=.00910

PLATFORM LONGITUDINAL DISPLACEMENT FOR RUN B6

ω = 4.00 RAD./SEC., ω_h = 4.05 RAD/SEC. $\Big\}$ $\frac{\omega}{\omega_h}$ = 0.988

$\frac{r}{c_c}$ = 0.0613

k = 0.625 LB./IN.

ϕ_{RL} = 44°

$\Theta_{AT\ FRONT\ LEGS}$	30°	60°	90°	120°	150°	180°	210°	240°	270°	300°	330°	360°
sin ωt = sin(angle →)	30°	60°	90°	120°	150°	180°	210°	240°	270°	300°	330°	360°
sin 3ωt = sin(angle →)	90°	180°	270°	360°	90°	180°	270°	360°	90°	180°	270°	360°
cos ωt = sin(angle →)	120°	150°	180°	210°	240°	270°	300°	330°	360°	30°	60°	90°
cos 2ωt = sin(angle →)	150°	210°	270°	330°	30°	90°	150°	210°	270°	330°	30°	90°

N LEGS	FOURIER SERIES FORCE TERM	$\frac{h\omega}{\omega_h}$	$\phi / h\phi_{RL}$										
N'=2 FRONT LEGS	sin ωt	.988	80°	310°	340°	10°	40°	70°	100°	130°	160°	190°	220°	250°	280°
	sin 3ωt	2.96	177°	273°	3°	93°	183°	273°	3°	93°	183°	273°	3°	93°	183°
	cos ωt	.988	80°	40°	70°	100°	130°	160°	190°	220°	250°	280°	310°	340°	10°
	cos 2ωt	1.98	175°	335°	35°	95°	155°	215°	275°	335°	35°	95°	155°	215°	275°
N'=2 REAR LEGS	sin ωt		44°	266°	296°	326°	356°	26°	56°	86°	116°	146°	176°	206°	236°
	sin 3ωt		132°	141°	231°	321°	51°	141°	231°	321°	51°	141°	231°	321°	51°
	cos ωt		44°	356°	26°	56°	86°	116°	146°	176°	206°	236°	266°	296°	326°
	cos 2ωt		88°	247°	307°	7°	67°	127°	187°	247°	307°	7°	67°	127°	187°

N LEGS	FOURIER SERIES FORCE TERM	FORCE COEF.=F (LBS.)	$\frac{h\omega}{\omega_h}$	$\frac{X_o}{X_{STATIC}}$	$X_o = \frac{X_o}{X_{ST.}} \cdot \frac{N'F}{k}$										
N=4	constant	.00094	—	1.00	.006	.006	.006	.006	.006	.006	.006	.006	.006	.006	.006	.006	.006
N'=2 FRONT LEGS	sin ωt	.00757	.988	7.79	.188	-.144	-.064	.033	.121	.177	.185	.144	.064	-.033	-.121	-.177	-.185
	sin 3ωt	-.00151	2.96	.13	-.001	.001	0	-.001	0	.001	0	-.001	0	.001	0	-.001	0
	cos ωt	.00910	.988	7.79	.227	.146	.214	.224	.174	.078	-.039	-.146	-.214	-.224	-.174	-.078	.039
	cos 2ωt	-.00094	1.98	.34	-.001	0	-.001	-.001	0	.001	.001	0	-.001	-.001	0	.001	.001
N'=2 REAR LEGS	sin ωt				.188	-.188	-.169	-.105	-.004	.082	.156	.188	.169	.105	.004	-.082	-.156
	sin 3ωt				-.001	-.001	.001	.001	-.001	-.001	.001	.001	-.001	-.001	.001	.001	-.001
	cos ωt				.227	-.016	.100	.188	.226	.204	.127	.016	-.100	-.188	-.226	-.204	-.127
	cos 2ωt				-.001	.001	.001	0	-.001	-.001	0	.001	.001	0	-.001	-.001	0
PLATFORM LONGITUDINAL DISPLACEMENT (INCHES)						-.195	.088	.345	.521	.547	.437	.209	-.076	-.335	-.511	-.535	-.423

FIGURE XVI - TABULAR CALCULATION FOR PLATFORM DISPLACEMENT

the Fourier series (57) are listed. It is apparent that a cosine varying force term leads the sine varying force term of the same frequency by a 90° time phase angle. In order to fit the cosine terms to the classical differential equation of forces (32) 90° is added to each of the cosine term reference angles, after which the term is treated as a sine function.

In the middle portion of the table the actual values of the angles for each of the terms are listed. For the front legs the angle ϕ is determined from (40) or Table II for each value of $\frac{n\omega}{\omega_n}$, where n is the coefficient of ωt. The angle ϕ is subtracted from the reference angle for each case, because displacement lags force (33). At the rear legs the force lags the force at the front legs by the lag angle $n\phi_{RL}$ (58). For each specific case the angle at the rear legs is found by subtracting $n\phi_{RL}$ from the corresponding angle at the front legs.

In the lower portion of the table the values of x_o (33) are calculated for each term of the Fourier series for displacement. The expression for the force coefficients F are given in (57). Values of the magnification factor $\frac{x_o}{x_{STATIC}}$ are determined from (38) or Table I.

The reader is cautioned that linear interpolation of Tables I or II may be poor in the immediate vicinity of resonance ($\frac{\omega}{\omega_n} = 1.0$).

In each of the twelve columns the value of x_o is multiplied by the sine of the appropriate angle from above, and the result is recorded. These results are added in each column to give values of platform longitudinal displacement x.

For this sample calculation the ratio of the maximum positive theoretical displacement to the maximum positive experimental displacement is 1.17.

C. Summary of Theoretical Calculations

Forces and Force Centroids

Table IV describes the 4 waves used in this thesis. The values H and L are measured, while $\frac{d+\eta_o}{d}$ is read directly from the computer output in Appendix D (or from (6)). For all runs d = 2.25 ft. Frequency (radians/second) is calculated from (8) by use of the relation $\omega = 2\pi C/L$.

TABLE IV - Wave Characteristics

Wave	H(ft.)	L(ft.)	d/L	H/L	J=2πd/L	$\frac{d+\eta_o}{d}$	$\frac{d+(\eta_o-H)}{d}$	ω
A	0.240	15.23	0.1476	0.01575	0.928	1.0557	0.949	3.10
B	0.313	10.86	0.207	0.0289	1.300	1.0715	0.932	4.00
C	0.361	8.82	0.255	0.0409	1.603	1.0817	0.921	4.60
D	0.404	7.33	0.307	0.0552	1.930	1.0908	0.911	5.13

Table V lists parameters used for computing drag forces. The multipliers A and B are read directly from the computer output (or from Figures IV and V, respectively), $\mathbb{R}$ and $\mathbb{R}_{trough}$ are computed from (18) and (19), respectively, while C_D and $C_{D\ trough}$ are read from Figure II.

TABLE V - Various Coefficients for Drag Force Determination

Wave	A	B	$\mathbb{R}$	C_D	$\mathbb{R}_{trough}$	$C_{D\ trough}$
A	0.00272	0.00191	1410	0.846	1188	0.846
B	0.00421	0.00276	1804	0.925	1591	0.885
C	0.00538	0.00318	2070	0.925	1720	0.925
D	0.00674	0.00342	2290	0.962	1795	0.925

Table VI lists the theoretical forces and force centroids on a single leg of the structure. F_D and $(F_D)_t$ are computed from (12) and (13), respectively, while F_I is computed from (25). The centroids $\bar{S}'$ and $(\bar{S}')_t$ are read directly from the computer output (or from Figure III), and $\bar{S}_I$ is computed from (28). Centroidal distances are measured from the bottom of the tank.

TABLE VI - Theoretical Forces and Force Centroids on a Single Leg

Wave	F_D(lbs.)	$\bar{S}'$(ft.)	$(F_D)_t$(lbs.)	$(\bar{S}')_t$(ft)	F_I(lbs)	$\bar{S}_I$(ft.)
A	0.01755	1.375	-0.01242	1.180	0.01485	1.200
B	0.0266	1.542	-0.01702	1.258	0.02295	1.260
C	0.0337	1.680	-0.0203	1.330	0.0283	1.328
D	0.0425	1.813	-0.0216	1.408	0.0329	1.380

Structure Natural Frequencies

Theoretical natural frequencies of the structure are computed by (47) and (61), using numbers from Appendix E. In Table VII run 3, for example, designates the unbraced model with 3 pounds of added weight on the platform. The letter Z designates the braced model. Experimental values of ω_n (Appendix F) are also given in Table VII for convenience of comparison. The units of all frequencies are radians/second.

TABLE VII - Structure Natural Frequencies

Run	ω_n theoretical	ω_n exp. in air	ω_n exp. in water
0	5.25	6.01	6.13
3	4.53	4.67	4.79
6	4.05	4.00	4.02
10	3.59	3.21	3.27
0Z	5.20	5.97	6.09
3Z	4.50	4.95	5.00
6Z	4.02	4.10	4.11
10Z	3.57	3.25	3.44

D. Computer Programs

Two separate IBM 7090 FORTRAN computer programs were written for use with this thesis. Part 1, "MAX DRAG FORCE MULTIPLIER AND DRAG CENTROID," was used both to develop the curves families of Figures III, IV, and V, and to supply exact values for force and centroid determination for the 4 waves studied.

Part 2, "TOWER DISPLACEMENTS," was used to supply the theoretical platform displacements for the 32 experimental runs of this thesis. The output from this program is shown plotted as Figures XIIa-p. The output from Part 1, although comprising data for 76 waves of differing characteristics, is included in this Appendix only for those waves which were the object of experimental study in this thesis. (The remaining output data has been submitted to the Thesis Supervisor under separate cover.)

Because the designer may want to make use of the programs, a brief description of their characteristics is included.

Part 1

This program was developed to facilitate solutions of drag forces and drag force centroids for crest and

trough regions. It is applicable only for those wave parameters for which Stokes' 3rd approximation applies. Its primary use is for development of curve families such that A, B, $\frac{\bar{S}'}{d}$ and $\frac{(\bar{S}')t}{d}$ in the formulas listed below may be read directly by the designer if no computer is available.

$$F_D = \frac{\gamma D d^2 C_D A}{2} \tag{12}$$

$$(F_D)_t = \frac{-\gamma D d^2 C_{D \text{ trough}} B}{2} \tag{13}$$

$$\frac{\bar{S}'}{d} = \frac{\int_0^{1+\eta_o/d} \frac{S'}{d} \frac{u_{max}^2}{gd} d(S'/d)}{A} \tag{26}$$

$$\frac{(\bar{S}')t}{d} = \frac{\int_0^{1+\frac{\eta_o - H}{d}} \frac{S'}{d} \frac{u_{trough}^2}{gd} d(S'/d)}{B} \tag{27}$$

where $A \equiv \int_0^{1+\eta_o/d} \frac{u_{max}^2}{gd} . d(S'/d)$ (14)

$$B \equiv \int_{0}^{\frac{1+\eta_o-H}{d}} \frac{u^2_{trough}}{gd} . d(S'/d) \qquad (15)$$

Integration of (26,27,14, and 15) is performed by the trapezoidal rule with 21 unequally special stations.

The curve families developed (Figures III, IV, V) show lines of constant H/L on graphs whose coordinates are the desired values vs. d/L.

A secondary function of the program is to supply horizontal-component velocity profiles at wave angles $\theta = 90°$ and $270°$. Two uses of these profiles are to give specific indication of the limit of applicability of the authors' design procedure and to supply required information for an analysis of transverse vortex shedding forces (Appendix I).

Supplementary information which may be read directly from the output includes:

$$\frac{d + \eta_o}{d} , \frac{d + (\eta_o - H)}{d} , \frac{U_{max}}{\sqrt{gd}} , \frac{U_{trough}}{\sqrt{gd}}$$

Wave celerity C, although determined internally as $\frac{C}{\sqrt{gd}}$, is not included in the output. However, the simple inclusion of this parameter (called "T" in the program) in the WRITE OUTPUT TAPE, DIMENSION, and output FORMAT statements would cause it to be written output.

Variables to be read into the program on data cards are defined as follows:

$X = d/H$

$Y = L/H$

The above data for each run is put on the same card in accordance with FORMAT statement 10. Variables written as output are:

$X = d/H$

$Y = L/H$

A

$CENTC = \frac{\bar{S}'}{d}$

B

$CENTT = \frac{(\bar{S}')t}{d}$

$PC = (S'/d)n \qquad n = 0, 20$

$UC = (\frac{u_{max}}{\sqrt{gd}})_n \qquad n = 0, 20$

$$UCSQ = \left(\frac{u_{max}^2}{gd}\right)_n \qquad n = 0, 20$$

$$PT = \left(\frac{S'_{trough}}{d}\right)_n \qquad n = 0, 20$$

$$UT = \left(\frac{u_{trough}}{\sqrt{gd}}\right)_n \qquad n = 0, 20$$

$$UTSQ = \left(\frac{u_{trough}^2}{gd}\right)_n \qquad n = 0, 20$$

Values of PC, UC, UCSQ, PT, UT, and UTSQ are given in incremental steps of S/d (not S'/d) of 0.05 from the bottom to the still water level. At n = 20 it is seen that the following result:

$$PC = \frac{d + \eta_o}{d}$$

$$UC = \frac{U_{max}}{\sqrt{gd}}$$

$$UCSQ = \frac{U_{max}^2}{gd}$$

$$PT = \frac{d + (\eta_o - H)}{d}$$

$$UT = \frac{U_{trough}}{\sqrt{gd}}$$

$$UTSQ = \frac{U_{trough}^2}{gd}$$

The output is written in accordance with FORMAT statements 90 and 100, and is included in this appendix for the A, B, C, and D waves only.

If other than 36 input data cards are to be used, the program must be run separately for each set of 36, with blank cards being used to fill out any set not comprising 36 data cards. A card with zeros punched in the x columns should be used to separate the data from the blank cards.

Some of the interesting aspects of the output used to develop Figures III, IV, and V are discussed in Appendix G.

```
* M1933-1598,FMS,DEBUG,2,4,1000,0

*       XEQ
*       LIST

        W. C. NOLAN AND V. C. HONSINGER

C       WAVE INDUCED VIBRATIONS IN FIXED OFFSHORE STRUCTURES
C       PART 1, MAX DRAG FORCE MULTIPLIER AND DRAG CENTROID
C
        DIMENSION X(36),Y(36),A(36),B(36),CENTC(36),CENTT(36),PC(21,36),
       1PT(21,36),UC(21,36),UT(21,36),UCSQ(21,36),UTSQ(21,36)
        READ INPUT TAPE 4,10, (X(I),Y(I),I=1,36)
   10 FORMAT (2F10.4)
        DO 60 I=1,36
        N=I
        IF (X(I)) 70,70,20
   20 Z=6.2832*X(I)/Y(I)
        D=EXPF(Z)-EXPF(-Z)
        E=TANHF(Z)
        F=EXPF(2.*Z)+EXPF(-2.*Z)
        T=SQRTF((E/Z)*(1.+(9.8697/Y(I)**2.)*(F**2.+2.*F+10.)/D**4.))
        R=0
        DO 50 J=1,21
        GP=EXPF(Z*R)+EXPF(-Z*R)
        GM=EXPF(Z*R)-EXPF(-Z*R)
        HP=EXPF(2.*Z*R)+EXPF(-2.*Z*R)
        HM=EXPF(2.*Z*R)-EXPF(-2.*Z*R)
        PP=R+9.4248*HM/(2.*X(I)*Y(I)*D**4.)
        UU=(9.8697*T/((Y(I)**2.)*D**2.))*(-2.+6.*HP/D**2.+HP)
        PC(J,I)=PP+GM/(2.*X(I)*D)
        PT(J,I)=PP-GM/(2.X(I)*D)
        UC(J,I)=UU+3.1416*T*GP/(Y(I)*D)
        UCSQ(J,I)=UC(J,I)**2.
        UT(J,I)=UU-3.1416*T*GP/(Y(I)*D)
        UTSQ(J,I)=UT(J,I)**2.
        IF(J-1) 30,30,40
   30 A(I)=0
        B(I)=0
        WC=0
        WT=0
        GOTO 50
   40 A(I)=A(I)+(UCSQ(J,I)+UCSQ(J-1,I))*(PC(J,I)-PC(J-1,I))/2.
        B(I)=B(I)+(UTSQ(J,I)+UTSQ(J-1,I))*(PT(J,I)-PT(J-1,I))/2.
        WC=WC+(UCSQ(J,I)+UCSQ(J-1,I))*(PC(J,I)**2.-PC(J-1,I)**2.)/4.
        WT=WT+(UTSQ(J,I)+UTSQ(J-1,I))*(PT(J,I)**2.-PT(J-1,I)**2.)/4.
   50 R=R+.05
        CENTC(I)=WC/A(I)
   60 CENTT(I)=WT/B(I)
   70 DO 80 M=1,N
        WRITE OUTPUT TAPE 2,90,X(M),Y(M),A(M),CENTC(M),B(M),CENTT(M),
       1PC(1,M),UC(1,M),UCSQ(1,M),PT(1,M),UT(1,M),UTSQ(1,M)
        WRITE OUTPUT TAPE 2,100,(PC(J,M),UC(J,M),UCSQ(J,M),PT(J,M),UT(J,M
       1),UTSQ(J,M), J=2,21  )
   80 CONTINUE
   90 FORMAT (2F10.6,10F9.6)
  100 FORMAT(56X,6F9.6)
        CALL EXIT
        END(1,1,0,0,0,0,0,0,0,0,0,0,0,0,0)
```

d/H	L/H	A	$\frac{\bar{s}'}{d}$	B	$\frac{\bar{s}_t}{d}$	$\frac{s'}{d}$	$\frac{u_{max}}{gd}$	$\frac{u^2_{max}}{gd}$	$\frac{s'_{trough}}{d}$	$\frac{u_{trough}}{gd}$	$\frac{u^2_{trough}}{gd}$
9.380000	63.500000	0.002722	0.611706	0.001910	0.524623	0.	0.042524	0.001808	0.	-0.040005	0.001600
						0.052390	0.042578	0.001813	0.047752	-0.040039	0.001603
						0.104785	0.042740	0.001827	0.095500	-0.040144	0.001612
						0.157191	0.043011	0.001850	0.143239	-0.040319	0.001626
						0.209614	0.043391	0.001883	0.190965	-0.040563	0.001645
						0.262060	0.043882	0.001926	0.238673	-0.040877	0.001671
						0.314534	0.044486	0.001979	0.286354	-0.041262	0.001703
						0.367043	0.045204	0.002043	0.334019	-0.041717	0.001740
						0.419591	0.046040	0.002120	0.381648	-0.042242	0.001784
						0.472186	0.046994	0.002208	0.429241	-0.042837	0.001835
						0.524833	0.048072	0.002311	0.476794	-0.043503	0.001893
						0.577539	0.049277	0.002428	0.524303	-0.044240	0.001957
						0.630310	0.050612	0.002562	0.571762	-0.045047	0.002029
						0.683153	0.052082	0.002713	0.619166	-0.045926	0.002109
						0.736075	0.053692	0.002883	0.666512	-0.046875	0.002197
						0.789083	0.055449	0.003075	0.713795	-0.047895	0.002294
						0.842185	0.057358	0.003290	0.761008	-0.048985	0.002400
						0.895387	0.059425	0.003531	0.808148	-0.050145	0.002515
						0.948699	0.061659	0.003802	0.855209	-0.051375	0.002639
						1.002129	0.064067	0.004105	0.902186	-0.052675	0.002775
						1.055685	0.066658	0.004443	0.949075	-0.054043	0.002921
7.180000	34.700000	0.004206	0.685431	0.002759	0.559225	0.	0.044294	0.001962	0.	-0.043083	0.001856
						0.052704	0.044401	0.001971	0.047370	-0.043160	0.001863
						0.105420	0.044724	0.002000	0.094730	-0.043393	0.001883
						0.158160	0.045263	0.002049	0.142068	-0.043780	0.001917
						0.210935	0.046024	0.002118	0.189374	-0.044323	0.001965
						0.263759	0.047009	0.002210	0.236637	-0.045024	0.002027
						0.316644	0.048225	0.002326	0.283846	-0.045882	0.002105
						0.369602	0.049680	0.002468	0.330990	-0.046900	0.002200
						0.422646	0.051382	0.002640	0.378057	-0.048078	0.002312
						0.475791	0.053342	0.002845	0.425036	-0.049419	0.002442
						0.529050	0.055572	0.003088	0.471915	-0.050925	0.002593
						0.582438	0.058087	0.003374	0.518681	-0.052596	0.002766
						0.635970	0.060901	0.003709	0.565322	-0.054435	0.002963
						0.689663	0.064033	0.004100	0.611824	-0.056444	0.003186
						0.743532	0.067505	0.004557	0.658175	-0.058623	0.003437
						0.797597	0.071337	0.005089	0.704360	-0.060974	0.003718
						0.851875	0.075557	0.005709	0.750369	-0.063497	0.004032
						0.906386	0.080192	0.006431	0.796172	-0.066192	0.004381
						0.961152	0.085275	0.007272	0.841769	-0.069059	0.004769
						1.016196	0.090841	0.008252	0.887139	-0.072095	0.005198
						1.071540	0.096930	0.009395	0.932264	-0.075296	0.005670
6.230000	24.450000	0.005381	0.746012	0.003177	0.590742	0.	0.041733	0.001742	0.	-0.041139	0.001692
						0.052724	0.041884	0.001754	0.047315	-0.041254	0.001702
						0.105465	0.042338	0.001793	0.094613	-0.041598	0.001730
						0.158243	0.043100	0.001858	0.141878	-0.042173	0.001779
						0.211074	0.044176	0.001951	0.189091	-0.042981	0.001847
						0.263979	0.045575	0.002077	0.236236	-0.044024	0.001938
						0.316974	0.047310	0.002238	0.283295	-0.045306	0.002053
						0.370081	0.049396	0.002440	0.330250	-0.046830	0.002193
						0.423321	0.051853	0.002689	0.377081	-0.048601	0.002362
						0.476713	0.054702	0.002992	0.423769	-0.050623	0.002563
						0.530282	0.057970	0.003361	0.470293	-0.052902	0.002799
						0.584050	0.061688	0.003805	0.516633	-0.055442	0.003074
						0.638043	0.065890	0.004341	0.562765	-0.058249	0.003393
						0.692287	0.070616	0.004987	0.608668	-0.061327	0.003761
						0.746812	0.075914	0.005763	0.654312	-0.064680	0.004183
						0.801648	0.081835	0.006697	0.699675	-0.068310	0.004666
						0.856828	0.088440	0.007822	0.744729	-0.072220	0.005216
						0.912388	0.095798	0.009177	0.789443	-0.076407	0.005838
						0.968365	0.103985	0.010813	0.833786	-0.080869	0.006540
						1.024800	0.113090	0.012789	0.877726	-0.085597	0.007327
						1.081740	0.123214	0.015182	0.921227	-0.090581	0.008205
5.575000	18.140000	0.006742	0.806107	0.003418	0.624576	0.	0.036887	0.001361	0.	-0.036639	0.001342
						0.052578	0.037079	0.001375	0.047440	-0.036791	0.001354
						0.105180	0.037655	0.001418	0.094856	-0.037246	0.001387
						0.157831	0.038624	0.001492	0.142224	-0.038008	0.001445
						0.210556	0.039998	0.001600	0.189521	-0.039081	0.001527
						0.263380	0.041792	0.001747	0.236721	-0.040470	0.001638
						0.316330	0.044031	0.001939	0.283798	-0.042182	0.001779
						0.369435	0.046741	0.002185	0.330726	-0.044227	0.001956
						0.422724	0.049958	0.002496	0.377477	-0.046614	0.002173
						0.476227	0.053723	0.002886	0.424020	-0.049354	0.002436
						0.529978	0.058086	0.003374	0.470325	-0.052458	0.002752
						0.584013	0.063106	0.003982	0.516357	-0.055937	0.003129
						0.638371	0.068849	0.004740	0.562080	-0.059801	0.003576
						0.693093	0.075398	0.005685	0.607456	-0.064062	0.004104
						0.748225	0.082844	0.006863	0.652442	-0.068725	0.004723
						0.803816	0.091297	0.008335	0.696994	-0.073796	0.005446
						0.859920	0.100882	0.010177	0.741063	-0.079275	0.006285
						0.916597	0.111747	0.012487	0.784596	-0.085155	0.007251
						0.973913	0.124064	0.015392	0.827536	-0.091421	0.008358
						1.031938	0.138031	0.019053	0.869820	-0.098046	0.009613
						1.090752	0.153882	0.023680	0.911380	-0.104989	0.011023

PART 2

This program performs the tabular calculation of Figure XVI. It is written for the specific case of N = 4 legs and k = 0.625 lb./in. In the expressions for S, T, U, V, and W the constants are recognized to be $\frac{N}{k}$ or $\frac{N'}{k}$. For different values of N or k the constants may be changed by substituting new values in the program.

Variables to be read into the program on data cards are defined as follows:

y = run number

A = ω/ω_n

B = C/C_c

C = ϕ_{RL} (radians)

DD = $\frac{F_1 - F_2}{4}$ (lbs.)

P = $\frac{4}{3\pi}$ $(F_1 + F_2)$ (lbs.)

Q = $-\frac{4}{15\pi}$ $(F_1 + F_2)$ (lbs.)

R = F_3 (lbs.)

The above data for each run is put all on the same card in accordance with FORMAT statement 10.

Variables written as output are:

y = run number

x = platform longitudinal displacement (in.)

This output is written on a single line for each run, in accordance with FORMAT statement 100. For each input data card 12 values of platform displacement are computed, these values corresponding to the 12 angular wave positions θ indicated at the top of Figure XVI.

If more than 32 runs are to be used, the program must be run separately for each set of 32, with blank cards being used to fill out any set not comprising 32 data cards.

```
*M1933-1598,FMS,DEBUG,2,4,500,0

*       XEQ
*       LIST

        W.C.NOLAN AND V.C.HONSINGER

C       WAVE INDUCED VIBRATIONS IN FIXED OFFSHORE STRUCTURES
C       PART 2, TOWER DISPLACEMENTS

        DIMENSION Y(32),A(32),B(32),C(32),DD(32),P(32),Q(32),R(32),THETA(4
       1,12),X(32,12)
        READ INPUT TAPE 4,10,(Y(I),A(I),B(I),C(I),DD(I),P(I),Q(I),R(I),I=1
       1,32)
   10 FORMAT (IF 3.0,7F8.5)
        DO 90 I=1,32
        D=2.*C(I)
        E=3.*C(I)
        FF=2.*A(I)*B(I)/(1.-(A(I))**2.)
        IF(FF) 20,30,30
   20 FF=FF+3.14159
   30 CONTINUE
        F=ATANF (FF)
        GG=4.*A(I)*B(I)/(1.-4.*(A(I))**2.)
        IF(GG) 40,50,50
   40 GG=GG + 3.14159
   50 CONTINUE
        G=ATANF (GG)
        HH=6.*A(I)*B(I)/(1.-9.*(A(I))**2.)
        IF(HH) 60,70,70
   60 HH=HH + 3.14159
   70 CONTINUE
        H=ATANF (HH)
        AA=1./SQRTF((1.-A(I)**2.)**2. + (2.*A(I)*B(I))**2.)
        BB=1./SQRTF((1.-4.*(A(I))**2.)**2. + (4.*A(I)*B(I))**2.)
        CC=1./SQRTF((1.-9.*(A(I))**2.)**2. + (6.*A(I)*B(I))**2.)
        S=6.4*DD(I)
        T=3.2*P(I)*AA
        U=3.2*Q(I)*CC
        V=3.2*R(I)*AA
        W=-3.2*DD(I)*BB
        DO 80 J=1,12
        Z=J
        THETA(1,J)=0.5236*Z
        THETA(2,J)=1.5708*Z
        THETA(3,J)=1.5708 + 0.5236*Z
        THETA(4,J)=1.5708 + 1.0472*Z
        X(I,J)=S + T*SINF(THETA(1,J)-F) + U*SINF(THETA(2,J)-H) + V*SINF(TH
       1ETA(3,J)-F) + W*SINF(THETA(4,J)-G) + T*SINF(THETA(1,J)-F-C(I)) + U
       2*SINF(THETA(2,J)-H-E) + V*SINF(THETA(3,J)-F-C(I)) + W*SINF(THETA(4
       3,J)-G-D)
   80 CONTINUE
   90 CONTINUE
  100 FORMAT(1F6.0,12F7.3)
        DO 110 I=1,32
        WRITE OUTPUT TAPE 2,100,Y(I),(X(I,J),J=1,12)
  110 CONTINUE
        CALL EXIT
        END(1,1,0,0,0,0,0,0,0,0,0,0,0,0,0)
```

E. Sample Calculations for Experimental Data

B wave

Wave period T:

Sanborn recorder speed = 25 mm/sec.

Wave length as measured on recorder = 40 mm.

Therefore $T = 40/25 = 1.60$ sec.

Wave circular frequency ω:

$$\omega = \frac{2\pi}{T} = \frac{2\pi}{1.60} = 3.93 \text{ radians/sec.}$$

Wave height H is read from the experimental wave profile (Figure XVIIb).

Wave forces:

Wave drag and inertia forces are read directly from the experimental force record (Figure XVIIb).

$$F_D \quad (\theta = 90°) = 0.044 \text{ lbs.}$$
$$(F_D)_t \quad (\theta = 270°) = -0.039 \text{ lbs.}$$
$$F_I \quad (\theta = 180°) = 0.017 \text{ lbs.}$$

Properties of the Structure Model

Consider run 6 and calculate the structural damping by (42) and (44).

$$\text{average } \frac{x_1}{x_2} = \frac{1}{5}\left(\frac{.92}{.64} + \frac{.93}{.63} + \frac{.64}{.43} + \frac{.62}{.43} + \frac{.43}{.29}\right) = 1.47$$

$$\delta = \log_e(1.47) = 0.385 \qquad (42)$$

$$\frac{c}{c_c} = \frac{0.385}{2\pi} = 0.0613 \qquad (44)$$

Damped natural frequency:

$$q = \frac{3 \text{ cycles}}{4.73 \text{ sec.}}(2\pi) = 3.99 \text{ radians/second}$$

From (45):

$$\omega_n = \frac{3.99}{\sqrt{1 - (0.0613)^2}} = 4.00 \text{ radians/second}$$

The volume of plastic in the unbraced model (including base) is:

$$\left[(18\tfrac{1}{16})^2 - \tfrac{\pi}{4}(\tfrac{7}{16})^2\right]\left[0.610\right] + 4\tfrac{\pi}{4}(0.505)^2(42) + (30\tfrac{1}{8} - \tfrac{1}{4})(22)(\tfrac{1}{2})$$

$$= 199 + 33.6 + 329 = 561.6 \text{ in}^3$$

For one leg:

$$wl = (\tfrac{1}{4})(\tfrac{33.6}{561.6})(22\tfrac{3}{4}) = 0.340 \text{ lb.}$$

For the platform:

The bolt weighs 0.200 lb.

$$W = \left(\frac{199}{561.6}\right)\left(22\frac{3}{4}\right)(4) + 0.200 = 8.25 \text{ lb.}$$

Calculate the following non-dimensional ratios.

From (59):

$$r_m = \frac{(4)(0.340) + 0.4}{(4)(0.340)} = 1.29$$

From (63):

$$r_D = 1 + \left[\frac{149}{(4)(27)}\right]\left[\frac{\frac{1}{4}}{\frac{1}{2}}\right] = 1.69$$

From (65):

$$r_I = 1 + \left[\frac{149}{(4)(27)}\right]\left[\frac{\frac{1}{4}}{\frac{1}{2}}\right]^2 = 1.34$$

F. Summary of Calculations for Experimental Data

Wave Characteristics

Wave profiles for waves A-D are shown in Figure XVII a-d, respectively. The crest is in all cases the 8th wave crest to pass the cylinder. Wave phase angle θ is set equal to 90° at the crest.

TABLE VIII - Experimental Wave Characteristics

Wave	H(ft.)	L(ft.)	d(ft.)	T (sec.)	ω (radians/sec)
A	0.240	15.23	2.25	2.00	3.14
B	0.313	10.86	2.25	1.60	3.93
C	0.361	8.82	2.25	1.40	4.49
D	0.404	7.33	2.25	1.26	4.99

Longitudinal Wave Forces

Experimental and theoretical longitudinal forces associated with waves A-D are shown in Figure XVIIa-d, respectively. The forces are read as follows:

F_D at $\theta = 90°$

$(F_D)_t$ at $\theta = 270°$

F_I at $\theta = 0°$

Figure XVIIa also shows experimental transverse forces caused by vortex shedding in the A wave.

The experimental longitudinal forces read from Figure XVII are given in Table IX.

TABLE IX - Experimental Wave Forces, $\frac{1}{2}$" Cylinder

Wave	F_D (lbs.)	$(F_D)_t$ (lbs.)	F_I (lbs.)
A	0.014	-0.019	0.017
B	0.044	-0.039	0.023
C	0.060	-0.055	0.022
D	0.085	-0.039	0.032

Figure XVIIa

Longitudinal and Transverse Forces

1/2" Cylinder - A Wave

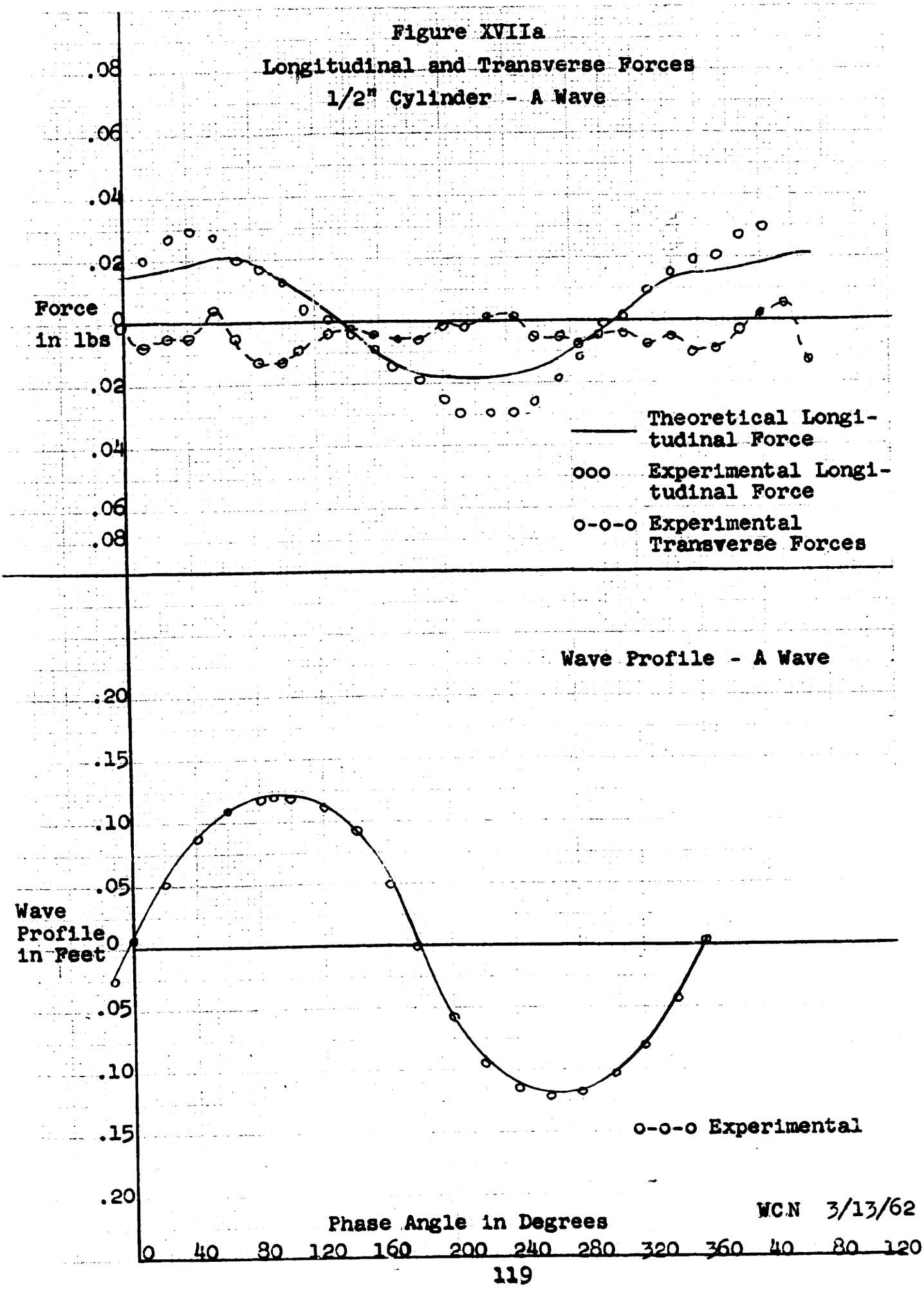

WCN 3/13/62

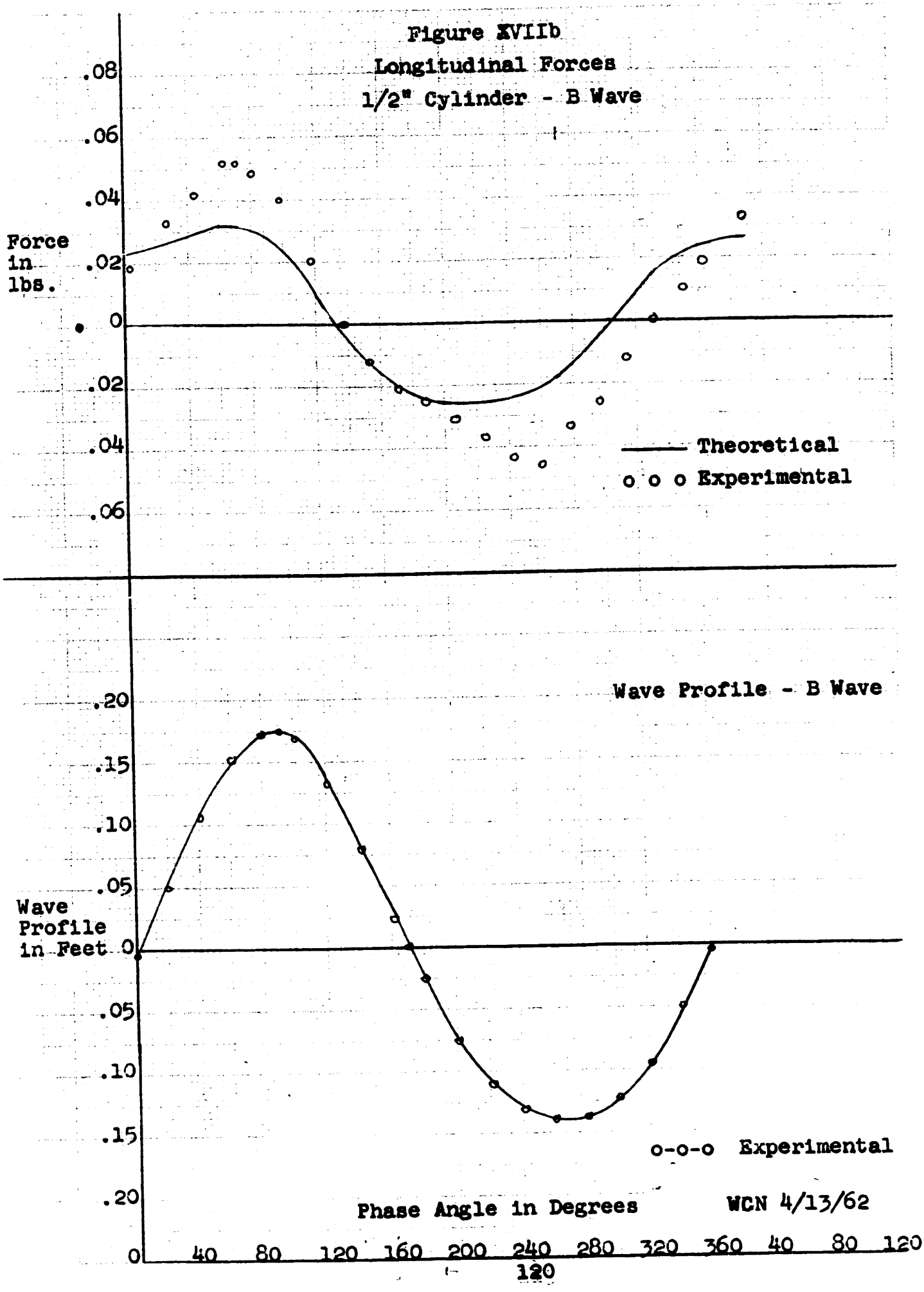
Figure XVIIb
Longitudinal Forces
1/2" Cylinder - B Wave
Force in lbs.
.08
.06
.04
.02
0
.02
.04
.06
Theoretical
o o o Experimental
Wave Profile - B Wave
Wave Profile in Feet
.20
.15
.10
.05
0
.05
.10
.15
.20
o-o-o Experimental
Phase Angle in Degrees
WCN 4/13/62
0
40
80
120
160
200
240
280
320
360
40
80
120
120

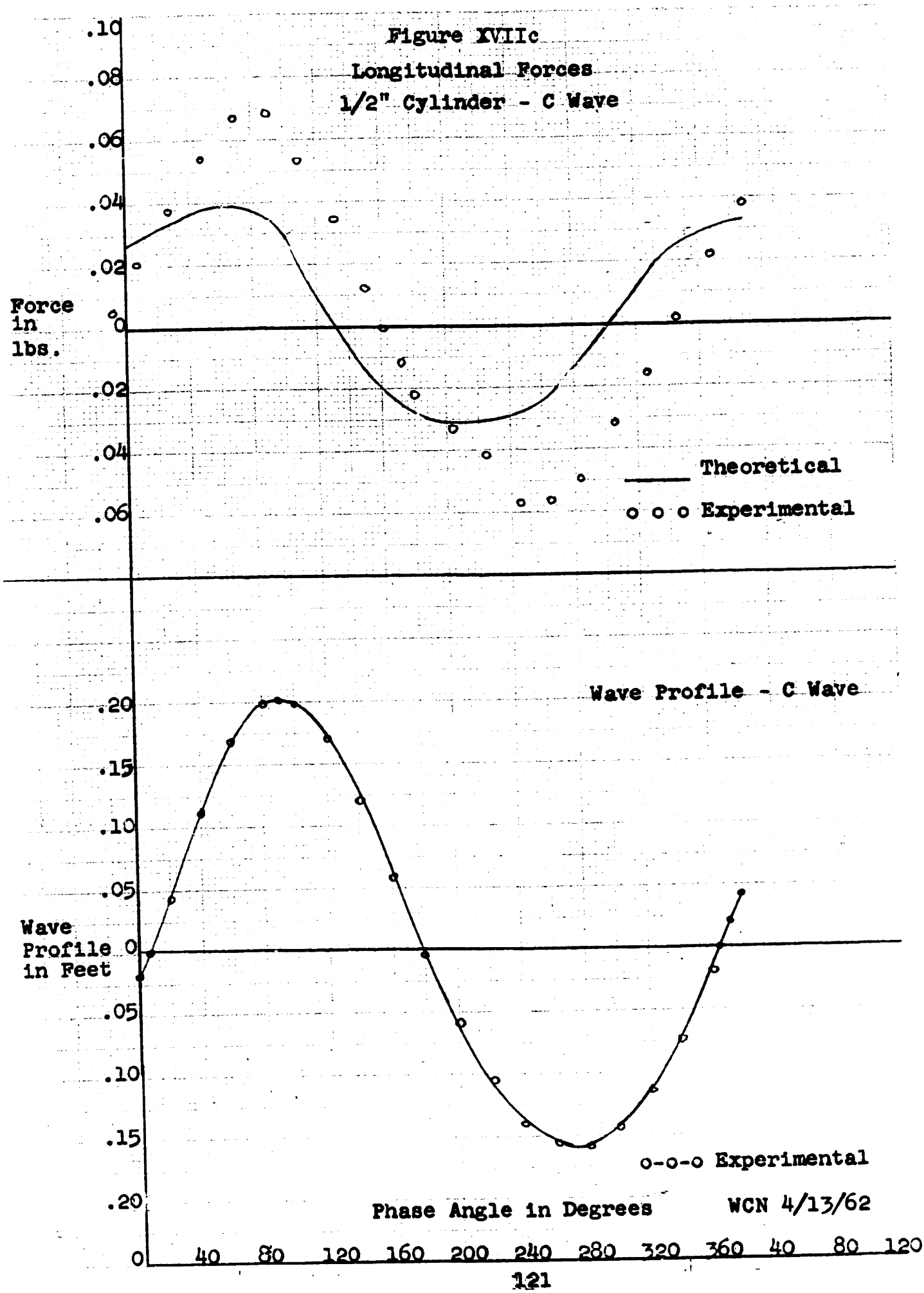
Figure XVIIc
Longitudinal Forces
1/2" Cylinder - C Wave
.10
.08
.06
.04
.02
0
.02
.04
.06
Force in lbs.
Theoretical
o o o Experimental
Wave Profile - C Wave
.20
.15
.10
.05
0
.05
.10
.15
.20
Wave Profile in Feet
o-o-o Experimental
Phase Angle in Degrees
WCN 4/13/62
0
40
80
120
160
200
240
280
320
360
40
80
120

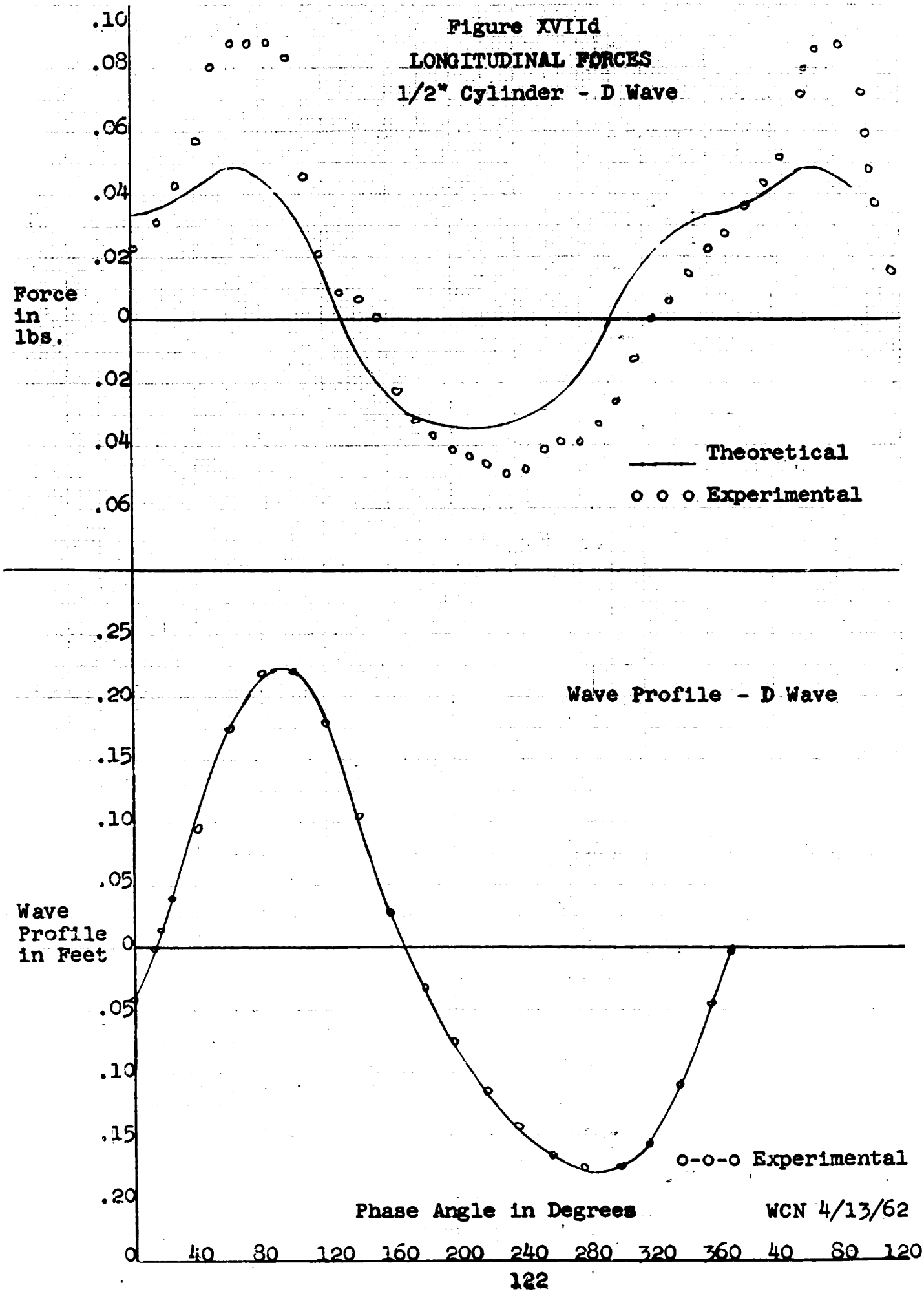
Figure XVIId
LONGITUDINAL FORCES
1/2" Cylinder - D Wave
.10
.08
.06
.04
.02
Force in lbs.
0
.02
.04
.06
Theoretical
o o o Experimental
.25
.20
.15
.10
.05
Wave Profile - D Wave
Wave Profile in Feet
0
.05
.10
.15
.20
o-o-o Experimental
Phase Angle in Degrees
WCN 4/13/62
0
40
80
120
160
200
240
280
320
360
40
80
120

Properties of the Structure Model

TABLE X - Experimental Damping and Structure Natural Frequencies

Run	Total Damping (as fraction of critical)	Structural damping $\frac{C}{C_c}$	Viscous damping (as fraction of critical)	Damped Natural Frequency q (rad/sec)	Undamped Natural Frequency ω_n (rad/sec)
0	0.0501	0.0501	0	6.00	6.01
3	0.0548	0.0548	0	4.66	4.67
6	0.0613	0.0613	0	3.99	4.00
10	0.0748	0.0748	0	3.20	3.21
0-W	0.0558	0.0501	0.0057	6.12	6.13
3-W	0.0580	0.0548	0.0032	4.78	4.79
6-W	0.0655	0.0613	0.0042	4.01	4.02
10-W	0.0748	0.0748	0	3.26	3.27
0Z	0.0501	0.0501	0	5.96	5.97
3Z	0.0559	0.0559	0	4.94	4.95
6Z	0.0613	0.0613	0	4.09	4.10
10Z	0.0738	0.0738	0	3.24	3.25
0Z-W	0.0547	0.0501	0.0046	6.08	6.09
3Z-W	0.0592	0.0559	0.0033	4.99	5.00
6Z-W	0.0645	0.0613	0.0032	4.10	4.11
10Z-W	0.0730	0.0738	--	3.43	3.44

Spring constant k (46) was determined experimentally:

$k = 0.625$ pounds/inch

G. Supplementary Discussion of Results

1. Theory and Experiment

Longitudinal Forces

A glance at the longitudinal force plots of Figures XVII a-d shows considerable disagreement between theory and experiment. Theoretical forces (drag and inertia) are tabulated in Table VI, and experimental forces are in Table IX. These tables show close agreement of inertia forces, with the drag forces differing by a factor of 2, in cases.

Prior users of the force gage have indicated that the dynamic response of the gage to exciting forces may indicate forces greater than the actual [28]. However, the authors conclude that for the frequencies associated with the waves used in this thesis any magnification factor applied to force gage displacements would in all cases be less than 1.1.

The proposal to use the rms velocity in the Reynolds numbers for drag coefficient determination is based upon the assumption that C_D and $C_{D\ trough}$ are independent of depth [17]. For the waves studied the lowest velocity encountered in the crest region is (theoretically) at the

bottom of the tank for the D wave. From Appendix D it is seen that $\frac{u_{max}}{\sqrt{gd}} = 0.0369$ for this situation. Therefore, $u_{max} = 0.315$ ft./sec. and $R = 1092$ for this region. When this value is compared with the Reynolds numbers listed in Table V, a glance at Figure II shows that the above assumption is valid for the waves studied in this thesis. However, if a local R at the bottom of a structure leg becomes less than about 100 in ocean waves, the assumption will lead to inaccuracies.

The drag and inertia components were of the same order of magnitude for the experimental runs of this thesis. Harleman and Shapiro [27] have found that for this particular situation agreement is not good between the proposed theoretical forces and the experimental forces. Because the theoretical and experimental inertia forces of this thesis agree quite closely, (Tables VI and IX), it is suspected that the discrepency is due to the method of evaluating the drag force component. Experiments conducted by Wiegel, Beebe, and Moon [5] to determine average values of C_D in a wave train show much scatter, with C_D varying between 0.2 and 2.5 for Reynolds numbers of around 10^4. They suggest that a factor of between 2.0 and 2.5 be applied to the drag force if an average value of C_D is used.

Keulegan and Carpenter [32], in their work with horizontal cylinders, have related C_D to the period parameter $\frac{u_{max}T}{D}$ rather than to some Reynolds number. If the drag coefficient is to be averaged over the height of a vertical cylinder, the authors suggest that C_D and $(C_D)_{trough}$ be included with A and B in the computer program (Appendix D). A look-up table for drag coefficient, based upon the curve of C_D vs $\frac{u_{max}T}{D}$ in [32], would have to be included in the program.

Free Oscillations and Natural Frequencies of the Structure Model

In Appendix H it will be seen that the free oscillation data is somewhat odd in that when the structure swings from a negative peak to a positive peak the amplitude of displacement often increases. Theoretically for the damped system this amplitude must decrease [22]. When the authors saw this result they immediately suspected unequal spring constants in the two directions, but a test showed that the spring constants were the same. The authors are unable to explain this oddity.

It is seen in Appendix F (or C) that in all configurations the natural frequency of the model is higher in still water than in air. One expects just the reverse,

because of viscous damping by the water and the added mass effect. The authors cannot explain this result, but they conclude that the added mass effect is negligible.

It is also seen that for all runs with the added weights the frequency of the braced structure model is higher than that for the unbraced structure model, both in air and in water. Theoretically spring constant k was not changed when the model was braced. Consequently, the addition of the bracing mass should have lowered the natural frequency $\omega_n (= \sqrt{k/m})$. Because the frequency is higher, however, for the braced model, it is probable that the bracing increased the stiffness k slightly. The authors did not suspect this result at the time of the experiment, however, and consequently stiffness k was not measured for the braced model.

2. Computer

It is mentioned in Appendix D that velocity profiles at crest and trough regions were written as output for the computer program used to develop Figures III, IV and V. These profiles, most of which are not submitted in this thesis (see comment, p. 103), show some interesting aspects relative to the boundary limits on Figure V. The

profiles of particular interest are those for the trough region. The computer output gives values of $\frac{u_{trough}}{\sqrt{gd}}$ vs $\frac{S'_{trough}}{d}$.

For certain critical values of wave parameters d/L and H/L, the peak value of $|u_{trough}|$ is shown to occur at some level other than at the surface, sometimes at the ocean bottom. In the extreme situation u_{trough} at the surface ($= U_{trough}$) becomes positive. Table XI gives the values of $\frac{u_{trough}}{\sqrt{gd}}$ associated with these critical parameters. The dimensionless velocity $\frac{U_{trough}}{\sqrt{gd}}$ refers to the velocity at the surface, and $\frac{u_{bottom}}{\sqrt{gd}}$ refers to the velocity at the ocean bottom under the wave trough. The dimensionless parameter $(\frac{S'_{trough}}{d})_{max}$ refers to the surface elevation of the trough, and $(\frac{S'_{trough}}{d})_{crit}$ refers to the elevation at which the absolute velocity is either a maximum or zero, as appropriate. Values of d/H and L/H are included in Table XI because the computer output is identified by these terms.

The authors suggest that the reader refer to Figure V while interpreting the information in Table XI.

First, for d/L = 0.07 and H/L = 0.04, it is seen from Table XI that the predicted height of the trough is above the still water level. This result, then, can be

TABLE XI - Trough Velocities Associated with Critical Wave Parameters

d/L	H/L	d/H	L/H	$\frac{U_{trough}}{\sqrt{gd}}$	$(\frac{S'_{trough}}{d})_{max}$	$\frac{u_{bottom}}{\sqrt{gd}}$	$(\frac{S'_{trough}}{d})_{crit}$
0.20	0.10	2.000	10.00	-0.1809	0.777	-0.1636	0.680
0.25	0.14	1.786	7.14	-0.1937	0.739	-0.1592	0.650
0.10	0.03	3.333	33.33	-0.0960	--	-0.1057	--
0.15	0.08	1.875	12.50	-0.1588	--	-0.1904	--
0.07	0.04	1.750	25.00	+0.1269	1.030	+0.0021	1.030
0.08	0.05	1.600	20.00	+0.0788	0.976	-0.0646	0.650
0.10	0.08	1.250	12.50	+0.0685	0.901	-0.1686	0.775

discarded as being outside the range of possibility. It is interesting to note that this situation is reached when Stokes' 3rd approximation predicts positive velocities in the trough region from surface to bottom.

If the remainder of the data is compared with the curve families of Figure V, the following observations are noted:

1. Each curve of the curve families reaches a peak value, which occurs approximately where Stokes' 3rd approximation predicts a positive velocity for trough regions above some $(\frac{S'_{trough}}{d})_{crit}$.

2. Values of the parameters corresponding to the above situation are seen to fall approximately on line H/d = 0.653, which has been stated to be the theoretical limit for wave characteristics in the ocean. The profile of positive velocity, beginning at the surface and extending down as d/L is decreased, is a result of the increasing significance of mass transport in Stokes' 3rd approximation.

3. Values of the parameters for which u_{trough} is never positive (and for which its peak value does not occur at the surface) are seen to fall approximately on the line for which H/d = 0.603. This line corresponds to the limit of applicability of Stokes' theory.

With regard to the statements made above, it is to be noted that, when plotted on the curve families of Figures III, IV, and V, lines of constant H/d converge for low values of d/L. Also, in explanation of observation number 1 above, it must be remembered that in solving for the force multiplier B from (15) it is

assumed that u_{trough} is negative for all $\frac{S'_{trough}}{d}$. If the proposed procedure is to be extended to regions for which this is not true, then $|u_{trough}|\ u_{trough}$ should be substituted for u^2_{trough} in (15).

H. Original Experimental Data

Water temperatures (°F) for the various runs are given in Table XII.

TABLE XII. Water Temperatures (°F)

Wave	Unbraced Structure	Braced Structure	Forces on Single Cylinder
A	62	57	63
B	62	61	63
C	62	61	63
D	62	61	63

A typical wave gage calibration curve is shown in Figure XVIII. A typical force gage calibration curve is shown in Figure XIX. "Record reading" on these curves refers to the deflection of the stylus needle on the Sanborn recorder. The wave gage is calibrated about the still water level, while the force gage is calibrated about the zero force position. Typical Sanborn recorder wave profile traces are shown in Figures XX and XXI.

The damped natural frequency of the 0.5 in. dia. cylinder/force-gage combination was 4.8 cps, while for the 1 in. dia. cylinder/force-gage combination (used for transverse forces) it was 17.85 cps.

Figure XVIII

Typical Wave Gage Calibration

(For B Wave Profile)

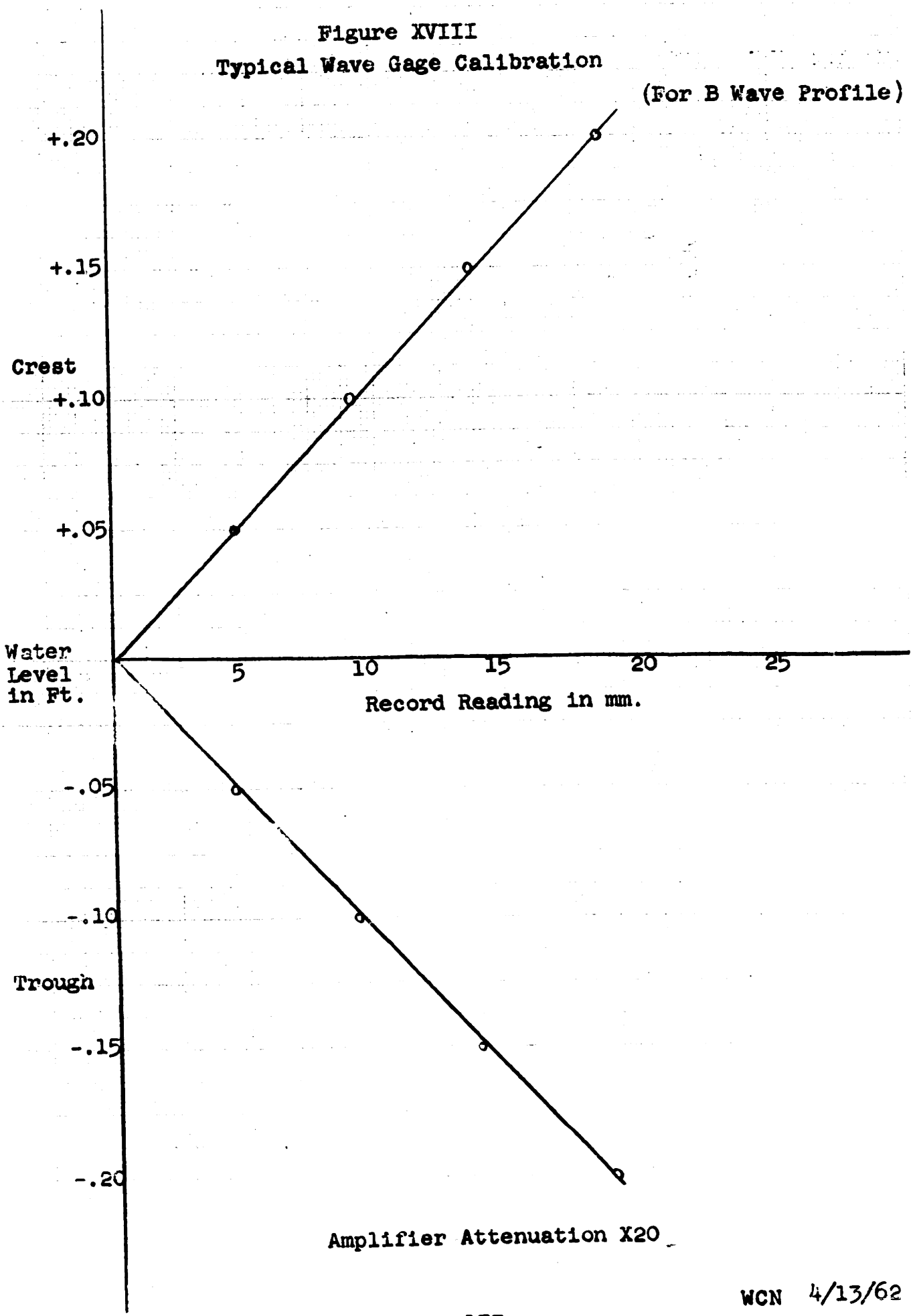

Amplifier Attenuation X20

WCN 4/13/62

Figure XIX

TYPICAL FORCE GAGE CALIBRATION

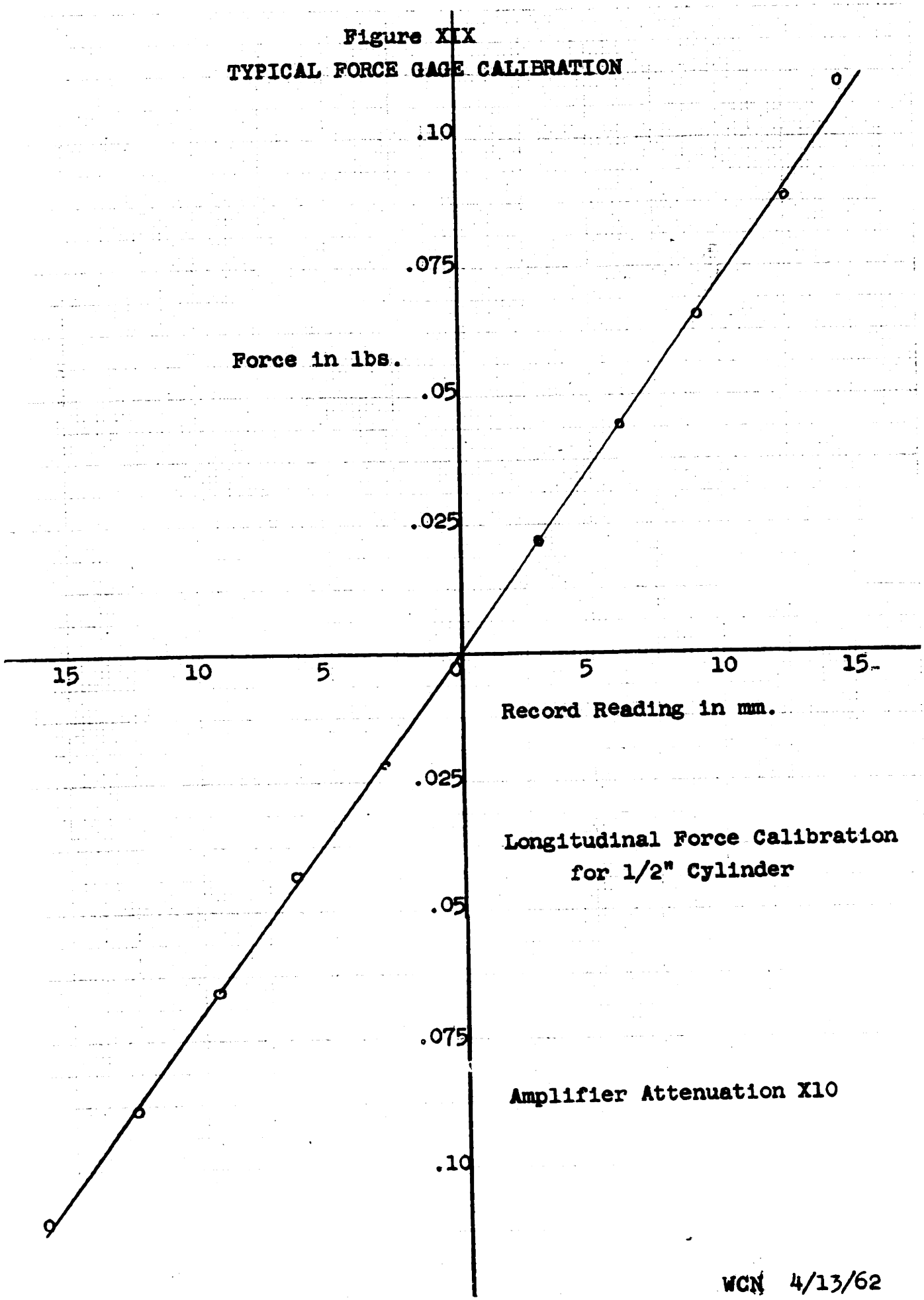

Longitudinal Force Calibration
for 1/2" Cylinder

Amplifier Attenuation X10

WCN 4/13/62

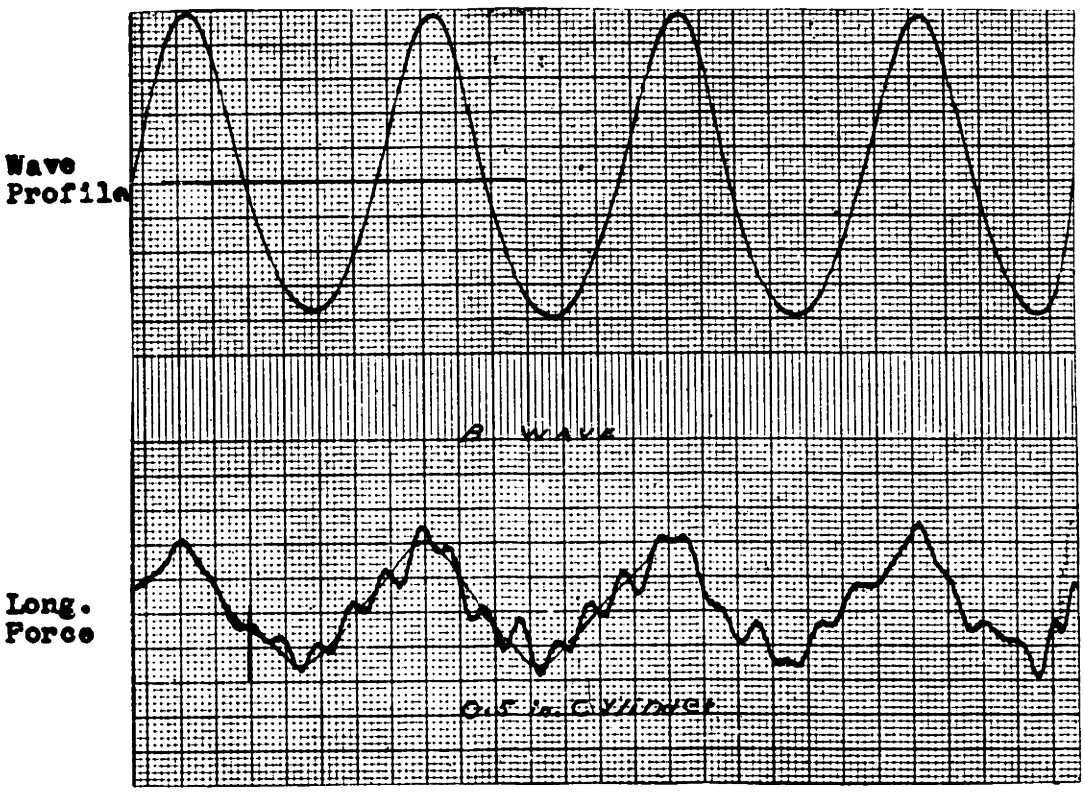

Figure XX - Sample Sanborn Record, Wave Profile And Longitudinal Forces

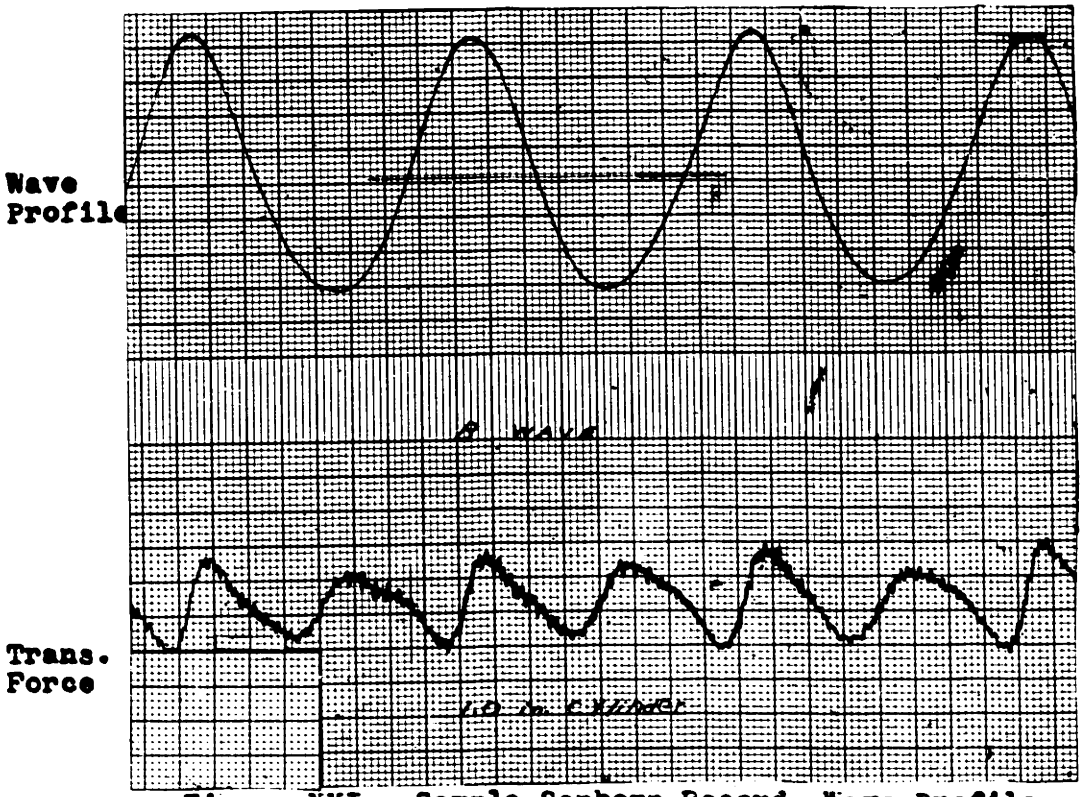

Figure XXI - Sample Sanborn Record, Wave Profile And Transverse Forces

Properties of the Structure Model

Experimental data for free (natural) oscillations of the model is given in Table XIII. Run 3, for example, designates a run in air with the unbraced model with 3 pounds of added weight on the platform. The letter Z designates the braced model. The letter W indicates runs with the model in still water. The tabulated numbers are peak displacements as obtained from movies. A number may not represent the actual peak, which might have occurred between frame exposures. After viewing the movies the authors deduced that in those few cases in which an error could exist it could be only about 0.01 inch. The elapsed time listed is between the first and last recorded peak-displacements.

The weight of plastic in the unbraced model (including base) is 22-3/4 lb. The weight of plastic bracing is about 0.4 lb. The weight of the bolt is 0.200 lb.

The total length of bracing is 186 inches. The length of bracing ℓ_B below the still water level is 149 inches.

TABLE XIII - Experimental Data for Free (Natural) Oscillations of the Structure Model

Run:	0	3	6	10	0-W	3-W	6-W	10-W
Time:	3.14	4.04	4.73	5.88	3.08	3.94	4.70	5.79
Peak Displ.	-.89	-.90	-.92	-.81	-.98	-.96	-.90	-.89
	.98	.99	.93	.83	.95	.91	.89	.87
	-.68	-.66	-.64	-.51	-.70	-.68	-.60	-.56
	.70	.68	.62	.51	.67	.62	.59	.54
	-.48	-.46	-.43	-.31	-.49	-.48	-.40	-.35
	.51	.49	.43	.32	.47	.43	.40	.34
	-.36	-.32	-.29	-.20	-.35	-.33	-.26	-.19
Run:	0Z	3Z	6Z	10Z	0Z-W	3Z-W	6Z-W	10Z-W
Time:	3.16	3.82	4.61	5.81	3.10	3.78	4.60	5.49
Peak Displ.	-.67	-.69	-.84	-.83	-.97	-.94	-.88	-.78
	.74	.67	.98	.92	.71	.93	.87	.74
	-.48	-.48	-.58	-.50	-.67	-.65	-.59	-.49
	.54	.47	.66	.57	.50	.63	.58	.51
	-.36	-.34	-.39	-.32	-.47	-.46	-.39	-.30
	.41	.34	.46	.37	.36	.43	.39	.33
	-.25	.24	-.26	-.18	-.34	-.32	-.26	-.18

I. Vortex Shedding on a Vertical Cylinder in a Wave Train

General

It has been mentioned in this thesis that in the development of a practical offshore structure design transverse or "lift" forces caused by vortex shedding may be included. It is to be expected that these reactive forces are periodic in nature, with magnitudes and frequencies being functionally related to the horizontal component of wave orbital particle velocity u. Furthermore, since $u = 0$ at discrete values of wave phase angle θ, it may also be expected that this periodicity in vortex shedding is repetitive with the passage of each wave in a regular train.

As an illustration let

F_{ij} = magnitude of transverse force caused by a vortex being shed

θ_{ij} = wave phase angle corresponding to F_{ij}.

where $i = 1,2,\ldots n$ = sequential number of a wave in a regular wave train ($i = 1$ for the first wave, etc.)

$j = 1,2,\ldots m$ = sequential number of the vortex shed during the passage of one wave ($j = 1$ for the first vortex shed during the passage of each wave, etc.)

Then

$$F_{ij} = \text{constant} \quad (i = 1,n)$$

$$\theta_{ij} = \text{constant} \quad (i = 1,n)$$

but since F_{ij} is a function of u_{ij},

$$F_{ij} \neq \text{constant} \quad (j = 1,m)$$

Thus it is seen that, because of the repetitive nature of these forces, if their magnitudes and frequencies can be predicted a Fourier series representation could be utilized in developing a procedure for calculating transverse platform displacements. This procedure would not differ appreciably from that presented in this thesis for longitudinal wave forces. It is the intent of this appendix to present an approach for the determination of these vortex forces and shedding frequencies and to show the results of experiments performed by the authors to substantiate this approach.

A. Theory

Transverse Forces

Before the transverse forces are discussed, it might be well first to make some qualitative remarks concerning the significance of considering these forces in a structure design. Mention has been made (Introduction)

of the reported failure, due to fatigue, of a piling subjected to transverse vibrations in ocean waves.

It is to be noted also that the frequency of this force will be at least equal to wave frequency, and for very long ocean waves it could be many times greater than wave frequency. It is possible that this force could create a resonance situation in an offshore structure.

Nothing has been found in the literature relative to the magnitudes of these forces as a vertical cylinder in a wave train, and, to the authors' knowledge, no measurements of the forces have been made in surface waves. However, if one relates the magnitude of this force to the maximum drag force by applying other type measurements and steady state theory, some interesting observations can be made.

Let

F_L = maximum transverse force acting on vertical cylinder of length ℓ

F_D = maximum longitudinal drag force acting on vertical cylinder of length ℓ

Then

$$dF_L = C_L \frac{\rho}{2} D u_{max}^2 d\ell \qquad (66)$$

$$dF_D = C_D \frac{\rho}{2} D u_{max}^2 d\ell \qquad (67)$$

In steady state flow Landweber [33] deduced that $C_L = 3.44 \approx 4\ C_D$, while for a vertical cylinder moving longitudinally with simple harmonic motion in a stationary liquid Laird [34] found $C_L = 0.37$ by measurement. Laird's measurement was for a cylinder diameter of 1" and with $u_{max} = 1.7$ ft./sec. Laird, Johnson, and Walker [35] found experimentally that $C_L \cdot 0.3\ C_D$ for a 2" diameter cylinder moving under the same circumstances as mentioned above. If C_D is taken as approximately equal to 1, this observation substantiates the value of $C_L = 0.37$. The above values of C_L represent the extremes which the literature gives as bases for comparing transverse and drag forces.

It is suspected that the value of C_L given by Laird most closely approximates the real situation. However, two important factors must be considered. First, the artifice employed by Laird in approximating a vertical cylinder in surface waves is deficient in that the water velocity past his cylinder is not a function of the distance from the water surface. In the real situation not only is u_{max} continually varying from bottom to surface, but also, as a wave crest passes a cylinder, the length over which any force acts is not the water depth d but rather $d + \eta_o$ (η_o = height of wave crest above the still water level).

Secondly, the experimental value of $C_L = 0.37$ was for a given cylinder diameter D and given u_{max}. It is to be expected that C_L, like C_D, is a variable with dependence on some defined Reynolds number.

From (66) it is seen that $dF_L = f(u_{max}^2)$. From the definition of u_{max} it is seen then that dF_L is that incremental force which would result if a vortex were shed at the instant that the crest passed the cylinder. Generally the vortex is not shed exactly under the crest. However, if one is interested in the maximum force which might occur, as is the designer, he can justify an assumption that the vortex is shed under the crest, where the particle horizontal velocities are maximum. Therefore, it is assumed that a vortex is shed when $\theta = 90°$.

Because waves of finite height are being considered, it must be noted further that the design force for the crest region will not be equal in magnitude to the design force for the trough region.

As a further complication it was noted by the authors in the experimental phase of this thesis that some vortices shed in the crest region were swept back over the cylinder by velocity reversal during trough passage. These cause significant additional forces on the cylinder, but how they add, detract, or interfere with new vortices about

to be shed is a matter of conjecture. By the time these vortices arrive back at the cylinder, some of their vorticity has been diffused out of the vortex street. Thus it is difficult to determine if the reduction in force in the trough region is the result of new vortices being shed in a region of lower orbital velocity or if the reduction is caused by vorticity diffusion of the swept-back vortices. Visual observation must be made at the same instant that force is recorded to resolve this issue.

In the ocean, where for long waves u is in the same direction for a relatively long period of time, it is proposed that most forces resulting in the wave trough will be caused by new vortices being shed, with only relatively few crest-shed vortices being swept back by velocity reversal - these few being immediately after $\theta = 180°$. The circumstances imposed by laboratory techniques where short wave periods are used make it impractical to verify predications on transverse forces in way of wave troughs. The authors feel that field tests must be employed for this type of verification.

For this reason, it is suggested that if a value for F_L for the wave crest region is predicted and verified experimentally, then a value for the trough region equal in magnitude to $K F_L$ $(K < 1)$ could be used in the

design stage. It is proposed further that for the structure displacement solution a forcing function of the following type be used.

$0° \leq \theta < 180°$

$$F = F_L \sin \omega_c t \tag{68}$$

$180° \leq \theta < 360°$

$$F = K F_L \sin \omega_t t \tag{69}$$

where ω_c = vortex shedding circular frequency in crest region.

ω_t = vortex shedding circular frequency in trough region.

K = constant ($K < 1$) whose value is dependent upon the assumed origin of the force.

More will be said about shedding frequencies later. The sine function results from the assumption [22] that a vortex shedding force is varying sinusoidally.

The remainder of this section on forces will be concerned with the prediction of F_L and K, where K will be that value based upon the assumption of new vortices being shed in the trough region. Several references may be cited (for example [33,34,36,37] which can be used to

derive values of C_L by the steady state Von Kármán vortex street analysis, and this procedure will not be repeated here. Rather, the previously specified values of $C_L = 3.44$ and $C_L = 0.37$ will be used to place limits on the predicted force in formula (66). $C_L = 3.44$ must be considered to be very conservative, however, since its value is based upon the assumption that $u = u_{max}$ for $0° \leq \theta \leq 180°$.

From (66), $$F_L = \int C_L \frac{\rho}{2} D \, u_{max}^2 \, dl \qquad (70)$$

where the limits of integration are as yet unspecified. Before attempting to solve this equation for F_L, it might be well to first consider what criterion may be used to indicate the boundaries for which vortex shedding forces are to be considered. For steady flow a regular Karman vortex street in the wake of cylinders has been observed only in the range of Reynolds numbers $R(= \frac{uD}{\nu})$ from about 60 to 5000. At lower values of R the flow is laminar, and no vortices are shed. For higher R there is complete turbulent mixing [18].

For the non-steady flow associated with wave passage, Keulegan and Carpenter [32] have developed a more realistic dimensionless parameter called the period parameter. From experiments with horizontal cylinders located at various depths in a sinusoidal wave train,

they found that the lower boundary for vortex street development was coincident with a value of the "period parameter" between 12.5 and 15.

$$\text{where period parameter} = \frac{u_{max}T}{D} \qquad (71)$$

u_{max} = horizontal particle velocity under crest at the cylinder depth

T = wave period

The significance of the period parameter lies in the critical distance a particle must travel in one direction for a given velocity in order to produce a vortex. For a complete discussion of this approach the reader is referred to the original work [32].

In this thesis the conservative value of $\frac{u_{max}T}{D} = 12.5$ will be used for the lower boundary of vortex shedding, while it is noted that Keulegan and Carpenter observed regular shedding for $\frac{u_{max}T}{D}$ as high as 110.

Two alternatives are therefore proposed for supplying the limits of integration to (70). First, it may be considered that the vortex extends from the surface down only to the depth where $\frac{u_{max}T}{D} = 12.5$. Secondly, it may be considered that the vortex, once started on the surface, extends all the way to the bottom of the cylinder. This second proposal presupposes that $\frac{u_{max}T}{D} = 12.5$ is the critical value for starting a vortex on the surface, but,

once the starting inertia is overcome, the period parameter is no longer critical in cutting off the vortex at a specified point along the cylinder.

Regardless of which proposal is followed, $\frac{U_{max}T}{D} = 12.5$ ($U_{max} = u_{max}$ at surface) affords the limiting boundary below which no vortices are shed. Intuitively the authors feel that the true solution is a compromise between the two proposals outlined above. However, both proposals will be tried for the specific waves of this thesis.

For descriptive purposes the solutions proposed thus far are designated as follows:

(a) vortex extends to cylinder bottom.

$$F_L = \int_y^{d+\eta_o} C_L \frac{\rho}{2} D\, u_{max}^2\, d\ell \quad \text{for crest region} \qquad (72)$$

$$F_L = \int_y^{d-(H-\eta_o)} C_L \frac{\rho}{2} D\, u_{trough}^2\, d\ell \quad \text{for trough region} \qquad (73)$$

where y is the distance of the bottom of the cylinder above the bottom of the tank (or ocean).

(b) vortex extends only to a depth where $\frac{u_{max}T}{D} = 12.5$ and $\frac{u_{trough}T}{D} = 12.5$ for crest and trough regions, respectively.

$$F_L = \int_{y'}^{d+\eta_o} C_L \frac{\rho}{2} D\, u_{max}^2\, d\ell \quad \text{for crest region} \qquad (74)$$

$$F_L = \int_{y'}^{d-(H-\eta_o)} C_L \frac{\rho}{2} D\, u_{trough}^2\, d\ell \quad \text{for trough region} \qquad (75)$$

where y' is that depth where $\frac{u_{max}T}{D} = 12.5$ and $\frac{u_{trough}T}{D} = 12.5$ for (74) and (75), respectively.

(1) $C_L = 3.44$ (Landweber - steady flow) (76)

(2) $C_L = 0.37$ (Laird - simple harmonic motion) (77)

As an example,

solution (a-2) refers to (72) and (73), using a value of C_L from (77). As mentioned previously, it is expected that the true solution lies between (a-2) and (b-2) with solutions (a-1) and (b-1) being the conservative extremes.

The solutions of (72,73,74,75) are of the following form:

$$F_L = C_L \frac{\rho}{2} \bar{u}^2 \ell \qquad (78)$$

where

$\bar{u}^2$ is the mean square velocity over the length to be considered. If the vortex and the cylinder extend to the bottom of the water $\bar{u}^2$ can be determined directly from (20) and (21).

$$\bar{u}^2_{max} = \frac{A\, g\, d^2}{d + \eta_o} \tag{20}$$

$$\bar{u}^2_{trough} = \frac{B\, g\, d^2}{d + (\eta_o - H)} \tag{21}$$

where A is determined from Figure IV and B, from Figure V.

$$\frac{\eta_o}{d} = \frac{1}{2\, d/H}\left\{1 + \frac{3}{8}\frac{\pi}{L/H}\frac{\sinh(2J)}{(\sinh J)^4}\right\} \tag{6}$$

The parameter $\frac{\eta_o}{d}$ may also be read from the computer output (not plotted), Appendix D. If the vortex does not extend to the bottom the following simplification may be used. Reference [17] shows that for distances removed from the bottom u^2 vs. S is approximately linear, where S is the distance above the bottom. A conservative value of $\bar{u}^2$ may then be taken as

$$\bar{u}^2 = \frac{U^2 + u^2(uT/D = 12.5)}{2} \tag{79}$$

This equation requires use of (10) and (11) or the computer output in Appendix D only two times to get $\overline{u}^2$. The authors feel that any loss of accuracy is justified when the procedure as a whole is viewed.

The proposed solutions therefore reduce to the following forms:

(a-1) crest: $$F_L = 3.44 \frac{\rho}{2} D \overline{u}^2_{max} \left[d + \eta_o - y \right] \quad (80)$$

trough: $$F_L = 3.44 \frac{\rho}{2} D \overline{u}^2_{trough} \left[d - (H - \eta_o) - y \right] \quad (81)$$

(a-2) crest: $$F_L = 0.37 \frac{\rho}{2} D \overline{u}^2_{max} \left[d + \eta_o - y \right] \quad (82)$$

trough: $$F_L = 0.37 \frac{\rho}{2} D \overline{u}^2_{trough} \left[d - (H - \eta_o) - y \right] \quad (83)$$

(b-1) crest: $$F_L = 3.44 \frac{\rho}{2} D \overline{u}^2_{max} \left[d + \eta_o - y' \right] \quad (84)$$

trough: $$F_1 = 3.44 \frac{\rho}{2} D \overline{u}^2_{trough} \left[d - (H - \eta_o) - y' \right] \quad (85)$$

(b-2) crest: $$F_L = 0.37 \frac{\rho}{2} D \overline{u}^2_{max} \left[d + \eta_o - y' \right] \quad (86)$$

trough: $$F_L = 0.37 \frac{\rho}{2} D \overline{u}^2_{trough} \left[d - (H - \eta_o) - y' \right] \quad (87)$$

y = distance of bottom of cylinder above water bottom

y' = distance from bottom to point where $\frac{uT}{D} = 12.5$

and the $\overline{u}^2$'s refer to the mean square velocity over the vortex length.

The force centroids are exactly the same as the drag force centroids (Figure III) if the vortex extends to the bottom, and for any other vortex length the centroids may be assumed in a manner analogous to the assumed $\overline{u}^2_{max}$ and $\overline{u}^2_{trough}$.

Shedding Frequencies

Let S_c = cylinder Strouhal number for steady flow

$$S_c = \frac{\omega_s D}{2\pi u} \tag{88}$$

where ω_s is the vortex shedding circular frequency and u is the steady state velocity. For values of R between 10^3 and 10^4 experiments by Roshko [36] show an average value of S_c of about 0.206. This is the range of concern in the experimental work of this thesis. For other ranges of Reynolds numbers, one is referred to the reference cited above.

Using $S_c = 0.206$, one obtains for ω_s,

$$\omega_s = \frac{0.206\ u\ (2\pi)}{D} \tag{89}$$

From (89) it is seen that in a wave train the shedding frequency (and number of vortices shed per wave cycle) is a function of the orbital particle velocity on

The force centroids are exactly the same as the drag force centroids (Figure III) if the vortex extends to the bottom, and for any other vortex length the centroids may be assumed in a manner analogous to the assumed $\overline{u}^2_{max}$ and $\overline{u}^2_{trough}$.

Shedding Frequencies

Let S_c = cylinder Strouhal number for steady flow

$$S_c = \frac{\omega_s D}{2\pi u} \tag{88}$$

where ω_s is the vortex shedding circular frequency and u is the steady state velocity. For values of R between 10^3 and 10^4 experiments by Roshko [36] show an average value of S_c of about 0.206. This is the range of concern in the experimental work of this thesis. For other ranges of Reynolds numbers, one is referred to the reference cited above.

Using $S_c = 0.206$, one obtains for ω_s,

$$\omega_s = \frac{0.206\ u\ (2\pi)}{D} \tag{89}$$

From (89) it is seen that in a wave train the shedding frequency (and number of vortices shed per wave cycle) is a function of the orbital particle velocity on

the surface of the water (U). This statement is made because vortex shedding is initiated at the surface. The question next arises as to what value to assign to U.

Laird [34] found that for his cylinders moving in simple harmonic motion no vortices were shed until the velocity reached 70% of the peak velocity. If this result is to be considered it seems reasonable that (89) may be written as

$$\omega_c = \frac{0.206(0.7\ U_{max} + U_{max})(2\pi)}{2D} = \frac{0.206(0.85\ U_{max})(2\pi)}{D} \quad (90)$$

where $\frac{(0.7\ U_{max} + U_{max})}{2}$ = "average velocity" at the surface during vortex shedding in the crest region

and

$$\omega_t = \frac{0.206(0.85\ U_{trough})(2\pi)}{D} \quad \text{for the trough region.} \quad (91)$$

Keulegan and Carpenter [32], on the other hand, in their work on horizontal cylinders in sinusoidal waves propose that the shedding frequency be related to the average velocity over a half cycle. If this reasoning is applied to (89) the result is

$$\omega_c = \frac{0.206(0.5\ U_{max})(2\pi)}{D} \quad \text{for the crest} \quad (92)$$

and

$$\omega_t = \frac{0.206(0.5\ U_{trough})(2\pi)}{D} \quad \text{for the trough} \tag{93}$$

The authors feel that it would be reasonable to use (90) and (91) for laboratory work and for steep waves in the ocean, while (92) and (93) may be used for long, low ocean waves where the period is long enough to permit many vortices to be shed. Equations (90) and (91) are used by the authors to obtain shedding frequency. The designer may want to modify this selection, however, when it is realized that the worst frequency to use is that frequency which most closely approaches the natural frequency ω_n of the structure. In any case the vortex force, of this frequency, would be applied to the legs of the structure only for the time duration between $\frac{UT}{D}$ being equal to 12.5 on either side of the crest and trough. The forcing function proposed by the authors assumes the force to be active for the entire wave passage.

Let $(T_s)_c$ = time required to shed 1 vortex in the crest = $\frac{2\pi}{2\omega_c}$ (94)

$(T_s)_t$ = time required to shed 1 vortex in the trough = $\frac{2\pi}{2\omega_t}$ (95)

Then from (90) and (91)

$$(T_s)_c = \frac{D}{2(0.206)(0.85)U_{max}} = \frac{2.86\ D}{U_{max}} \tag{96}$$

and

$$(T_s)_t = \frac{2.86\ D}{U_{trough}} \tag{97}$$

$\frac{T}{2}$ = time for passage of wave crest or wave trough.

Let

n_c = number of vortices shed during crest passage.

n_t = number of vortices shed during trough passage.

Then

$$n_c = \frac{T}{2(T_s)_c} = \frac{T\ U_{max}}{5.72\ D} \tag{98}$$

$$n_t = \frac{T}{2(T_s)_t} = \frac{T\ U_{trough}}{5.72\ D} \tag{99}$$

Because n_c and n_t must be integral numbers, it is proposed to accept the next lower whole numbers in lieu of the values computed from (98) and (99). These integral values of n_c and n_t then give

$$\omega_c = n_c \omega \tag{100}$$

$$\omega_t = n_t \omega \tag{101}$$

where ω is the wave circular frequency.

The proposed theoretical procedure is to use (80) through (87) to determine transverse forces, and (98) through (101) to determine the forcing frequencies.

B. Results, Theoretical and Experimental

For the experimental runs the same waves (A, B, C, and D) were used that were used for longitudinal force determination. Transverse force measurements were attempted by using the 0.5 in. dia. cylinder described in Section II-B. However, it was found that the B, C, and D waves caused resonant vibrations of the cylinder/force-gage combination in the transverse direction, with the A wave being the only wave which gave usable results. For comparative purposes the transverse forces caused by the A wave are plotted with the longitudinal forces and the results are shown in Figure XVIIa.

As a consequence of these results it was decided to center investigation on a 1 in. dia. cylinder. This cylinder cleared the bottom of the tank by 12-5/8". Therefore, in (80,81,82,83) y is taken as 12-5/8" = 1.052 ft. By measurement the damped natural frequency of the 1 in. dia. cylinder arrangement was

17.85 cps, as compared to 4.8 cps for the 0.5 in. dia. cylinder arrangement.

Before the results are presented it would be interesting to predict whether or not vortex shedding is expected for the various runs. Table XIV lists values of wave period, as well as $\frac{U_{max}T}{D}$ and $\frac{U_{trough}T}{D}$, for the 4 waves of the experiment. Wave periods are determined from (8), while the velocities are taken directly from the computer output (Appendix D). All other values in the following analysis are taken from Appendix D, unless a particular equation is specified.

TABLE XIV- Wave Periods and Period Parameters

Wave	T(sec.)	$\frac{U_{max}T}{D}$	$\frac{U_{trough}T}{D}$
A	2.015	13.75	-11.13
B	1.558	15.45	-12.00
C	1.350	17.07	-12.53
D	1.200	18.90	-12.90

Since the critical value of $\frac{uT}{D}$ is considered to be 12.5, it is doubtful that the trough region can support vortex shedding. In fact, all forces in the trough region were observed to be caused (in part at least) by crest-shed vortices being swept back to

the cylinder during velocity reversal. Hence, trough-shed vortices are not considered further, except to state that for the runs performed by the authors, $\omega_t = \omega_c$.

Parameters used in the solution of (80, 82, 84, 86) are shown in tabulated form in Table XV. The parameter $(u_{max})_{crit}$ refers to the velocity for which the period parameter is equal to 12.5 and is used as the entering argument in Appendix D to determine y'. The parameter $(u_{max})_y$ is the velocity under the crest at the bottom of the cylinder. The parameter $(\bar{u}_{max}^2)_a$ is for use with (80) and (82) and is equal to $\frac{U_{max}^2 + (u_{max}^2)_y}{2}$. The parameter $(\bar{u}_{max}^2)_b$ is for use with (84) and (86) and is equal to $\frac{U_{max}^2 \times (u_{max}^2)_{crit}}{2}$. Velocities are in ft./sec.

TABLE XV - Wave Parameters for Transverse Force Determination

Wave	η_o(ft)	U_{max}	$(u_{max})_{crit}$	$(u_{max})_y$	y'(ft)	$(\bar{u}_{max}^2)_a$	$(\bar{u}_{max}^2)_b$
A	0.120	0.568	0.518	0.399	2.09	0.241	0.296
B	0.173	0.825	0.669	0.452	2.00	0.442	0.563
C	0.200	1.050	0.774	0.462	1.97	0.657	0.879
D	0.227	1.310	0.870	0.453	1.95	0.958	1.334

The transverse forces (F_L) as determined experimentally are shown plotted with the corresponding wave profiles in Figures XXII a-d. Table XVI compares theoretical and experimental results for values of F_L and n_c (number in parenthesis is integral value). The value of ω_c (= ω_t for reasons mentioned) is determined from (100). The theoretical values of n_c are determined from (98), and the various F_L's from the appropriate formulas (80, 82, 84, 86), with inputs from Table V.

ρ = 1.94 slugs/ft.^{3} d = 2.25 ft.

TABLE XVI - Comparison of Theoretical and Experimental Transverse Force Results

	F_L					n_c		$\omega_c/2\pi$ (cps)	
	Method					Theory	Exp.	Theory	Exp.
Wave	a-1	a-2	b-1	b-2	Exp.				
A	0.0883	0.0095	0.0230	0.00248	0.014	2.4(2)	2	0.993	0.993
B	0.1680	0.0181	0.0654	0.00704	0.072	2.7(2)	2	1.283	1.283
C	0.2550	0.0274	0.1167	0.01255	0.128	3.0(2)	2	2.220	1.482
D	0.3800	0.0408	0.1950	0.02100	0.088	3.3(2)	2	2.500	1.667

C. Discussion of Results

From Table XVI and Figures XXII a-d it is seen that the assumption of vortex shedding frequency being equal to an integral multiple of wave frequency is

FIGURE XXIIa

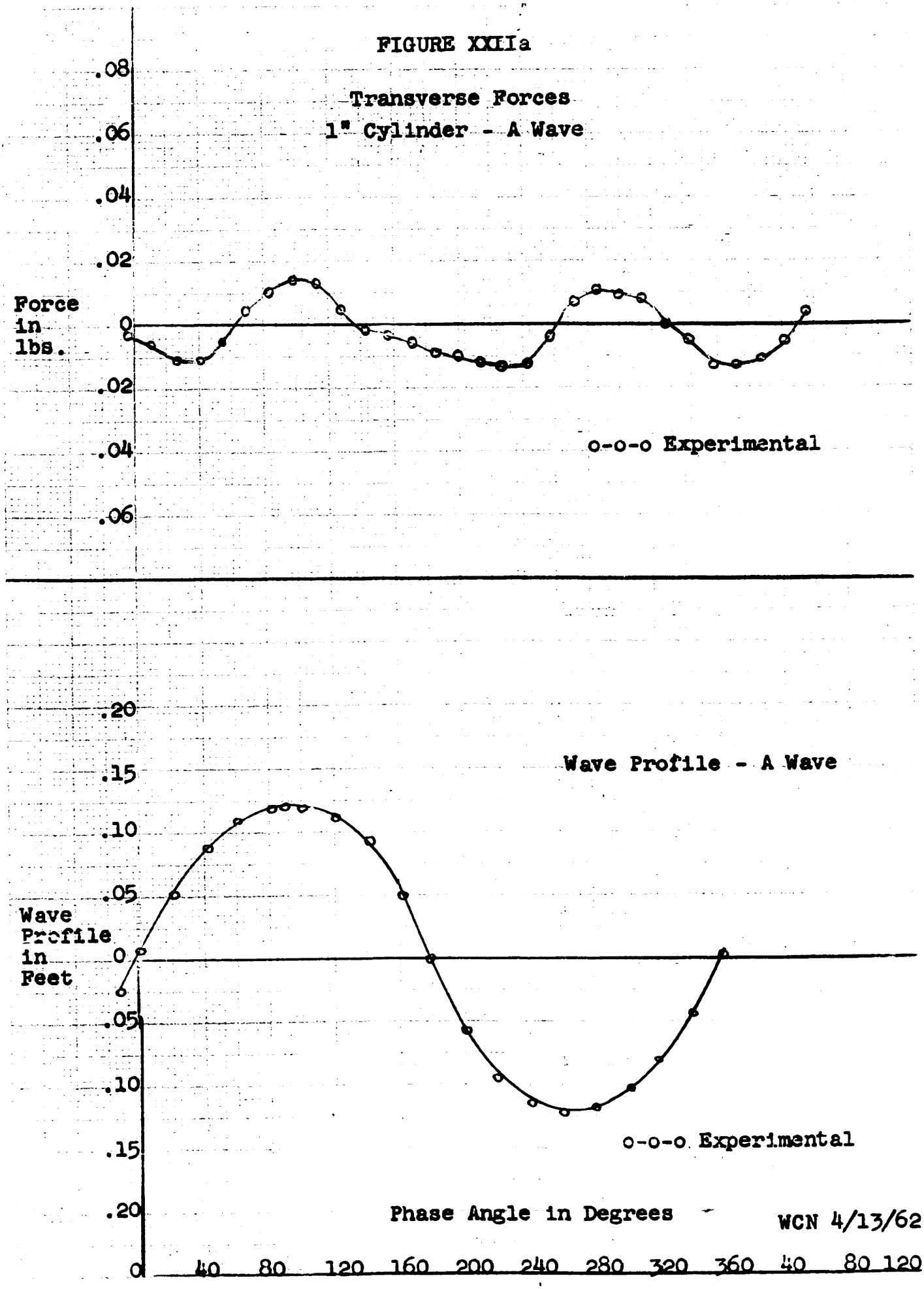

FIGURE XXIb

Transverse Forces

1" Cylinder - B Wave

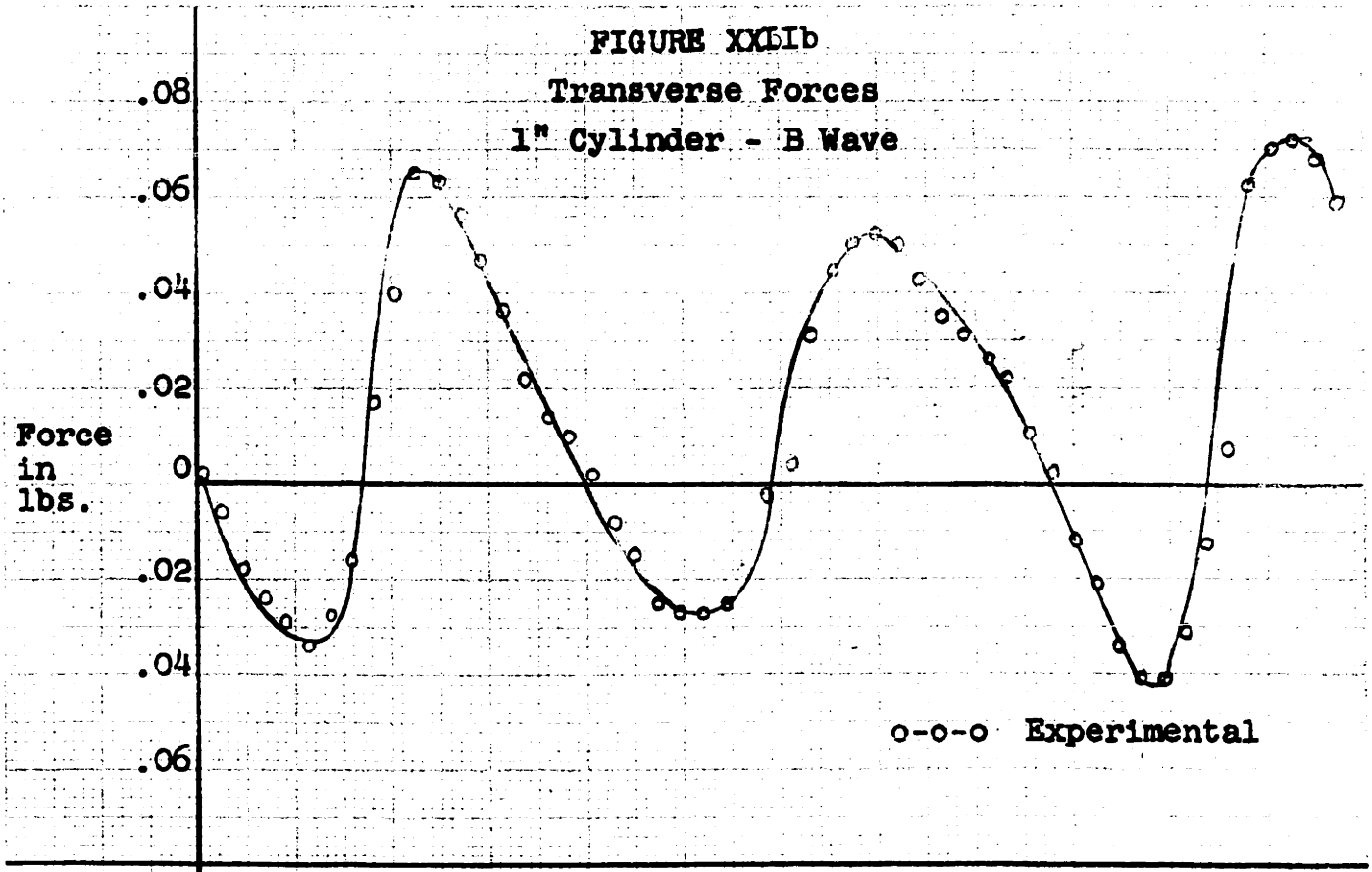

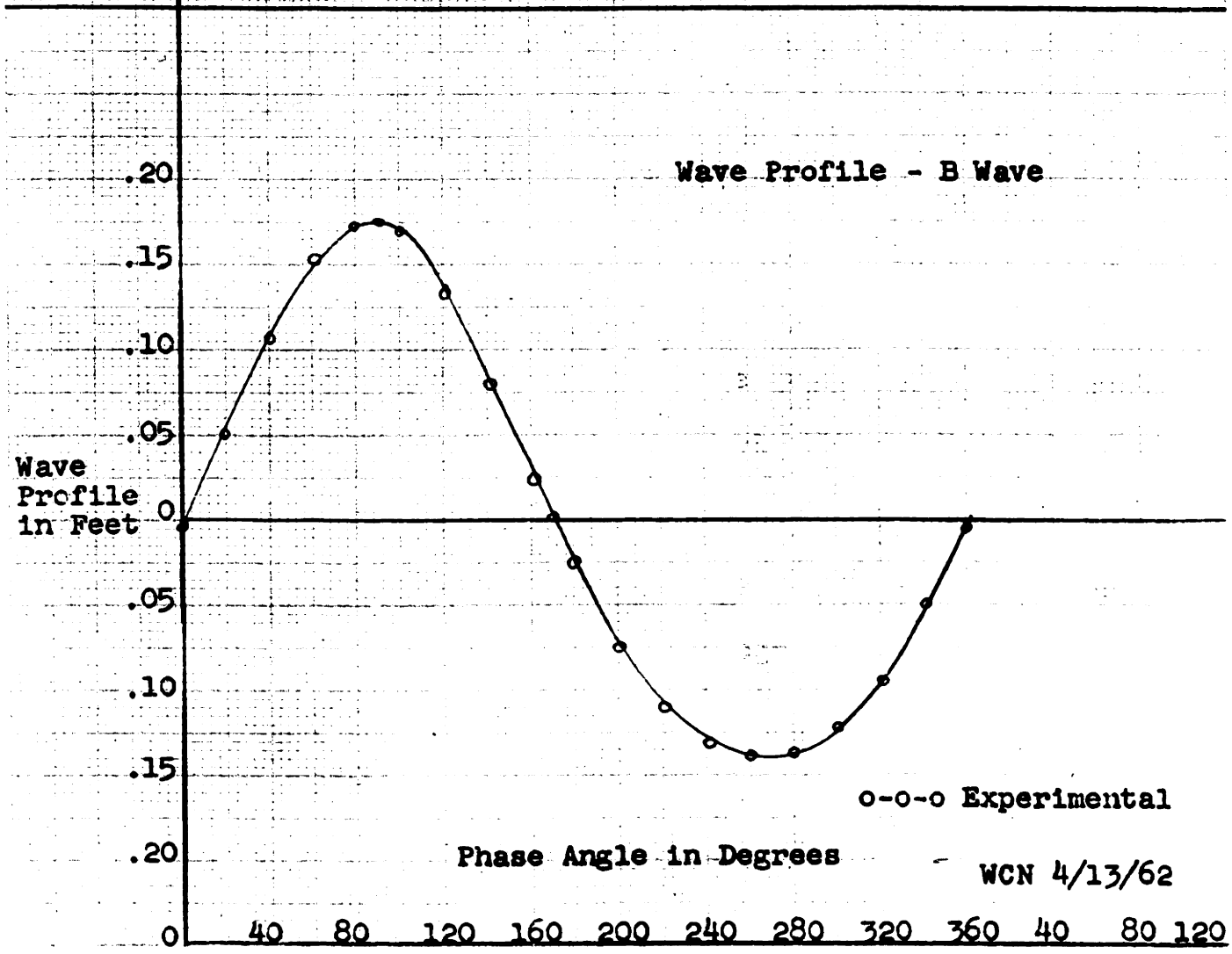

WCN 4/13/62

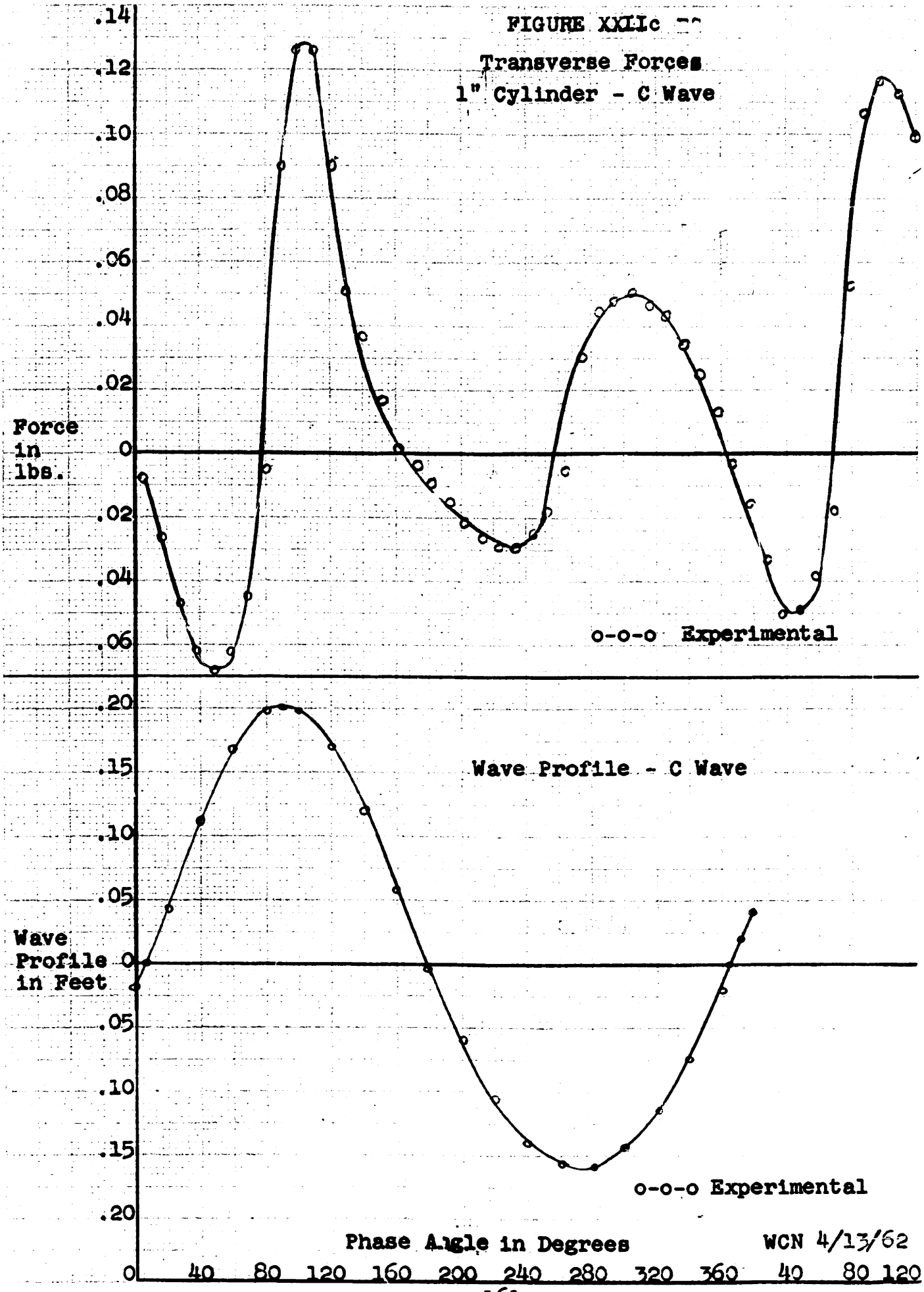
FIGURE XXIIc
Transverse Forces
1" Cylinder - C Wave
.14
.12
.10
.08
.06
.04
.02
Force in lbs.
0
.02
.04
.06
o-o-o Experimental
.20
.15
.10
.05
Wave Profile in Feet
0
.05
.10
.15
.20
Wave Profile - C Wave
o-o-o Experimental
Phase Angle in Degrees
0
40
80
120
160
200
240
280
320
360
40
80
120
WCN 4/13/62

FIGURE XXIId

Transverse Forces

1" Cylinder - D Wave

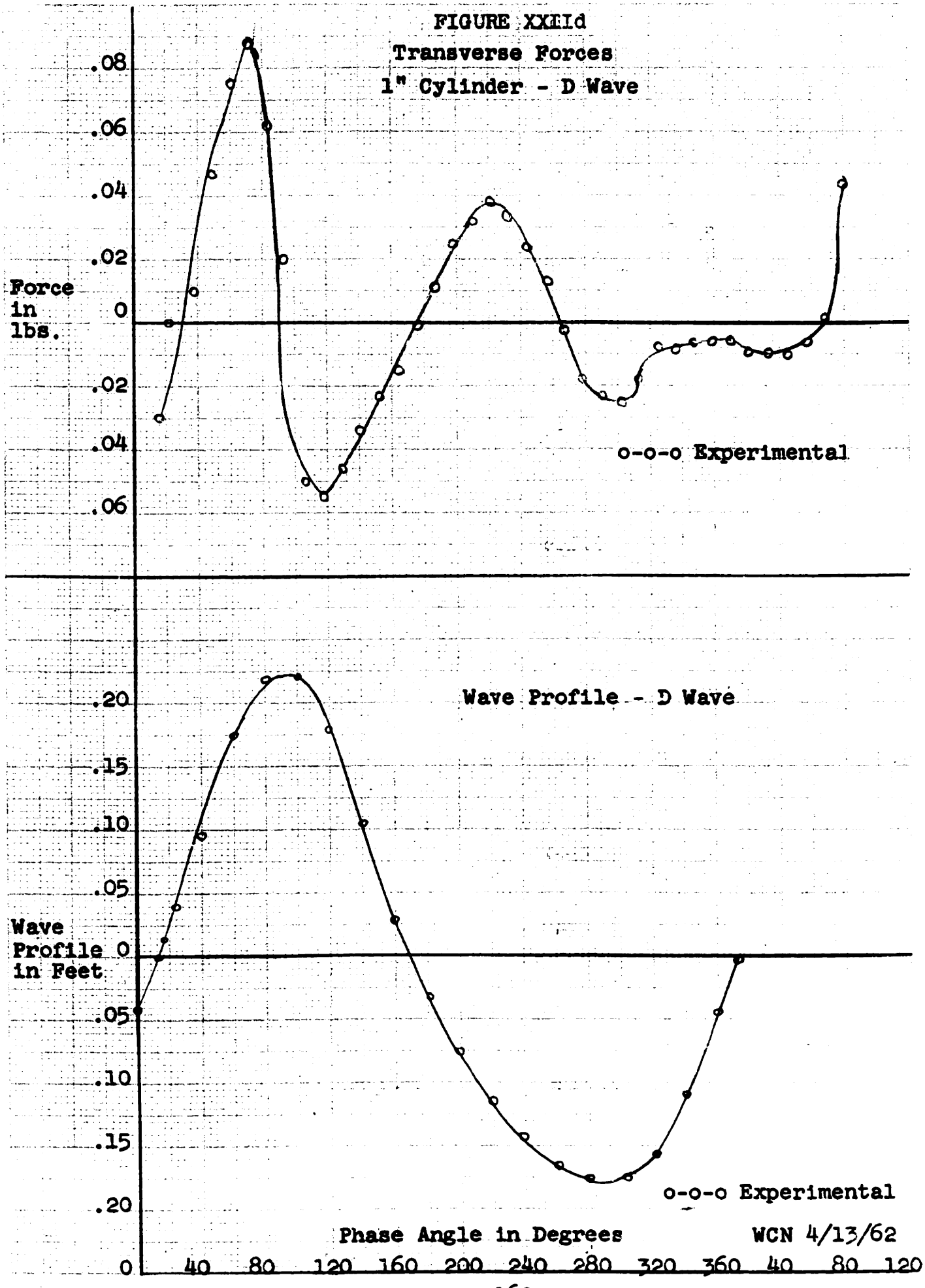

valid. Laird [34] found experimentally that vortex shedding appears to occur in pairs, and this may be why the experimental values of n_c for the C and D waves are equal to 2 rather than 3. For all experimental runs trough shedding frequency ω_t was equal to crest shedding frequency ω_c, as explained previously.

The vortex forces in the trough region were not determined analytically, because, for the experimental runs of this thesis, these forces are caused (in part) by back-sweeping crest-shed vortices from which some of the vorticity has been diffused out of the street. From Figure XVIIa for the 0.5 in. dia. cylinder, it is seen that the experimental maximum vortex force is 43.4% of the experimental longitudinal total force and 90% of the experimental longitudinal drag force. This 90% value is considerably higher than the 30% value found experimentally by Laird, Johnson, and Walker [35].

From Table XVI it is seen that method (b-1) agrees most closely with the experimental force results. Method (b-1) refers to (84), where C_L is taken as 3.44, and the vortex length terminates where $\frac{u_{max}^T}{D} = 12.5$. Methods (a-2) and (b-2), which assume $C_L = 0.37$, are seen to give forces which are far too small. It is seen, therefore, that a method of solution between (a) and (b) together with a method between (1) and (2), would give analytical

results most closely approximating the experimental results of this thesis. The 90% ratio of C_L/C_D, determined experimentally for the 0.5 in. dia. cylinder (Figure XVIIa), may indicate a basis for selection of C_L. More experimental tests are required to narrow the boundaries for the analytical forces, as shown in Table XVI, but it is reassuring that the experimental forces lie within the range defined by the proposed theories.

D. Conclusions and Recommendations

1. The proposed method of determining a design vortex shedding frequency is valid. It is suggested that the designer pick a value of n_c which is on the side of the computed value to cause ω_c (or ω_t) to approach the structure natural frequency ω_n.

2. Until a more accurate prediction may be made of the vortex shedding forces, a safe design is to assume $C_L = C_D$.

3. It is recommended that field tests be conducted with ocean waves of long period to verify the authors' procedure for the case of trough-shed vortices.

4. If platform rotation is considered, vortex shedding forces will assume added importance.

J. Literature Citations

1. Wylie, E.M., "Tragedy on Tower Four," True, the Man's Magazine, April 1962, as condensed in The Reader's Digest, April 1962, pp. 94-102.

2. Report 173, "Texas Tower No. 4, Platform Motion Study," Brewer Engineering Laboratories, Inc., Marion, Massachusetts, June 10, 1959, pp. E, F, 36.

3. "Design Calculations for Buzzards Bay Light Station, U.S. Coast Guard," J. Ray McDermott & Co., Inc., New Orleans, 1960-61.

4. Rechtin, E.C., Steele, J.E., and Scales, R.E., "Engineering Problems Related to the Design of Offshore Mobile Platforms," Transactions of the Society of Naval Architects and Marine Engineers, Volume 65, 1957, pp. 633-681.

5. Wiegel, R.L., Beebe, K.E., and Moon, J., "Ocean Wave Forces on Circular Cylindrical Piles," Proceedings of the American Society of Civil Engineers, Hydraulics Division, Volume 83, 1957, pp. 1199-1 through 1199-36.

6. Putz, R.R., "Statistical Distribution for Ocean Waves," Transactions, American Geophysical Union, Volume 33, No. 5, 1952, pp. 685-691.

7. Chadwick, J.H., and Chang, S.S.L., "A Recording-Analyzing System for Wave-Induced Forces and Motions," Proceedings, Symposium on the Behavior of Ships in a Seaway, Volume II, 1957, pp. 691-711.

8. "Analysis of Ocean Wave Forces on the Concrete Pile Foundation for St. John's Fog Signal," U.S. Coast Guard Civil Engineering Report No. 16, CG-250-16, 1955, pp. 7-27.

9. Brewer, G., of Brewer Engineering Laboratories, Inc., Marion, Massachusetts, correspondence to Mr. Mildram of Lincoln Laboratories, November 12, 1956.

10. Blueprint "Key Plan and General Arrangement of Texas Tower No. 4," Department of the Navy, Bureau of Yards and Docks drawing no. 678257, September 8, 1955.

11. Hartman, E.L., "Proximity Effects on the Drag Coefficient for Circular Cylinders," B.S. thesis in Department of Civil Engineering at Massachusetts Institute of Technology, 1957, p. 31.

12. Lamb, H., Hydrodynamics, Second Edition, Cambridge University Press, 1895, pp. 404-428.

13. Wiegel, R.L., and Johnson, J.W., "Elements of Wave Theory," Proceedings of First Conference on Coastal Engineering, 1950, pp. 5-21.

14. Bretschneider, C.L., "Selection of Design Wave for Offshore Structures," Proceedings of the American Society of Civil Engineers, Journal of the Waterways and Harbors Division, 1958, pp. 1-37.

15. Bigelow, H.B., and Edmondson, W.T., Wind Waves at Sea-Breakers and Surf, Hydrographic Office Publication No. 602, 1947, pp. 2-126.

16. "Summary of Theories for Waves and Wave Forces on Cylindrical Piles," Appendix A of Feasibility Report on Texas Towers, p. A28.

17. Harleman, D.R.F., and Shapiro, W.C., "Experimental and Analytical Studies of Wave Forces on Offshore Structures, Part I; Results for Vertical Cylinders," Technical Report No. 19 of the Hydrodynamics Laboratory of Massachusetts Institute of Technology, May 1955, pp. 1-24.

18. Schlichting, H., Boundary Layer Theory, Fourth Edition, McGraw-Hill Book Co., Inc., New York, 1960, pp. 16, 30.

19. "Argus Island - Deflection Study," J. Ray McDermott & Co., Inc., New Orleans, February 1961, p. 2.

20. "The Collapse of Texas Tower No. 4," Report by Preparedness Investigating Subcommittee of the Committee on Armed Services, United States Senate, 87th Congress, 1st Session, U S. Government Printing Office, Washington, 1961, pp. 12, 35.

21 "Inquiry into the Collapse of Texas Tower No. 4," Hearings before the Preparedness Investigating Subcommittee of the Committee on Armed Services, United States Senate, 87th Congress, 1st Session, U.S. Government Printing Office, Washington, May 1961, p. 180.

22. Den Hartog, J.P., Mechanical Vibrations, Fourth Edition, McGraw-Hill Book Co., Inc., New York, 1956, pp. 17-20, 23-54, 141-155, 305.

23. "Argus Island - Vibration Study," J. Ray McDermott & Co., Inc., New Orleans, February 1961, p. 5.

24. Harris, C.M., and Crede, C.E., editors, Shock and Vibration Handbook, McGraw-Hill Book Co., Inc., 1961, pp. 37-2, 50-20.

25. Norris, C.H., and Wilbur, J.B., Elementary Structural Analysis, Second Edition, McGraw-Hill Book Co., Inc., 1960, pp. 57-58, 84-85, 256-273, 296-300, 318-343, 380-392, 472-473.

26. Harleman, D.R.F., Shapiro, W.C., and Marlow, T.A., II, "Experimental and Analytical Studies of Wave Forces on Offshore Drilling Structures, Part II; Buoyancy Components for Floating Platforms," Technical Report No. 24 of the Hydrodynamics Laboratory of Massachusetts Institute of Technology, June 1957, pp. 12-13, 16, 32-35, 40.

27. Harleman, D.R.F., and Shapiro, W.C., "Investigations on the Dynamics of Moored Structures in Waves," Technical Report No. 28 of the Hydrodynamics Laboratory of Massachusetts Institute of Technology, July 1958, pp. 13, 35-38, 44-46.

28. Dean, R.G., and Ursell, F., "Interaction of a Fixed Semi-Immersed Circular Cylinder with a Train of Surface Waves," Technical Report No. 37 of the Hydrodynamics Laboratory of Massachusetts Institute of Technology, September 1959, pp. 27-38.

29. Den Hartog, J.P., Strength of Materials, McGraw-Hill Book Co., Inc., New York, 1949, pp. 79-85.

30. Thomson, W.T., Mechanical Vibrations, Second Edition, Prentice-Hall, Inc., Englewood Cliffs, N.J., 1953, p. 11.

31. Rouse, H., editor, Advanced Mechanics of Fluids, John Wiley & Sons, Inc., New York, 1959, pp. 94-95, 156.

32. Keulegan, G.H., and Carpenter, L.H., "Forces on Cylinders and Plates in an Oscillatory Fluid," Journal of Research of the National Bureau of Standards, Volume 60, Number 5, May 1958, pp. 423-440.

33. Landweber, L., "Flow About a Pair of Adjacent Parallel Cylinders Normal to a Stream: Theoretical Analysis," David W. Taylor Model Basin Report Number 485, Navy Department, July 1942.

34. Laird, A.D.K., "Eddy Forces on Rigid Cylinders," Proceedings of the American Society of Civil Engineers, Journal of the Waterways and Harbors Division, Volume 84, Number WW4, November 1961, pp. 53-68.

35. Laird, A.D.K., Johnson, C.A., and Walker, R.W., "Water Eddy Forces on Oscillating Cylinders," Proceedings of the American Society of Civil Engineers, Journal of the Hydraulics Division, Volume 86, Number HY9, November 1960, pp. 43-54.

36. Roshko, A., "On the Drag and Shedding Frequencies of Two-Dimensional Bluff Bodies," National Advisory Committee for Aeronautics Technical Note 3169, July 1954.

37. Prandtl, L., and Tietjens, O.G., Applied Hydro- and Aeromechanics, translated by J.P. Den Hartog, Dover Publications, Inc., New York, 1957, pp. 130-136, 161-173.

Other References

38. Bowden, K.F., "Some Observations of Waves and Other Fluctuations in a Tidal Current," Proceedings, Royal Society of London, Serial A, Volume 192, 1948, 403-428.

39. Bretschneider, C.L., "The Generation and Decay of Wind Waves in Deep Water," Transactions, American Geophysical Union, Volume 33, Number 5, 1952, pp. 382-383.

40. Bretschneider, C.L., "Hurricane Design Wave Practices," Proceedings of the American Society of Civil Engineers, Journal of the Waterways and Harbors Division, 1957, pp. 1-33.

41. Bretschneider, C.L., "Selection of Design Wave for Offshore Structures," Transactions, American Society of Civil Engineers, Volume 125, 1960, pp. 388-414.

42. Collipp, B.G., "The Design of an Offshore Oil-drilling Rig," M.S. thesis in the Department of Naval Architecture and Marine Engineering at Massachusetts Institute of Technology, August 23, 1954, pp. 27, 89.

43. Freeman, J.C., Jr., and Goode, H., "Winds, Tides, Waves, and Wave Forces in Hurricane Flossy of 1956," paper presented before the Gulf Section, Society of Naval Architects and Marine Engineers, 1957, pp. 1-4.

44. Johnson, J.W., and Rice, E.K., "A Laboratory Investigation of Wind Generated Waves," Transactions, American Geophysical Union, Volume 33, Number 6, 1952, pp. 848-853.

45. Kolodzey, C.E., "Offshore Drilling Platforms - Structural Details, Wave Forces, and Safety Precautions," paper presented before the Gulf Section, Society of Naval Architects and Marine Engineers, 1954, from SNAME Bulletin, Volume X, Number 2, 1955, pp. 14-19.

46. MacCamy, R.C., and Fuchs, R.A., "Wave Forces on Piles: A Diffraction Theory," Technical Memorandum Number 69, Beach Erosion Board, 1954.

47. Morison, J.R., O'Brien, M.P., Johnson, J.W., and Schaaf, S.A., "The Force Exerted by Surface Waves on Piles," Petroleum Transactions, American Insitute Min. and Metal. Eng., Volume 189, 1950, pp. 149-154.

48. Norris, C.H., Hansen, R.J., Holley, M.J., Jr., Biggs, J.M., Namyet, S., and Minami, J.K., Structural Design for Dynamic Loads, McGraw-Hill Book Co., Inc., New York, 1959.

49. Pierson, W.J., and Marks, W., "The Power Spectrum Analysis of Ocean-Wave Records," Transactions, American Geophysical Union, Volume 33, Number 6, 1952, pp. 834-842.

50. Pierson, W.J., Neumann, G., and James, R.W., Observing and Forecasting Ocean Waves by Means of Wave Spectra and Statistics, Hydrographic Office Publication 603, 1958.

51. Rogers, G.L., Dynamics of Frame Structures, John Wiley & Sons, Inc., New York, 1959, pp. 28, 104, 319.

52. Roll, H.U., "Height, Length, and Steepness of Sea Waves in the North Atlantic and Dimension of Sea Waves as Functions of Wind Force," Technical and Research Bulletin Number 1-19, Society of Naval Architects and Marine Engineers, 1958, pp. 1-8.

53. Roll, H.U., "Some Results of Comparison Between Observed and Computed Heights of Wind Waves," Proceedings, Symposium on the Behavior of Ships in a Seaway, Volume I, 1957, pp. 418-426.

54. Rouse, H., Fluid Mechanics for Hydraulic Engineers, McGraw-Hill Book Co., Inc., New York, 1938, pp. 217-220.

55. Skjelbreia, L., "Gravity Waves - Stokes' Third Approximation Table of Functions," Council of Wave Research, The Engineering Foundation, 1959.

56. Timoshenko, S., and Young, D.H., Vibration Problems in Engineering, Third Edition, D. Van Nostrand Co., Inc., 1955, pp. 31-33.

47. Morison, J.R., O'Brien, M.P., Johnson, J.W., and Schaaf, S.A., "The Force Exerted by Surface Waves on Piles," Petroleum Transactions, American Insitute Min. and Metal. Eng., Volume 189, 1950, pp. 149-154.

48. Norris, C.H., Hansen, R.J., Holley, M.J., Jr., Biggs, J.M., Namyet, S., and Minami, J.K., Structural Design for Dynamic Loads, McGraw-Hill Book Co., Inc., New York, 1959.

49. Pierson, W.J., and Marks, W., "The Power Spectrum Analysis of Ocean-Wave Records," Transactions, American Geophysical Union, Volume 33, Number 6, 1952, pp. 834-842.

50. Pierson, W.J., Neumann, G., and James, R.W., Observing and Forecasting Ocean Waves by Means of Wave Spectra and Statistics, Hydrographic Office Publication 603, 1958.

51. Rogers, G.L., Dynamics of Frame Structures, John Wiley & Sons, Inc., New York, 1959, pp. 28, 104, 319.

52. Roll, H.U., "Height, Length, and Steepness of Sea Waves in the North Atlantic and Dimension of Sea Waves as Functions of Wind Force," Technical and Research Bulletin Number 1-19, Society of Naval Architects and Marine Engineers, 1958, pp. 1-8.

53. Roll, H.U., "Some Results of Comparison Between Observed and Computed Heights of Wind Waves," Proceedings, Symposium on the Behavior of Ships in a Seaway, Volume I, 1957, pp. 418-426.

54. Rouse, H., Fluid Mechanics for Hydraulic Engineers, McGraw-Hill Book Co., Inc., New York, 1938, pp. 217-220.

55. Skjelbreia, L., "Gravity Waves - Stokes' Third Approximation Table of Functions," Council of Wave Research, The Engineering Foundation, 1959.

56. Timoshenko, S., and Young, D.H., Vibration Problems in Engineering, Third Edition, D. Van Nostrand Co., Inc., 1955, pp. 31-33.

Miscellaneous

57. Robinson, D.K., "United States Coast Guard Offshore Light Stations," The Engineer's Digest, U.S. Coast Guard, September-October, 1961, pp. 26-29.

58. Wiman, K.G., "Shop Fabrication of Buzzards Bay and Brenton Reef Light Stations," The Engineer's Digest, U.S. Coast Guard, November-December 1961, pp. 10-12.

59. Wiman, K.G., "Field Erection of Buzzards Bay Offshore Light Station," The Engineer's Digest, U.S. Coast Guard, January-February 1962, pp. 2-4.

60. "Texas Towers Aid German Bridge Erection," Engineering News-Record, March 22, 1962, pp. 138-140.